Arch Computat Methods Eng (2015) 22:1–65
DOI 10.1007/s11831-014-9108-x

Mass Matrix Templates: General Description and 1D Examples

Carlos A. Felippa · Qiong Guo · K. C. Park

Received: 24 August 2013 / Accepted: 24 August 2013 / Published online: 26 May 2014

Abstract This article is a tutorial exposition of the template approach to the construction of customized mass-stiffness pairs for selected applications in structural dynamics. The main focus is on adjusting the mass matrix. Two well known discretization methods, described in FEM textbooks since the late 1960s, lead to diagonally lumped and consistent mass matrices, respectively. Those models are sufficient to cover many engineering applications but for some problems they fall short. The gap can be filled with a more general approach that relies on the use of templates. These are algebraic forms that carry free parameters. Templates have the virtue of producing a set of mass matrices that satisfy certain *a priori* constraint conditions such as symmetry, nonnegativity, invariance and momentum conservation. In particular, the diagonally lumped and consistent versions can be obtained as instances. Availability of free parameters, however, allows the mass matrix to be customized to special needs, such as high precision vibration frequencies or minimally dispersive wave propagation. An attractive feature of templates for FEM programming is that only one element implementation as module with free parameters is needed, and need not be recoded when the application problem class changes. The paper provides a general overview of the topic, and illustrates it with one-dimensional structural elements: bars and beams.

C. A. Felippa (✉) · Q. Guo · K. C. Park
Department of Aerospace Engineering Sciences,
University of Colorado at Boulder, Boulder, CO 80309-0429, USA
e-mail: carlos.felippa@colorado.edu

Q. Guo
Shanghai Aircraft Design and Research Institute,
Commercial Aircraft Corporation of China Ltd., Shanghai, China

K. C. Park
Department of Ocean Engineering, KAIST, Daejon, Republic of Korea

1 Introduction

This paper addresses the construction of mass matrices for dynamic models of structures treated by the finite element method (FEM). The goal is to introduce a general approach through which *customized mass matrices* can be constructed for specific structural elements. This is called the method of *templates*. The qualifier "customized" is defined more precisely later.

Two standard procedures for constructing FEM mass matrices are well known. They are outlined in Appendix 2 to make this paper reasonably self-contained. They lead to *consistent* and *diagonally lumped* forms, respectively. Conventional forms of those models are denoted by $\mathbf{M}_C$ and $\mathbf{M}_L$, respectively, in the sequel, with additional subscripts or superscripts as necessary or convenient. Abbreviations consistent mass matrix (CMM) and diagonally lumped mass matrices (DLMM), respectively, are also used. Collectively those two models take care of many engineering applications in structural dynamics. Occasionally, however, they fall short. The gap can be filled with a more general approach that relies on *templates*. These are algebraic forms that carry free parameters. The set of parameters is called the *template signature*. When given numerical values, the signature uniquely characterizes a mass matrix *instance*.

This paper presents basic concepts and techniques that underlie the template approach. This methodology is applied to several one-dimensional (1D) structural elements as expository examples.

The template approach has the virtue of generating a set of mass matrices that satisfy certain *a priori* constraints; for example symmetry, nonnegativity, invariance and linear momentum conservation. A mass matrix that satisfies those will be called *admissible*. In particular, the diagonally lumped and consistent mass matrices should

Table 1 Template customization scenarios

Acronym	Customization
LFCF	Low-frequency continuum fit: matching acoustic branch (AB) to continuum model
AMC	Angular momentum conservation: useful for transverse motions
RHFP	Reduced high-frequency pollution (spurious noise) in direct time integration (DTI)
MSTS	Maximum stable time step in conditionally stable direct time integration (DTI)
RDAW	Reduced directional anisotropy in wave propagation (not relevant to 1D meshes)

be obtained as instances. Thus those standard models are not excluded. Availability of free parameters, however, allows the mass matrix to be *customized* to special requirements.

Several customization scenarios are listed in Table 1, along with their acronyms. The last one: reduction of directional anisotropy in wave propagation, is not applicable to 1D elements and therefore not treated in this paper.

The versatility of application will be evident from the examples. It will be also seen that optimizing templates for one scenario generally does not help with others, and in fact may make things worse. Thus, ability to adapt the mass matrix to particular needs as well as problem regions is an important virtue. Note that mesh and freedom configuration need not be modified in any way; only template signatures are adjusted.

An attractive feature of templates for FEM programming is that each "custom mass matrix" need not be coded and tested individually. It is sufficient to implement the template as a single element-level module, with free parameters as arguments (alternatively, useful instances may be identified by predefined mnemonic character strings, and converted to numerical signatures internally). The signature is adjusted according to goals and needs. In particular the same module should be able to produce the conventional DLMM and CMM models as instances. This can provide valuable cross-checking with well established programs while doing benchmarks.

In problems characterized by rapid transients, such as contact-impact and fragmentation, templates allow a flexible customization: reduced high-frequency pollution in elements in or near shock regions while maintaining low-frequency continuum fit away from such regions. In those scenarios, signatures may evolve in time.

2 Is Customization Worth the Trouble?

The ability to customize a mass matrix is not free of development costs. The presence of free parameters makes template derivations considerably more complicated than those based on the two standard procedures noticed in Sect. 1 and outlined in Appendix 2. Reason: everything must be carried along *symbolically*: geometry, material and fabrication properties, in addition to the free parameters. Consequence: hand computations rapidly become unfeasible, even for fairly simple 1D elements. Help from a computer algebra system (CAS) is needed to get timely results. A key issue is: when is this additional work justified? Two specific cases may be mentioned.

One is *high fidelity systems*. Dynamic analysis covers a wide range of applications. There is a subclass that calls for a level of simulation accuracy beyond that customary in engineering analysis. Examples are deployment of precision space structures, resonance analysis of machinery or equipment, adaptive active control systems, medical imaging, phononics (long wave guidance at molecular level), vehicle signature detection, radiation loss in layered circuits, and molecular- and crystal-level simulations in micro- and nanomechanics.

In static structural analysis an error of 20 or 30 % in peak stresses is not cause for alarm—such discrepancies are usually covered adequately by safety factors. But a similar error in frequency analysis or impedance response of a high fidelity system can be disastrous. Achieving acceptable precision with a fine mesh, however, can be expensive. Model adaptivity comes to the rescue in statics. This approach is less effective in dynamics, however, on account of the time dimension and the fact that irregular meshes are prone to develop numerical pollution. Customized elements may provide a practical solution: achieving adequate accuracy with a *coarse regular* mesh.

Another possibility is that the stiffness matrix comes from a method that avoids displacement shape functions (DSF). For example, assumed-stress or strain elements. Or, it could simply be an array of numbers provided by a black-box program, with no documentation explaining its source. If this happens the concept of CMM, in which velocity shape functions (VSF) are taken to coincide with DSF, loses the comfortable variational meaning outlined in Sect. 1. An expedient way out is to choose an element with similar geometry and freedom configuration derived with DSF and take those as VSF. But which element to pick? If time allows, constructing and customizing a template avoids uncritically rolling the dice.

3 Mass Parametrization Techniques

There are several ways to parametrize mass matrices. Techniques found effective in practice are summarized below.

Most of them are illustrated in the worked out examples of ensuing sections.

It is often advantageous to have several template expressions for the same element configuration. For example, to study the subset of DLMM it may be convenient to streamline the general form to one that produces only such matrices. Likewise for singular mass matrices. In that case we speak of template *variants*. These may overlap totally or partially: the DLMM variant is plainly a subset of the general mass template. The key difference between a template subset and a variant is that the latter *redefines free parameters from scratch*.

For the reader's convenience, acronyms often used in this paper are listed in Table 2. A set of definitions and abbreviations pertaining to templates are collected in Table 3.

Notational conventions for mathematical expressions that appear in this paper are summarized in Table 4. Specific conventions used for free template parameters are given in Table 5. As a general rule, template parameters are always dimensionless and denoted by lower case Greek letters.

3.1 Matrix-Weighted Parametrization

A *matrix-weighted* (MW) mass template for element e is a linear combination of $(k+1)$ component mass matrices, $k \geq 1$ of which are weighted by parameters $\mu_i, (i = 1, \ldots k)$:

$$\mathbf{M}^e \stackrel{\text{def}}{=} \mathbf{M}^e_0 + \mu_1 \mathbf{M}^e_1 + \cdots \mu_k \mathbf{M}^e_k. \tag{1}$$

Here $\mathbf{M}^e_0$ is the *baseline mass matrix*. This should be an admissible mass matrix on its own if $\mu_1 = \ldots \mu_k = 0$. The simplest instance of (1) is a linear combination of the CMM and a DLMM:

$$\mathbf{M}^e \stackrel{\text{def}}{=} (1-\mu)\mathbf{M}^e_C + \mu \mathbf{M}^e_L. \tag{2}$$

This can be reformatted as (1) by writing $\mathbf{M}^e = \mathbf{M}^e_C + \mu(\mathbf{M}^e_L - \mathbf{M}^e_C) = \mathbf{M}^e_0 + \mu\,\mathbf{M}^e_1$. Here $k = 1$, the baseline is $\mathbf{M}^e_0 \equiv \mathbf{M}^e_C$, $\mu \equiv \mu_1$ and $\mathbf{M}^e_1$ is the "mass deviator" $\mathbf{M}^e_L - \mathbf{M}^e_C$. The specialization (2) is often abbreviated to "linear combination of consistent and diagonally lumped masses," with acronym LCDM; cf. Table 2. The rationale behind (2) is that the CMM typically overestimates natural frequencies while a DLMM usually underestimates them. Thus a linear combination has a good chance of improving low-frequency accuracy for some $\mu \in [0, 1]$.

A MW mass template represents a tradeoff. It cuts down on the number of free parameters. Such a reduction is essential for 2D and 3D elements. It makes it easier to satisfy conservation and nonnegativity conditions through appropriate choice of the $\mathbf{M}^e_i$. On the minus side it gen-

Table 2 Acronyms used in paper

Acronym	Stands for
AB	Acoustic branch in DDD: has physical meaning in continuum models
ABTS	AB Taylor series in DWN κ, centered at $\kappa = 0$
BLCD	Best linear combination (LFF sense) of the CMM and a selected DLMM
BLFD	Best possible DLMM (LFF sense); acronym also applies to MS pair with this mass
BLFM	Best possible FPMM (LFF sense); acronym also applies to MS pair with this mass
CMM	Consistent mass matrix: a special VDMM in which VSM and DSF coalesce
CMS	Component Mode Synthesis: model reduction framework for structural dynamics
CMT	Congruential (also spelled congruent) mass transformation
COB	Constant optical branch: OB frequency is independent of wavenumber
COF	Cutoff frequency: OB frequency at zero wavenumber (lowest one if multiple OB)
DDD	Dimensionless dispersion diagram: DCF Ω versus DWN κ
DGVD	Dimensionless group velocity diagram: $\gamma_c = c/c_0$ versus DWN κ
DIMM	Directionally invariant mass matrix: repeats with respect to any RCC frame
DOF	Degree(s) of freedom
DLMM	Diagonally lumped mass matrix; qualifier "diagonally" is often omitted
DSF	Displacement shape functions to interpolate displacements over element
DSM	Direct Stiffness Method: the most widely used FEM implementation
DTI	Direct time integration of EOM
DCF	Dimensionless circular frequency, always denoted by Ω
DWN	Dimensionless wavenumber, always denoted by κ
EOM	Equations of motion
FEM	Finite Element Method
FFB	Flexural frequency branch in Bernoulli–Euler or Timoshenko beam models
FPMM	Fully populated mass matrix (at element level); includes CMM as special case
HF	High frequency: short wavelength, small DWN, typically $\kappa > 1$
LCDM	Mass matrix obtained as linear combination of the CMM and a selected DLMM
LF	Low frequency: long wavelength, small DWN, typically $\kappa < 1$
LFF	Low frequency fitting of AB to that of continuum
LLMM	Lobatto lumped mass matrix: a DLMM based on a Lobatto quadrature rule
MOF	Maximum overall frequency: largest frequency in DDD over Brillouin zone

Table 2 continued

Acronym	Stands for
MSA	Matrix Structural Analysis: invented by Duncan and Collar at NPL [23,24]
NCT	Non-continuum term: a term in the ABTS that is not present in the continuum
NND	Nonnegative definite; a qualifier reserved for symmetric real matrices
PD	Positive definite; a qualifier reserved for symmetric real matrices
PVP	Parametrized variational principle
OB	Optical branch (or branches) in DDD: no physical meaning in continuum models
OBTS	OB Taylor series in DWN κ, centered at $\kappa = 0$
RCC	Rectangular Cartesian Coordinate: qualifier to frame, system, axes, etc.
SDAV	Structural dynamics and vibration applications: low frequency range important
SF	Shape function
SFB	Shear frequency branch in the Timoshenko beam model
SLMM	Simpson lumped mass matrix: a LLMM based on Simpson's 3-pt quadrature rule
SMS	Selective mass scaling: modifying a mass matrix by adding a scaled stiffness
VDMM	Variational derived mass matrix: Hessian of discretized kinetic energy
VP	Variational principle
VSF	Velocity shape functions to interpolate velocities and produce a VDMM

erally spans only a subspace of admissible mass matrices.

3.2 Spectral Parametrization

A spectrally parametrized (SP) mass template has the form

$$\mathbf{M}^e \stackrel{\text{def}}{=} \mathbf{H}^T \mathbf{D}_\mu \mathbf{H}, \qquad \mathbf{D}_\mu = \mathbf{diag}\big[\, c_0\mu_0 \; c_1\mu_1 \; \ldots \; c_k\mu_k \,\big]. \tag{3}$$

in which $\mathbf{H}$ is typically a full matrix. Parameters $\mu_0 \ldots \mu_k$ appear as entries of the diagonal matrix $\mathbf{D}_\mu$. Scaling coefficients c_i may be introduced for convenience so the μ_i are dimensionless. Often the values of μ_0 and/or μ_1 are preset from conservation conditions.

Configuration (3) occurs naturally when $\mathbf{M}^e$ is constructed first in generalized coordinates, followed by congruential transformation to physical coordinates via $\mathbf{H}$. If the generalized mass is derived using mass-orthogonal functions (for example, Legendre polynomials in 1D elements), the unparametrized generalized mass $\mathbf{D} = \mathbf{diag}\big[\, c_0 \quad c_1 \quad \ldots c_k \,\big]$ is diagonal. Parametrization is effected by scaling its entries.

Table 3 Template related nomenclature

Term or abbreviation	Meaning
Template	An algebraic expression for a FEM matrix that contains free parameters So far used to construct stiffness and mass matrices of linear FEM models
Signature	The set of free parameters that uniquely defines a template
Instance	Matrix (or matrices) obtained by setting the signature to numeric values
Subset	Generic term for template specialization: includes families and variants
Family	A template subset in which some free parameters are linked by constraints
Variant	A template subset that introduces free parameters from scratch (the "subset" may be the original template if reparametrized)
Admissible	Qualifier applied to instances that satisfy predefined conditions such as positiveness, element mass conservation, and fabrication symmetries
MS template	Mass-stiffness pair template: both **M** and **K** have free parameters
FD template	Frequency-dependent template: free parameters may depend on frequency
FDM template	Frequency-dependent mass template
FDS template	Frequency-dependent stiffness template
FDMS template	Frequency-dependent mass-stiffness template
EW template	Entry weighted parametrization of a template; see Sect. 3.3
ML template	Multilevel parametrization of a template; see Sect. 3.4
MW template	Matrix weighted parametrization of a template; see Sect. 3.1
SP template	Spectral parametrization of a template; see Sect. 3.2

As noted, some entries may be left fixed to satisfy *a priori* constraints such as mass conservation.

Expanding (3) and collecting matrices that multiply each μ_i leads to a matrix weighted combination form (1) in which each $\mathbf{M}_i^e$ is a rank-one matrix. The analogy with the spectral representation theorem of symmetric matrices is obvious. But in practice it is usually better to work directly with the congruent representation (3).

As remarked later in Sect. 3.6, SP is especially convenient for constructing *singular* mass matrices under customization scenario RHFP of Table 1.

3.3 Entry-Weighted Parametrization

An entry-weighted (EW) mass template applies free parameters directly to each entry of the mass matrix, except for

Table 4 General notational conventions for mathematical expressions

Letter symbol[a]	Used for	Examples
UC bold	Matrices	$\mathbf{K}$, $\mathbf{M}$
LC bold	Vectors	$\mathbf{u}$, $\dot{\mathbf{u}}$
US roman	Scalar coefficients or functions	a, b, $\bar{Q}$, $u(x,t)$
SS LC roman	Subscripted variants of scalar coefficients	$\hat{c}_1$, $\hat{c}_2$
SS LC roman	Vector entries conforming with vector symbol	u_i: entries of $\mathbf{u}$
DS UC roman	Matrix entries conforming with matrix symbol	K_{ij}: entries of $\mathbf{K}$
Greek letters	Dimensionless quantities except as noted below[b]	θ, ψ, Ω
Superposed dot	Temporal differentiation	$\ddot{\mathbf{u}} \equiv d^2\mathbf{u}(t)/dt^2$
Prime	1D spatial differentiation, usually with respect to x	$v'(x) \equiv dv(x)/dx$

[a] *UC* uppercase, *LC* lowercase, *US* unsubcripted, *SS* single subscripted, *DS* double subscripted
[b] Exemption made for well established symbols: e.g. ω frequency, or ρ mass density

Table 5 Notational conventions for template parameters

Symbol[a]	Used for
α_i	Free parameters in basic stiffness matrix template (not used in this paper)
β_i	Free parameters in higher order stiffness matrix template
μ_i	Original free parameters in mass template. Additional letter subscripts may be appended as appropriate to distinguish template families or variants
ν_i, χ_i	Alternative notations for mass template parameters. Often derived from the original μ_i to streamline expressions, or to identify families or variants

[a] The subscript index is suppressed if only one parameter appears; e.g. β, μ

a priori constraints on symmetry, invariance and conservation. As an example, for a 1D element with three translational DOF we may start from

$$\mathbf{M}^e \stackrel{\text{def}}{=} m^e \begin{bmatrix} \mu_{11} & \mu_{12} & \mu_{13} \\ \mu_{12} & \mu_{22} & \mu_{23} \\ \mu_{13} & \mu_{23} & \mu_{33} \end{bmatrix}, \tag{4}$$

in which m^e is the total element mass, and the sum of all row sums is one. EW is often applied to entries of a "deviator matrix" that measures the change from a baseline matrix such as $\mathbf{M}_C$. For example, see the three-node bar template (39).

Because of its generality, EW parametrization can be expected to lead to optimal customized instances. But it is restricted to simple (usually 1D) elements because the number of parameters grows quadratically in the matrix size, whereas for the foregoing two schemes either it grows linearly, or stays constant.

3.4 Multilevel Parametrization

A hierarchical combination of parametrization schemes can be used to advantage if the kinetic energy can be naturally decomposed from physical considerations. For example, the Timoshenko beam element covered in Sect. 7 uses a two-matrix-split template combined by a weighted form similar to (2) as top level (the energy split is between translational and rotational inertia). The two components are constructed by spectral and EW parametrization, respectively. Such combinations fall under the scope of multilevel (ML) parametrization.

3.5 Selective Mass Scaling

Selective mass scaling (SMS), is a method proposed recently (references given in Appendix Sect. 1.4), in which the mass matrix is modified by a scaled version of the stiffness matrix. Thus $\mathbf{M}$ becomes

$$\mathbf{M}_K = \mathbf{M} + \frac{\mu_K}{\omega_{ref}^2}\mathbf{K}. \tag{5}$$

Here $\mu_K \geq 0$ is a dimensionless scaling factor whereas ω_{ref}^2 is a "reference" frequency used to homogenize physical dimensions. The modification (5) may be done at the element or system level. The objective is to "filter down" high frequencies in explicit DTI for applications such as contact-impact; e.g., vehicle crash simulation. Filtering aims to reduce spurious noise as well as increasing the stable timestep. It thus follows under customization scenarios RHFP and MSTS of Table 1. The basic idea can be explained as follows. Let ω_i and $\mathbf{v}_i$ denote the natural frequencies and associated orthonormalized eigenvectors, respectively, whereas $\hat{\omega}_i$ and $\hat{\mathbf{v}}_i$ are their counterparts for the modified eigenproblem $(\mathbf{M}_K + \hat{\omega}_i^2\,\mathbf{K})\,\hat{\mathbf{v}}_i = \mathbf{0}$. By inspection the eigenvectors are preserved: $\hat{\mathbf{v}}_i = \mathbf{v}_i$. Taking the Rayleigh quotient shows that the modified frequencies are

$$\hat{\omega}_i^2 = \frac{\omega_i^2}{R_i}, \quad \text{in which} \quad R_i = 1 + \mu_K \frac{\omega_i^2}{\omega_{ref}^2}. \tag{6}$$

Choosing $\mu_K > 0$ cuts down each frequency by $R_i > 0$. For low frequencies the modification is negligible if μ_K and ω_{ref}^2 are appropriately selected so that $R_i \approx 1$. For nonphysical high frequencies (mesh modes) the reduction can be significant In fact note that if $\omega_i^2 >> \mu_K/\omega_{ref}^2$, $\hat{\omega}_i^2$ cannot exceed the fixed bound $\omega_{max}^2 = \omega_{ref}^2/\mu_K$. The downside is that low frequency accuracy may suffer significantly, as illustrated later.

Although SMS may be presented as a variant of the MW parametrization technique of Sect. 3.1, it deserves to be considered on its own for the reasons stated in Appendix Sect. 1.4.

3.6 Singular Mass Matrices

A thread linked to SMS but independently developed is that of *singular* mass matrices. This has been primarily advocated for multibody dynamics, as well as dynamical systems leading to differential-difference equations of motion (EOM) that occur in active or passive control with time lags. References are provided in Appendix Sect. 1.5. The objective is roughly similar to SMS: reduce high frequency noise pollution triggered by rapid transients and/or time lags. But now this is done by raising the optical branch (OB) (or branches) so as to widen the *acoustoptical gap* pictured described in Sect. 5.1 and illustrated in Fig. 8. Noisy frequencies that fall in the gap decay exponentially.

There are several ways to produce such matrices. Under the template framework, the use of SP is particularly convenient, as observed in Sect. 3.2. Other approaches include reduced numerical integration, as well as injection of a convenient null space using mass matrix projection.

3.7 Constant Optical Branch Variant

Instead of rising the OB (or branches) by making $\mathbf{M}^e$ singular, one may try to make the OB frequency independent. Templates that accomplish that feat are tagged as having a constant optical branch (COB) for short. They form subsets collectively identified as the COB variant. The group velocity pertaining to a COB vanishes, so associated waveforms with that particular frequency do not propagate. COB templates were discovered during the course of this work, and are briefly studied in Sect. 5.13 for the three-node bar element.

3.8 Mass-Stiffness Template Pairs

The concept of template was first developed for element stiffness matrices, as a natural generalization of its decomposition into basic and higher order parts. A brief historical account is provided in Appendix Sect. 1.6. Normally the stiffness template is optimized by imposing superconvergence conditions dealing with higher order patch tests while element aspect ratios are kept arbitrary. That optimal instance, if found, is kept fixed while a mass matrix template is subsequently investigated.

Maximum customization for dynamics can be expected if *both* stiffness and mass matrix templates can be simultanously adjusted. This is known as a mass-stiffness (MS) template. These may be of interest when improving dynamic behavior is paramount. Presently there is relatively little experience with this more ambitious approach. A note of caution: highly optimized MS templates may be abnormally sensitive to geometric or material perturbations away from a regular mesh.

3.9 Frequency Dependent Templates

One final generalization should be mentioned: allowing free parameters to be function of the frequency. If this is done for the mass matrix, we speak of a frequency dependent mass (FDM) template. If this is done for both the mass and stiffness matrices, we call the combination a FDM-stiffness (FDMS) template. Both cases are illustrated in Sects. 4.11–4.13 for the two-node bar element.

Although this ultimate complication is largely a curiosity, it might be occasionally useful in problems that profit from transformation to the frequency domain. For example: a linear dynamic system driven by a harmonic excitation of slowly varying frequency, if only the long term (steady-state) response is considered. Such systems may arise in parametric stability and active control.

4 The Two-Node Bar Element

The template approach is best grasped through an example that involves the simplest nontrivial structural finite element: a two-node prismatic bar of mass density ρ, area A and length ℓ, that can only move along the longitudinal axis x. See Fig. 1a. This element is often acronymed Bar2 for brevity's sake. The well known consistent and DLMM forms are

$$\mathbf{M}^e_C = \frac{m^e}{6}\begin{bmatrix} 2 & 1 \\ 1 & 2 \end{bmatrix}, \qquad \mathbf{M}^e_L = \frac{m^e}{2}\begin{bmatrix} 1 & 0 \\ 0 & 1 \end{bmatrix}. \tag{7}$$

in which $m^e = \rho A \ell$ is the total element mass. These are derived in Sect. 1.

4.1 Bar2 Entry Weighted Template

The most general mass matrix form for Bar2 is the EW template

$$\mathbf{M}^e = \begin{bmatrix} M^e_{11} & M^e_{12} \\ M^e_{21} & M^e_{22} \end{bmatrix} = \rho A\,\ell \begin{bmatrix} \mu_{11} & \mu_{12} \\ \mu_{21} & \mu_{22} \end{bmatrix} = m^e \begin{bmatrix} \mu_{11} & \mu_{12} \\ \mu_{21} & \mu_{22} \end{bmatrix}. \tag{8}$$

The first form is merely a list of entries. Next the element mass $m^e = \rho A\,\ell$ is factored out. The emerging parame-

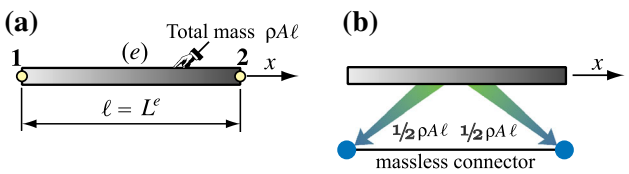

Fig. 1 The two-node prismatic bar element: **a** element configuration, **b** direct mass lumping to end nodes

ters μ_{11} through μ_{22} are numbers, which illustrates a general rule: *template free parameters should be dimensionless*. This simplifies analysis and implementation. To cut down on parameters one looks at *configuration constraints*. The most obvious ones are:

Matrix symmetry $\mathbf{M}^e = (\mathbf{M}^e)^T$. For the expression (8) this requires $\mu_{21} = \mu_{12}$.

Physical symmetry: For a prismatic bar, $\mathbf{M}^e$ in (8) must exhibit antidiagonal symmetry: $\mu_{22} = \mu_{11}$.

Conservation of total translational mass: same as conservation of linear momentum or of kinetic energy. Apply the uniform velocity field $\dot{u} = v$ to the bar. The associated nodal velocity vector is $\dot{\mathbf{u}}^e = \mathbf{v}^e = v\begin{bmatrix}1 & 1\end{bmatrix}^T$. The kinetic energy is $T^e = \frac{1}{2}(\mathbf{v}^e)^T\mathbf{M}^e\mathbf{v}^e = \frac{1}{2}m^e v^2(\mu_{11} + \mu_{12} + \nu_2 + \mu_{22})$. This must equal $\frac{1}{2}m^e v^2$, whence $\mu_{11} + \mu_{12} + \mu_{21} + \mu_{22} = 2(\mu_{11} + \mu_{12}) = 1$.

Nonnegativity: $\mathbf{M}^e$ should not be indefinite (this is not an absolute must, and it is actually relaxed in some elements discussed later). Whether checked by computing eigenvalues or principal minors, this constraint is nonlinear and of inequality type. Consequently it is not often applied *ab initio*, unless the element is quite simple, as in this case, or can be stated through simple expressions.

4.2 Bar2 One Parameter Mass Template

On applying the symmetry and conservation rules three parameters of (8) are eliminated. The remaining one, called μ, is taken for convenience to be $\mu_{11} = \mu_{22} = (2+\mu)/6$ and $\mu_{12} = \mu_{21} = (1-\mu)/6$. This rearrangement gives

$$\mathbf{M}^e_\mu = \tfrac{1}{6}\rho A\,\ell\begin{bmatrix}2+\mu & 1-\mu\\ 1-\mu & 2+\mu\end{bmatrix} = (1-\mu)\mathbf{M}^e_C + \mu\mathbf{M}^e_L. \quad (9)$$

Expression (9) shows that the general Bar2 mass template can be recast as a linear combination of the CMM and DLMM instances listed in (7). Summarizing, we end up with a one-parameter, matrix-weighted (MW) template that befits the LCD form (2). If $\mu = 0$ and $\mu = 1$, (9) reduces to $\mathbf{M}^e_C$ and $\mathbf{M}^e_L$, respectively. This illustrates another requirement: the CMM and DLMM forms *must be instances* of the mass template.

Finally we can apply the nonnegativity constraint. For the two principal minors of $\mathbf{M}^e_\mu$ to be nonnegative, $2+\mu \geq 0$ and $(2+\mu)^2 - (1-\mu)^2 = 3+6\mu \geq 0$. Both are satisfied if $\mu \geq -1/2$. Unlike the others, this constraint is of inequality type, and only limits the range of μ.

The remaining task is to select the parameter. This is done by introducing an *optimality criterion that fits the problem at hand*. This is where customization comes in. Even for this simple case the answer is not unique. Thus the statement "the best mass matrix for Bar2 is so-and-so" has to be qualified. Two specific optimization criteria are considered in Sects. 4.4 and 4.5.

4.3 Bar2 Alternative Parametrization

An alternative template expression that is useful in some investigations, such as those undertaken in Appendix 6, is obtained by reparametrizing via $\chi = 1 + 2\mu$, the inverse of which is $\mu = (\chi - 1)/2$. The resulting form is

$$\mathbf{M}^e_\chi = \tfrac{1}{12}\rho A\,\ell\begin{bmatrix}3+\chi & 3-\chi\\ 3-\chi & 3+\chi\end{bmatrix}. \quad (10)$$

This is called the "χ form" of the general Bar2 mass template. Because the determinant is $\rho A\,\ell\chi$, $\mathbf{M}^e_\chi$ is seen to be singular if $\chi = 0$, and nonnegative if $\chi \geq 0$.

4.4 Bar2 Angular Momentum Conservation

This criterion can only be applied in multiple dimensions, since element-transverse angular rotations do not exist in 1D. Accordingly we allow the bar to move in the $\{x, y\}$ plane by expanding its nodal DOF to $\mathbf{u}^e = \begin{bmatrix}u_{x1} & u_{y1} & u_{x2} & u_{y2}\end{bmatrix}^T$, whence (9) becomes a 4×4 matrix

$$\mathbf{M}^e_\mu = \tfrac{1}{6}\rho A\,\ell\begin{bmatrix}2+\mu & 0 & 1-\mu & 0\\ 0 & 2+\mu & 0 & 1-\mu\\ 1-\mu & 0 & 2+\mu & 0\\ 0 & 1-\mu & 0 & 2+\mu\end{bmatrix} \quad (11)$$

Apply a uniform angular velocity $\dot{\theta}$ about the midpoint. The associated node velocity vector at $\theta = 0$ is $\dot{\mathbf{u}}^e = \frac{1}{2}\ell\dot{\theta}\begin{bmatrix}0 & -1 & 0 & 1\end{bmatrix}^T$. The discrete and continuum energies are

$$T^e_\mu = \tfrac{1}{2}(\dot{\mathbf{u}}^e)^T\mathbf{M}^e_\mu\dot{\mathbf{u}}^e = \tfrac{1}{24}\rho A\ell^3(1+2\mu),$$
$$T^e = \int_{-\ell/2}^{\ell/2}\rho A\big(\dot{\theta}\,x\big)^2\,dx = \tfrac{1}{24}\rho A\ell^3. \quad (12)$$

Matching $T^e_\mu = T^e$ gives $\mu = 0$. So according to this criterion the optimal mass matrix is the consistent one (CMM). Note that if $\mu = 1$, $T^e_\mu = 3T^e$, whence the DLMM overestimates the element rotational (rotary) inertia by a factor of three.

4.5 Bar2 Fourier Analysis

For longitudinal motions, a more useful customization criterion is to improve accuracy in the long wavelength, low-frequency limit; this is labeled low frequency continuum fit (LFCF) in Table 1. This is carried out by a well known tool: *Fourier analysis*. Physical interpretation: probe the

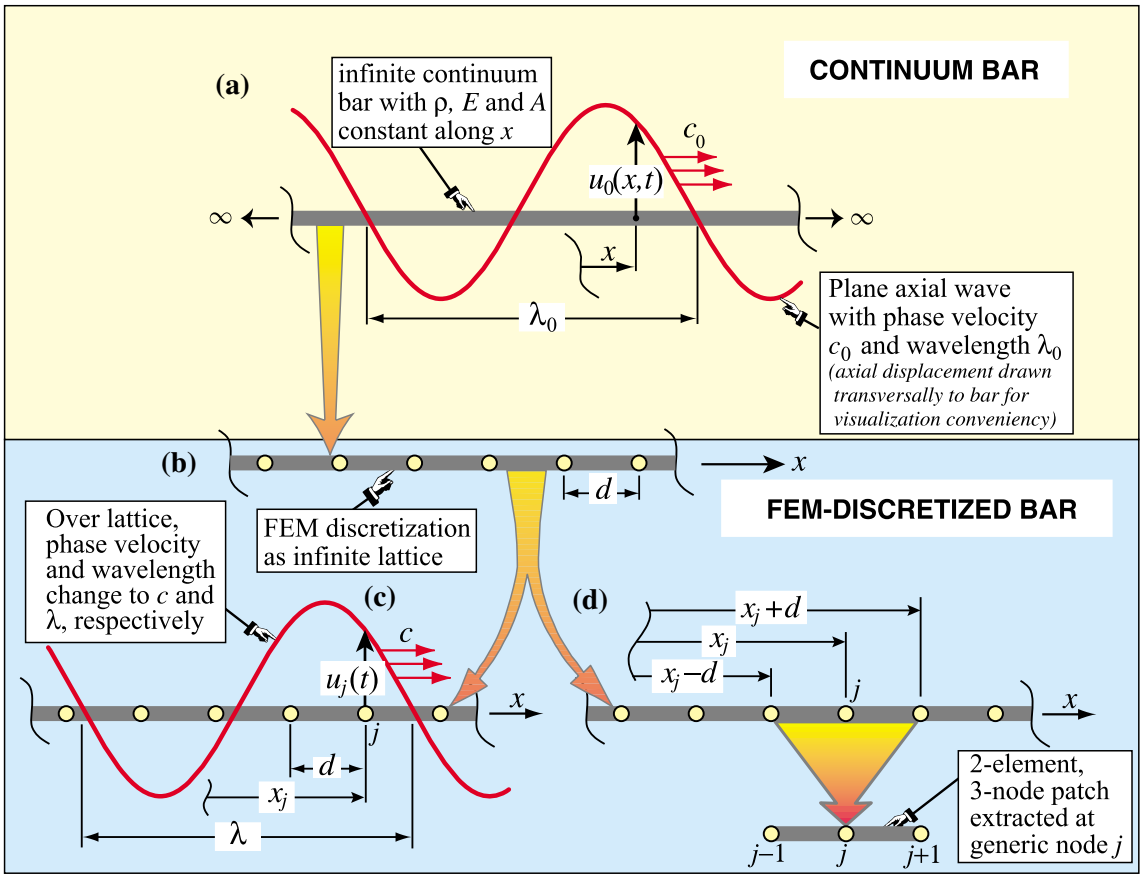

Fig. 2 Propagation of a harmonic plane wave over an infinite, prismatic, elastic bar: **a** propagation over a *continuum* bar, **b** FEM discretization as infinite regular lattice, **c** propagation of plane wave over Bar2-discretized lattice, **d** extraction of a typical two-element patch. For visualization convenience, the wave-profile axial displacement $u(x,t)$ is plotted *normal* to the bar

fidelity with which planes waves are propagated over a FEM-discretized regular lattice, when compared to the propagation over a *continuum* bar. The essentials are illustrated in Fig. 2. The top half depicts the continuum bar whereas the bottom half shows stages of the Fourier analysis of its FEM-discretized counterpart.

Symbols used for the analysis of plane wave propagation are collected in Table 6 for the reader's convenience (the same notation is reused in later Sections). Corresponding nomenclature for the FEM-discretized two-node bar lattice is collected in Table 7. The continuum-versus-lattice notational rule is: corresponding quantities use the same symbol but the zero subscript is suppressed in the lattice. For example, the continuum wavelength λ_0 becomes the lattice wavelength λ.

Plane wave propagation over a regular spring-mass lattice is governed by the semidiscrete linear EOM:

$$\mathbf{M}\ddot{\mathbf{u}}+\mathbf{K}\mathbf{u}=\mathbf{0}, \tag{13}$$

in which $\mathbf{M}$ and $\mathbf{K}$ are infinite, tridiagonal Toeplitz matrices. This EOM can be solved by Fourier methods. Figure 2b displays two characteristic lengths: λ and ℓ. The element length-to-wavelength ratio is called $\Upsilon = \ell/\lambda$. The floor function of its inverse: $N_{e\lambda} = \lfloor \lambda/\ell \rfloor$ is the number of elements per wavelength. Those ratios characterize the fineness of the discretization, as illustrated in Fig. 2b.

Within constraints noted later the lattice can propagate real, travelling, harmonic plane waves of wavelength λ and grpup velocity c, as depicted in Fig. 2b, c. The wavenumber is $k = 2\pi/\lambda$ and the circular frequency $\omega = 2\pi/T = 2\pi c/\lambda = k\,c$. The range of wavelengths that the lattice may transport is illustrated in Fig. 3.

To study plane wave solutions it is sufficient to extract a two-element patch, a process depicted in Fig. 2d. A harmonic plane wave of amplitude B is described by the function

$$\begin{aligned} u(x,t) &= B\,\exp\left[\jmath\,(kx-\omega t)\right] \\ &= B\,\exp\left[\jmath\left(\kappa x-\Omega\, c_0\, t\right)/\ell\right], \quad \jmath=\sqrt{-1}. \end{aligned} \tag{14}$$

Here the dimensionless wavenumber κ and dimensionless circular frequency Ω were introduced as $\kappa = k\,\ell = 2\pi\ell/\lambda = 2\pi\chi$ and $\Omega = \omega\,\ell/c_0$, respectively. Here $c_0 = \sqrt{E/\rho}$ is the elastic bar group velocity, which for the continuum is the

Table 6 Nomenclature for harmonic plane wave propagation over continuum bar

Quantity[a]	Meaning (physical dimension in brackets)
ρ, E, A	Mass density, elastic modulus, and cross section area of bar
$()'$, $\ddot{()}$	Abbreviations for derivatives with respect to space x and time t, respectively
$\rho\,\ddot{u}_0 = E\,u_0''$	Bar wave equation. Frequency domain forms: $-\omega_0^2 u = c_0^2\,u''$ and $u'' + k_0^2\,u = 0$
$u_0(x,t)$	Plane wave function $u_0 = B_0\,\exp\left(i(k_0 x - \omega_0 t)\right)$ [length], in which $i = \sqrt{-1}$
B_0	Wave amplitude [length]
λ_0	Wavelength [length]
k_0	Wavenumber $k_0 = 2\pi/\lambda_0$ [1/length]
κ_0	Dimensionless wavenumber $\kappa_0 = k_0\lambda_0$
ω_0	Circular (a.k.a. angular) frequency $\omega_0 = k_0 c_0 = 2\pi f_0 = 2\pi c_0/\lambda_0$ [radians/time]
f_0	Cyclic frequency $f_0 = \omega_0/(2\pi)$ [cycles/time: Hz if time in seconds]
T_0	Period $T_0 = 1/f_0 = 2\pi/\omega_0 = \lambda_0/c_0$ [time]
Ω_0	Dimensionless circular frequency $\Omega_0 = \omega_0 T_0 = \omega_0\lambda_0/c_0$
c_0	Group wave velocity $c_0 = \omega_0/k_0 = \lambda_0/T_0 = \sqrt{E/\rho}$ [length/time]. Often abbreviated to *wavespeed*. Physically, c_0 is the longitudinal speed of sound

[a] Unsubscripted counterpart symbols, such as k or c, pertain to a discrete FEM lattice; cf. Table 7

Table 7 Nomenclature for harmonic plane wave propagation over Bar2 lattice

Quantity[a]	Meaning (physical dimension in brackets)
$u(x,t)$	Plane wave function (14) [length]
$\mathbf{u}$	Node displacement vector, built by evaluating $u(x,t)$ at nodes [length]
$\mathbf{M\ddot{u}+Ku = 0}$	Lattice wave equation (13). $\mathbf{K}$ and $\mathbf{M}$ are infinite Toeplitz matrices
B	Wave amplitude [length]
ℓ	Bar element length [length]
λ	Wavelength $\lambda = 2\pi/k = 2\pi\ell/\kappa$ [length]
k	Wavenumber $k = 2\pi/\lambda = \kappa/\ell$ [1/length]
κ	Dimensionless wavenumber $\kappa = k\,\ell = 2\pi\,\ell/\lambda$
$N_{e\lambda}$	Elements per wavelength: $\lfloor\lambda/\ell\rfloor$: same as signal sampling rate
ω	Circular (a.k.a. angular) frequency $\omega = \Omega\,c_0/\ell$ [radians/time]
f	Cyclic frequency $f = \omega/(2\pi)$ [cycles/time: Hz if time in seconds]
T	Period $T = 1/f = 2\pi/\omega = \lambda/c$ [time]
Ω	Dimensionless circular frequency $\Omega = \omega\,\ell/c_0$
c	Group velocity over lattice: $c = \partial\omega/\partial k = c_0(\partial\Omega/\partial\kappa)$ [length/time]
γ_c	Wavespeed ratio $c/c_0 = \partial\Omega/\partial\kappa$ from discrete to continuum

[a] Quantities unchanged from continuum to lattice, such as E, are not repeated in this Table. Note that the definition of Ω uses the *continuum* wavespeed $c_0 = \sqrt{E/\rho}$; *not* the discrete wavespeed c

same as the phase velocity (in physical acoustics c_0 is the *sound speed* of the material). Using the well-known Bar2 static stiffness matrix and the mass template (9) gives the patch equations

$$\frac{\rho A\ell}{6}\begin{bmatrix} 2+\mu & 1-\mu & 0 \\ 1-\mu & 4+2\mu & 1-\mu \\ 0 & 1-\mu & 2+\mu \end{bmatrix}\begin{bmatrix} \ddot{u}_{j-1} \\ \ddot{u}_j \\ \ddot{u}_{j+1} \end{bmatrix} + \frac{EA}{\ell}\begin{bmatrix} 1 & -1 & 0 \\ -1 & 2 & -1 \\ 0 & -1 & 1 \end{bmatrix}\begin{bmatrix} u_{j-1} \\ u_j \\ u_{j+1} \end{bmatrix} = 0. \tag{15}$$

From this one takes the middle (node j) equation, which repeats in the infinite lattice:

$$\frac{\rho A\ell}{6}\begin{bmatrix} 1-\mu & 4+2\mu & 1-\mu \end{bmatrix}\begin{bmatrix} \ddot{u}_{j-1} \\ \ddot{u}_j \\ \ddot{u}_{j+1} \end{bmatrix} + \frac{EA}{\ell}\begin{bmatrix} -1 & 2 & -1 \end{bmatrix}\begin{bmatrix} u_{j-1} \\ u_j \\ u_{j+1} \end{bmatrix} = 0. \tag{16}$$

Evaluate the wave motion (14) at $x = x_{j-1} = x_j - \ell$, $x = x_j$ and $x = x_{j+1} = x_j + \ell$ while keeping t continuous. Substitution into (16) gives the wave propagation condition

$$\frac{\rho A\,c_0^2}{3\ell}\Big[6 - (2+\mu)\Omega^2 - \big(6 - (1-\mu)\Omega^2\big)\cos\kappa\Big] \times \left(\cos\frac{\Omega\,c_0\,t}{\ell} - i\,\sin\frac{\Omega\,c_0\,t}{\ell}\right) B = 0. \tag{17}$$

If this is to be zero for any t and B, the expression in brackets, called the *characteristic equation*, must vanish. Solving gives the dimensionless frequency versus wavenumber relation

$$\Omega^2 = \frac{6(1-\cos\kappa)}{2+\mu+(1-\mu)\cos\kappa} = \kappa^2 + \frac{1-2\mu}{12}\,\kappa^4 + C_6\,\kappa^6 + \cdots \tag{18}$$

in which $C_6 = (1 - 10\mu + 10\mu^2)/360$. Its inverse is

$$\kappa = \arccos\left[\frac{6-(2+\mu)\Omega^2}{6+(1-\mu)\Omega^2}\right] = \Omega - \frac{1-2\mu}{24}\Omega^3 + \frac{9-20\mu+20\mu^2}{1920}\Omega^5 + \cdots \tag{19}$$

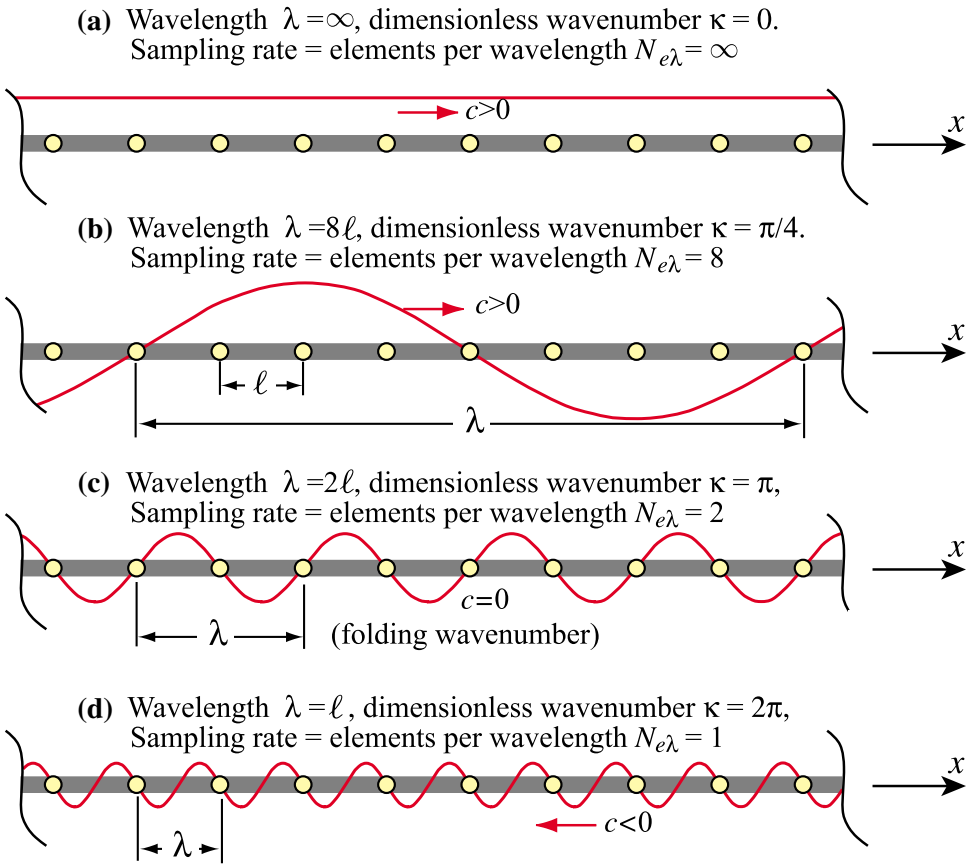

Fig. 3 Selected plane waves of various wavelengths, illustrating the physical meaning of the dimensionless wavenumber (DWN) $\kappa = k\ell = 2\pi\ell/\lambda$. **a, b, c, d** show cases $\kappa = 0, \pi/4, \pi$ and 2π, respectively. The number of elements per wavelength is $N_{e\lambda} = \lfloor\lambda/\ell\rfloor = \lfloor 2\pi/\kappa\rfloor$, in which $\lfloor . \rfloor$ denotes the floor function. (This is equivalent to the spatial *sampling rate* of filter technology). The case $\lambda = 2\ell$ pictured in **c** pertains to the folding or Nyquist frequency, at which $\kappa = \pi$, $N_{e\lambda} = 2$, and the group velocity c vanishes

Transforming (18) to physical wavenumber $k = \kappa/\ell$ and circular frequency $\omega = \Omega\, c_0/\ell$ gives

$$\omega^2 = \left(\frac{6c_0^2}{\ell^2}\right)\frac{1-\cos(k\ell)}{2+\mu+(1-\mu)\cos(k\ell)} = c_0^2 k^2\left(1+\frac{1-2\mu}{12}k^2\ell^2 + C_6\, k^4\ell^4 + \cdots\right) \tag{20}$$

4.6 Bar2 Dispersion Diagrams

An equation that links frequency and wavenumber: $\Omega = \Omega(\kappa)$ as in (18), or $\omega = \omega(k)$, as in (20), is a *dispersion relation*. A plot of the dispersion relation with k and ω along horizontal and vertical axes, respectively, is called a *dispersion diagram*. When this is done in terms of dimensionless wavenumber κ and dimensionless frequency Ω, the plot is called a dimensionless dispersion diagram (DDD). Such diagrams exhibit a 2π period: $\Omega(\kappa) = \Omega(\kappa + 2\pi n)$ for integer n. Thus it is enough to plot $\Omega(\pi)$ over either $[-\pi, \pi]$ or $[0, 2\pi]$, a range called a *Brillouin zone*. All DDD in this paper use the $[0, 2\pi]$ range choice.

Why is $\Omega = 0$ at $\kappa = 2\pi$? The wavelenth $\lambda = \ell$ pictured in Fig. 3d has the same value at all nodes for each time t. This nodal sampling cannot be distinguished from the case $\lambda = \infty$ (that is, $\kappa = 0$) shown in Fig. 3a. They must share the same frequency, which is zero. Associated plane waves propagate with the same speed but in opposite directions. Similar arguments can be adduced to justify the dispersion curve symmetry about wavenumber $\kappa = \pi$, as well as the 2π periodicity.

4.7 Best μ By Low Frequency Fitting

An oscillatory dynamical system is *nondispersive* if ω is linear in k, in which case $c = \omega/k$ is constant and the wavespeed (the group velocity) is the same for all frequencies. The physical dispersion relation for the continuum bar is $c_0 = \omega_0/k_0 = \sqrt{E/\rho}$. Hence all waves propagate with the same speed in this model. Group and phase velocities coalesce.

The FEM-discretized lattice group velocity is $c = \partial\omega/\partial k = c_0(\partial\Omega/\partial\kappa)$, which differs from c_0 except at $\omega = \kappa = 0$. The Bar2 discrete model is *dispersive* for any fixed μ, since from (20) we get

$$\gamma_c = \frac{c}{c_0} = \frac{\partial\Omega}{\partial\kappa} = \frac{1}{\kappa}\sqrt{\frac{6(1-\cos\kappa)}{2+\mu+(1-\mu)\cos\kappa}} = 1 + \frac{1-2\mu}{24}\kappa^2 + \frac{1-20\mu+20\mu^2}{1920}\kappa^4 + \cdots \tag{21}$$

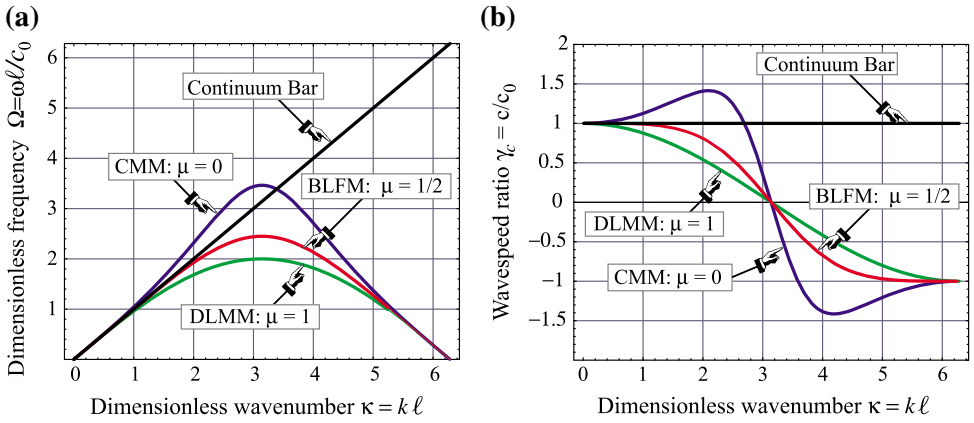

Fig. 4 Results from Fourier analysis of Bar2 infinite regular lattice for three choices of μ, plus continuum: **a** DDD, **b** dimensionless group velocity diagram (DGVD)

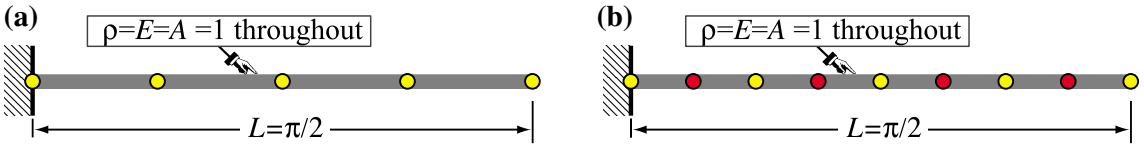

Fig. 5 Fixed-free homogeneous prismatic elastic bar member used in vibration test for Bar2 and Bar3 template instances. Both pictured discretizations display 4 elements. **a** Member modeled with Bar2 elements; results reported in Table 8 and Fig. 6, **b** member modeled with Bar3 elements; results reported in Fig. 12

Plainly the best fit to the continuum for *small wavenumbers* $\kappa = k\ell << 1$ is obtained by taking $\mu = 1/2$, which makes the second term of the series (18) or (21) vanish. So for LFCF customization the best mass matrix is the average of the lumped and consistent ones:

$$\mathbf{M}^e_{BLFM} = \mathbf{M}^e_{\mu}\big|_{\mu=\frac{1}{2}} = \tfrac{1}{2}\mathbf{M}^e_C + \tfrac{1}{2}\mathbf{M}^e_L = \frac{\rho A\ell}{12}\begin{bmatrix} 5 & 1 \\ 1 & 5 \end{bmatrix}. \tag{22}$$

This instance is labeled BLFM, for best low-frequency match. Figure 4a plots the dimensionless dispersion relation (18) for the CMM ($\mu = 0$), DLMM ($\mu = 1$) and BLFM ($\mu = \frac{1}{2}$) mass matrices, along with the continuum-bar relation $\Omega_0 = \kappa_0$. The superior small-κ fit provided by the BLFM is evident.

4.8 Folding Frequency

The maximum lattice frequency occurs at the *folding wavenumber* $\kappa = k\ell = \pi$ or $\lambda = 2\ell$, which is waveform (c) in Fig. 3. The sampling rate $N_{e\lambda}$ is then 2 elements per wavelength. This is called the *folding* or *Nyquist frequency*, and is denoted as

$$\Omega^2_{af} = \frac{12}{1 + 2\,\mu}. \tag{23}$$

(The "a" in the subscript stands for AB; this notation is explained in Sect. 5.1). This varies from $\Omega_{af} = \sqrt{12} = 2\sqrt{3}$ for the CMM through $\Omega_{af} = 2$ for the DLMM. Frequencies higher than Ω_{af} cannot be propagated over the lattice. As shown in Fig. 4b, the lattice wavespeed vanishes at the folding wavenumber $\kappa = \pi$, and is negative over the range $(\pi, 2\pi]$. Waveforms in that rage move with negative speed: $c < 0$. As discussed in Sect. 4.6, the waveform with $\ell = \lambda$, or $\kappa = 2\pi$, cannot be distinguished from a rigid motion such as that pictured in Fig. 3a, and the lattice frequency falls to zero.

4.9 Bar2 Test: Vibrations of a Fixed-Free Bar Member

Natural frequency predictions of three Bar2 template instances are compared for predicting natural frequencies of longitudinal vibrations of the fixed-free elastic bar member pictured in Fig. 5. The member is prismatic, with constant $E = 1$, $A = 1$, and $\rho = 1$. The total member length is taken as $L = \pi/2$ for convenience. With those numerical properties the continuum eigenfrequencies are

$$\omega_{0i} = \frac{(2i-1)\pi}{2L}\sqrt{\frac{E}{\rho}} = 2i - 1, \quad i = 1, 2, 3, \ldots \tag{24}$$

The member is divided into N_e identical elements, with $N_e = 1, 2, \ldots 16$. Figure 5a pictures the case $N_e = 4$. Three template instances are compared: CMM ($\mu = 0$), DLMM ($\mu = 1$) and BLFM ($\mu = 1/2$). Numerical results obtained for the first three frequencies are collected in Table 10. The $O(\kappa^4)$ convergence of BLFM is obvious. For exam-

Table 8 Bar2 instance results for vibrations of a fixed-free bar member

Instance	N_e	ω_1	ω_2	ω_3
CMM	1	1.102658	*	*
	2	1.025859	3.583726	*
	4	1.006437	3.174947	5.767394
	8	1.001607	3.043539	5.202396
	16	1.000402	3.010855	5.050339
DLMM	1	0.900316	*	*
	2	0.974495	2.352640	*
	4	0.993587	2.829496	4.234640
	8	0.998394	2.956815	4.801608
	16	0.999598	2.989169	4.949951
BLFM	1	0.986247	*	*
	2	0.999188	2.781352	*
	4	0.999950	2.987344	4.827222
	8	0.999997	2.999237	4.989971
	16	1.000000	2.999953	4.999389

* Frequency not provided by discrete FEM model

ple, 4 elements give ω_2 correct to 4 digits while both CMM and DLMM, which converge as $O(\kappa^2)$, give only 2. As expected, CMM overestimates the continuum frequencies while DLMM underestimates them.

The results of Table 8 are graphically reformatted in Fig. 6, as accuracy versus elements log-log plots. The horizontal axis shows number of elements N_e in $\log_2$ scale. The vertical axis displays correct digits of computed frequency, obtained as

$$d = -\log_{10}|\Delta\omega_i|, \quad \text{in which} \quad \Delta\omega_i = \omega_i - \omega_{0i}. \tag{25}$$

Here $\Delta\omega_i$ is the frequency error of computed values with respect to continuum frequencies $\omega_{0i} = 2\,i - 1$, given by (24). The plots clearly show at a glance that, for the same N_e, BLFM roughly doubles the number of correct digits provided by the other two instances. It also illustrates that CMM and DLMM give the same error magnitude (within plot accuracy) although of different signs. Thus log-log plots such as those in Fig. 6 are unable to show whether the convergence is from above or below, because of the taking of absolute values in (25). That visualization deficiency should be kept in mind should error signs become important.

4.10 Other Customization Options

The last three customization options listed in Table 1 are not relevant to this element. RHFP is unnecessary because the dispersion diagram does not have an OB. MSTS is pointless because the DLMM in (7) is unique. Finally, RDAW does not apply to 1D elements.

4.11 Bar2 Frequency Dependent Mass

As noted in Sect. 3.9, it is occasionally useful to make the mass and/or stiffness matrix frequency dependent. The goal is to exactly match the continuum dispersion relation $\Omega = \kappa$ for all frequencies, or at least a finite range that includes $\Omega = \kappa = 0$. Such an exact fit allows for coarser discretizations. The cost paid is that matrix entries become trigonometric functions of frequency. Both the EOM and associated eigenproblems become trascendental.

Unless the frequency is specified beforehand (for example, in pure harmonic excitation) an iterative process is unavoidable. Therefore "exactness" gains might be illusory: the dog chases its own tail. Early publications that follow this approach are cited in Sect. 1. For reasons indicated there, those formulations are *not* necessarily instances of the general template derived in Sect. 4.12.

The simplest way to introduce frequency dependency is to allow the mass template parameter μ in (9) to be frequency

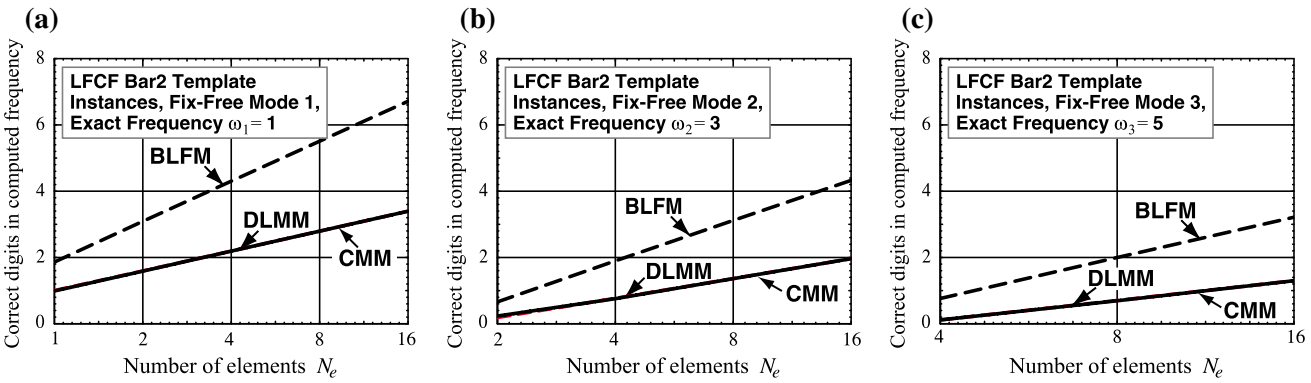

Fig. 6 Performance of selected Bar2 template instances in predicting the first three natural frequencies ω_i, $i = 1, 2, 3$ of the fixed-free prismatic homogeneous bar shown in Fig. 5a. **a, b, c** compare against frequencies $\omega 1 = 1$, $\omega 2 = 3$ and $\omega 3 = 5$, respectively. This is a graphical, log-log representation of the results of Table 8. *Horizontal axis* shows number of elements while *vertical axis* displays correct digits of computed frequency. See text for details of what is shown along each axis

dependent, while the stiffness matrix is held fixed. To find the expression of μ, set $\kappa \to \Omega$ in the characteristic equation extracted from (17):

$$6 - (2 + \mu^\omega)\Omega^2 - \left(6 - (1 - \mu^\omega)\Omega^2\right)\cos\Omega = 0, \tag{26}$$

in which μ has been renamed μ^ω. Solving for it gives

$$\mu^\omega = 1 + \frac{6}{\Omega^2} - \frac{3}{1-\cos\Omega} = \frac{1}{2} - \frac{\Omega^2}{40} - \frac{\Omega^4}{1008} - \frac{\Omega^6}{28800} - \cdots \tag{27}$$

Since $\kappa = \Omega$ for the continuum,

$$\mu^\omega = 1 + \frac{6}{\kappa^2} - \frac{3}{1-\cos\kappa} = \frac{1}{2} - \frac{\kappa^2}{40} - \frac{\kappa^4}{1008} - \frac{\kappa^6}{28800} - \cdots \tag{28}$$

As $\Omega \to 0$ or $\kappa \to 0$ both (27) and (28) approach 0/0. The indeterminacy is removed by the Taylor expansions given above, which show that the limit is $\mu^\omega \to \frac{1}{2}$, as may be expected. As Ω or κ grows, μ^ω decreases so the template gradually favors the CMM more. Two interesting values should be noted. If $\kappa = 3.38742306673364$, $\mu^\omega = 0$, which makes the CMM frequency exact; this occurs at the intersection of the continuum and CMM dispersion curves in Fig. 4a. If $\kappa = \kappa_{lim} = 4.05751567622863$, $\mu^\omega = -1/2$, which makes $\mathbf{M}^e$ singular. If $\kappa > \kappa_{lim}$, $\mathbf{M}^e$ becomes indefinite. It follows that the match (27) or (28) is practically limited to the DWN range $0 \le \kappa < 4$.

4.12 Bar2 Frequency Dependent Mass-Stiffness Pair

The most general FDMS template for Bar2 has 8 free parameters. These are chosen as deviations from the optimal frequency-independent matrices:

$$\begin{aligned}\mathbf{M}^e &= C_M\left(\begin{bmatrix}5 & 1\\ 1 & 5\end{bmatrix} + \begin{bmatrix}\mu^\omega_{11} & -\mu^\omega_{12}\\ -\mu^\omega_{21} & \mu^\omega_{22}\end{bmatrix}\right),\quad \mathbf{K}^e\\ &= C_K\left(\begin{bmatrix}1 & -1\\ -1 & 1\end{bmatrix} + \begin{bmatrix}\beta^\omega_{11} & -\beta^\omega_{12}\\ -\beta^\omega_{21} & \beta^\omega_{22}\end{bmatrix}\right),\end{aligned} \tag{29}$$

in which $C_M = \rho\, A\ell/12$ and $C_K = E\, A/\ell$. All parameters may be frequency dependent. For brevity that dependency will not be explicitly shown unless necessary. If all μ^ω_{ij} vanish, $\mathbf{M}^e$ reduces to (22), which is BLFM optimal. If all β^ω_{ij} vanish, $\mathbf{K}^e$ reduces to the well known stiffness of a 2-node prismatic bar. Thus in the zero-frequency (static) limit all parameters must vanish, which provides useful checks. To cut down on parameters, we impose diagonal and antidiagonal symmetry conditions *a priori*: $\mu^\omega_{21} = \mu^\omega_{12}$, $\mu^\omega_{22} = \mu^\omega_{11}$, $\beta^\omega_{21} = \beta^\omega_{12}$, and $\beta^\omega_{22} = \beta^\omega_{11}$. In addition setting $\beta^\omega_{12} = \beta^\omega_{21} = \beta^\omega_{11}$ avoids singularities in the static limit, as noted later. Thus (29) reduces to

$$\begin{aligned}\mathbf{M}^e &= C_M\left(\begin{bmatrix}5 & 1\\ 1 & 5\end{bmatrix} + \begin{bmatrix}\mu^\omega_{11} & -\mu^\omega_{12}\\ -\mu^\omega_{12} & \mu_{11}\end{bmatrix}\right),\quad \mathbf{K}^e\\ &= C_K\left(\begin{bmatrix}1 & -1\\ -1 & 1\end{bmatrix} + \begin{bmatrix}\beta^\omega_{11} & -\beta^\omega_{11}\\ -\beta^\omega_{11} & \beta^\omega_{11}\end{bmatrix}\right).\end{aligned} \tag{30}$$

which has 3 free parameters: μ^ω_{11}, μ^ω_{12} and β^ω_{11}. These matrices are nonnegative if

$$4 + \mu^\omega_{11} + \mu^\omega_{12} \ge 0,\quad 6 + \mu^\omega_{11} - \mu^\omega_{12} \ge 0,\quad 1 + \beta^\omega_{11} \ge 0. \tag{31}$$

Imposing the plane wave motion (14) on a two-element patch, extracting the middle node equation and dropping extraneous factors yields the complex characteristic equation

$$\begin{aligned}\Big[12(1+\beta_{11}) - (5+\mu^\omega_{11})\,\Omega^2 - \big(12 + 12\beta_{11}\\ + (1-\mu^\omega_{12})\,\Omega^2\big)\cos\kappa\Big]\,\exp(j\kappa) = 0.\end{aligned} \tag{32}$$

Since the complex exponential never vanishes, it may be dropped and (32) reduces to the real equation

$$\begin{aligned}12\,(1+\beta^\omega_{11}) - (5+\mu^\omega_{11})\,\Omega^2\\ - \big(12 + 12\beta^\omega_{11} + (1-\mu^\omega_{12})\,\Omega^2\big)\cos\kappa = 0.\end{aligned} \tag{33}$$

To match the continuum, Ω is replaced by κ, whence

$$\begin{aligned}f_{cm} = 12\,(1+\beta^\omega_{11}) - (5+\mu^\omega_{11})\,\kappa^2 - (12 + 12\beta^\omega_{11}\\ +(1-\mu^\omega_{12})\,\kappa^2)\cos\kappa = 0.\end{aligned} \tag{34}$$

This establishes a linear constraint among the 3 parameters. Consider these as functions of κ: $\beta^\omega_{11} = \beta^\omega_{11}(\kappa)$, $\mu^\omega_{11} = \mu^\omega_{11}(\kappa)$, and $\mu^\omega_{12} = \mu^\omega_{12}(\kappa)$. Expanding in Taylor series about $\kappa = 0$ yields

$$\begin{aligned}f_{cm} = \left(6\,\beta^\omega_{11}\big|_0 - \mu^\omega_{11}\big|_0 + \mu^\omega_{12}\big|_0\right)\kappa^2\\ + \left(6\,\frac{\partial\beta^\omega_{11}}{\partial\kappa}\bigg|_0 - \frac{\partial\mu^\omega_{11}}{\partial\kappa}\bigg|_0 + \frac{\partial\mu^\omega_{12}}{\partial\kappa}\bigg|_0\right)\kappa^3 + \cdots = 0,\end{aligned} \tag{35}$$

This shows that in the static limit $\Omega = \kappa = 0$ the continuum equation is identically satisfied. If $\beta_{12}|_0 \ne \beta^\omega_{11}|_0$, however, a term in κ^{-2} appears in (35); this is the reason for presetting $\beta^\omega_{12} = \beta^\omega_{11}$.

Further developments depend on which parameter pair is kept. Table 9 lists three possibilities: $(\beta^\omega_{11}, \mu^\omega_{11})$, $(\beta^\omega_{11}, \mu^\omega_{12})$, and $(\mu^\omega_{11}, \mu^\omega_{12})$.

4.13 Bar2 Frequency Dependent Mass Instances

Some relatively simple FDM instances can be obtained by setting $\beta^\omega_{11} = 0$ in (30). Taking $\mu^\omega_{12} = \mu^\omega_{11}$ and solving for the latter gives

Table 9 General FDMS template for Bar2

Free parameters[a]	Linkage equation (top line); Taylor series[b] at $\omega = \kappa = 0$ (bottom line)
$\mu_{11}^\omega, \mu_{12}^\omega$	$\beta_{11}^\omega = (\kappa^2(5+\mu_{11}^\omega) + (12+\kappa^2(1-\mu_{12}^\omega))\cos\kappa - 12)/(12(1-\cos\kappa))$
	$\beta_{11}^\omega\big\vert_{\kappa\to 0} = [\mu_{11}^\omega\big\vert_0 - \mu_{12}^\omega\big\vert_0]\kappa^2 + O(\kappa^3)$
$\beta_{11}^\omega, \mu_{12}^\omega$	$\mu_{11}^\omega = (12+12\beta_{11}^\omega - 5\kappa^2 - (12+12\beta_{11}^\omega + \kappa^2(1-\mu_{12}^\omega))\cos\kappa)/\kappa^2$
	$\mu_{11}^\omega\big\vert_{\kappa\to 0} = [\mu_{11}^\omega\big\vert_0 - \mu_{12}^\omega\big\vert_0]\kappa^2 + O(\kappa^3)$
$\beta_{11}^\omega, \mu_{11}^\omega$	$\mu_{12}^\omega = (12+12\beta_{11}^\omega + \kappa^2 - (12+12\beta_{11}^\omega - \kappa^2(5+\mu_{11}^\omega))\sec\kappa)/\kappa^2$
	$\mu_{12}^\omega\big\vert_{\kappa\to 0} = [\mu_{11}^\omega\big\vert_0 - \mu_{12}^\omega\big\vert_0]\kappa^2 + O(\kappa^3)$

Parameter arguments are usually omitted to reduce clutter unless necessary

[a] Template parameters are generally functions of κ or Ω; e.g., $\mu_{11}^\omega = \mu_{11}^\omega(\kappa) = \mu_{11}^\omega(\Omega)$, etc.

[b] In the bottom-line series, $\beta_{11}^\omega\big\vert_0$, $\mu_{11}^\omega\big\vert_0$ and $\mu_{12}^\omega\big\vert_0$ denote parameter values at $\kappa = \Omega = 0$

$$\mu_{11}^\omega = \mu_{12}^\omega = 1 + \frac{12}{\kappa^2} - \frac{6}{1-\cos\kappa} = -\frac{\kappa^2}{20} - \frac{\kappa^4}{540} - \frac{\kappa^6}{14400} - \cdots \tag{36}$$

The resulting $\mathbf{M}^e$ is indefinite if $\kappa > 4.05752$. This is the equivalent of the FDM instance considered in Sect. 4.11. The difference between (36) and (28) lies in the choice of baseline matrix for null free parameters. On the other hand, setting $\mu_{12}^\omega = 0$ along with $\beta_{11}^\omega = 0$ yields

$$\mu_{11}^\omega = \frac{-12 + 5\kappa^2 + (12+\kappa^2)\cos\kappa}{\kappa^2} = -\frac{\kappa^4}{40} - \frac{11\kappa^6}{14400} - \cdots, \tag{37}$$

This correction is smaller than (36) if $\kappa < \pi/2$. The resulting $\mathbf{M}^e$ is indefinite if $\kappa > 4.46192$.

5 The Three-Node Bar Element

The three-node bar element configuration is shown in Fig. 7a. The element is prismatic with length $\ell = L^e$, uniform cross section area A and mass density ρ. Midnode 3 is at the center. The element DOFs are arranged as $\mathbf{u}^e = \begin{bmatrix} u_1 & u_2 & u_3 \end{bmatrix}^T$. The element name is often abbreviated to `Bar3` in the sequel. We will consider only *frequency independent* templates here.

Despite its simplicity, the Bar3 template is sufficiently feature-rich so it can be used to illustrate most of the customization scenarios listed in Table 1. Two reasons: it has multiple dispersion branches, and the stiffness has a free parameter. But additional terminology on dispersion diagrams has to be introduced first. Readers familiar with that topic should skip to Sect. 5.2.

5.1 Dispersion Diagram Terminology

The characteristic equation of the Bar3 element, derived in Sect. 5.5 below, gives *two* positive real frequencies for each plane wave wavelength. The dimensionless forms are identified by Ω_a and Ω_o, ordered so $\Omega_a \le \Omega_o$. The functions $\Omega_a(\kappa)$ and $\Omega_o(\kappa)$, in which κ is the dimensionless wavenumber, are called *acoustic* and *optical* branches, respectively, of the DDD. This terminology originated in crystal physics, in which both branches have physical meaning in modeling molecular level oscillations (in crystallography, acoustic waves are lower frequency waves caused by sonic-like disturbances, in which adjacent molecules move in the same direction. Optical waves are higher frequency oscillations caused by interaction with light or electromagnetics, in which adjacent molecules move in opposite directions. Textbook references are provided in Sect. 1).

In FEM discretization work, only the AB has physical meaning because for small κ (that is, long wavelengths) it approaches the continuum bar relation $\Omega = \kappa$, as plainly illustrated by the Ω_a^2 series in Sect. 4.5. On the other hand, the OB is spurious. It is caused by the discretization and pertains to higher frequency lattice oscillations, also known as "mesh modes.'

Figure 8 displays nomenclature used for a two-branch dispersion diagram, such as that exhibited by the Bar3 element. As noted, the AB is the long-wavelength counterpart of the continuum model, for which $\Omega = \kappa$; thus $\Omega_a\vert_{\kappa\to 0} = 0$. On the other hand, the OB has a nonzero

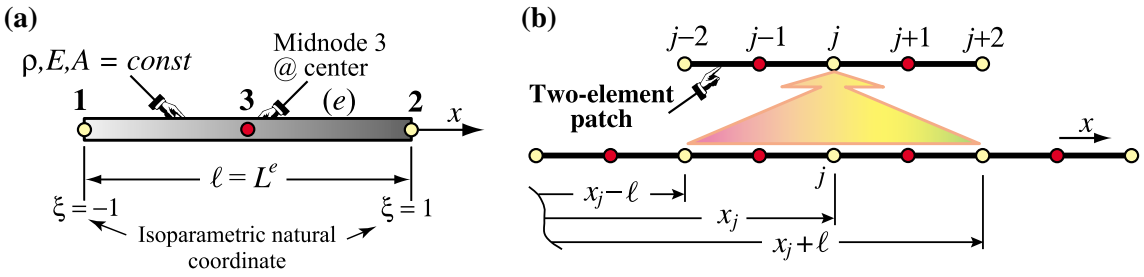

Fig. 7 Three-node prismatic bar element: **a** configuration, **b** extraction of two-element patch from a regular lattice

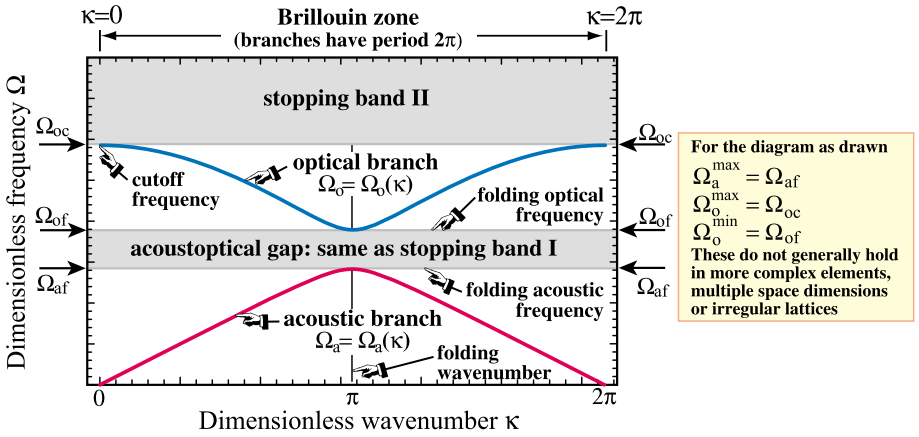

Fig. 8 Nomenclature for a two-branch dispersion diagram typical of 1D structural elements such as Bar3. The stopping band is the union of I and II (symmetry and monotonicity about the folding wavenumber $\kappa_f = \pi$ is typical of prismatic, simple 1D elements in regular lattices; else those features are typically lost. In addition, multiple optical branches will appear for characteristic equations with more than two roots for each κ)

frequency $\Omega_{oc} = \Omega_o|_{\kappa\to 0}$ called the *cutoff frequency* (COF) that cannot vanish, although it may go to infinity under certain conditions; such as a singular mass matrix. Also of interest are the values of Ω_a and Ω_o at the folding frequency $\kappa_f = \pi$; these are denoted by Ω_{af} and Ω_{of}, respectively. The lowest and highest values of Ω_o are called Ω_o^{max} and Ω_o^{min}, respectively, whereas the largest Ω_a is called Ω_a^{max}. For the plots drawn in Fig. 8 (note disclaimer on the right):

$$\Omega_a^{max} = \Omega_{af}, \quad \Omega_o^{min} = \Omega_{of}, \quad \Omega_o^{max} = \Omega_{oc}. \tag{38}$$

Often, but not always, Ω_o^{min} and Ω_a^{max} occur at $\kappa = \pi$, the folding (Nyquist) wavenumber at which group velocities vanish. In any case, if $\Omega_o^{min} > \Omega_a^{max}$, the frequency range $\Omega_o^{min} > \Omega > \Omega_a^{max}$ is called the *acoustoptical frequency gap*. Frequencies within the gap are said to pertain to portion I of the *stopping band* or *stop-band*, a term derived from filter technology. Frequencies $\Omega > \Omega_o^{max}$ pertain to portion II of the stopping band.

A frequency that falls within a stopping band cannot propagate as plane wave over the FEM lattice, since there the characteristic equation has complex roots with negative real parts. This causes exponential attenuation so any periodic disturbance with that frequency will die out.

5.2 Bar3 General Mass-Stiffness Template

We begin by introducing a general template for the MS pair. The mass template is given four parameters:

$$\mathbf{M}^e_\mu = \frac{m^e}{30}\begin{bmatrix} 4+\mu_1 & -1+\mu_3 & 2+\mu_4 \\ -1+\mu_3 & 4+\mu_1 & 2+\mu_4 \\ 2+\mu_4 & 2+\mu_4 & 16+\mu_2 \end{bmatrix} = \mathbf{M}^e_{CMM} + \frac{m^e}{30}\begin{bmatrix} \mu_1 & \mu_3 & \mu_4 \\ \mu_3 & \mu_1 & \mu_4 \\ \mu_4 & \mu_4 & \mu_2 \end{bmatrix}. \tag{39}$$

in which $m^e = \rho\, A\, \ell$. Here $\mathbf{M}^e_{CMM}$ is the CMM, obtained for $\mu_1 = \mu_2 = \mu_3 = \mu_4 = 0$, which is derived in Sect. 1. The template (39) incorporates matrix, geometric and fabrication symmetries *ab initio*. It includes all DLMM by setting $\mu_3 = 1$ and $\mu_4 = -2$. Because of its practical importance, however, that "lumped mass subset" is studied in Sect. 5.8 using a two-parameter template variant.

For (39) to be nonnegative definite (NND), three inequality constraints have to be satisfied. Those are more elegantly expressed in terms of the alternative "χ-form" derived in Sect. 5.3.

Conservation of total element mass $\rho\, A\, \ell$ (invariance of linear momentum) imposes the following homogeneous constraint:

$$2\mu_1 + \mu_2 + 2\mu_3 + 4\mu_4 = 0. \tag{40}$$

This constraint is not always preimposed as it may complicate intermediate expressions, but it is eventually applied at some point. Conservation of angular momentum in 2D or 3D requires $\mu_1 = \mu_3$, as verified by the CMM. This is ignored, however, as it hinders customization.

As regards the stiffness matrix, the following one-parameter template is used:

$$\mathbf{K}^e = \mathbf{K}^e_b + \mathbf{K}^e_h = k^e\begin{bmatrix} 1 & -1 & 0 \\ -1 & 1 & 0 \\ 0 & 0 & 0 \end{bmatrix} + \frac{4\,k^e\beta}{3}\begin{bmatrix} 1 & 1 & -2 \\ 1 & 1 & -2 \\ -2 & -2 & 4 \end{bmatrix}, \tag{41}$$

in which $k^e = EA/\ell$. Here $\mathbf{K}^e_b$ and $\mathbf{K}^e_h$ denote the basic and higher-order stiffness matrices, respectively. This decomposition was introduced by Bergan and coworkers in the 1980s for the development of the Free Formulation; references are provided in Appendix Sect. 1.7. The higher order stiffness is scaled by the free parameter $\beta \geq 0$. Setting $\beta = 1$ produces the well known stiffness of the quadratic (isoparametric) dis-

placement model, whereas $\beta = 0$ reduces $\mathbf{K}^e$ to the Bar2 stiffness considered in Sect. 4.2.

5.3 Bar3 Alternative Mass Template

An alternative configuration of the general Bar3 mass template is obtained by changing the four μ_i free parameters to three: χ_1, χ_2, and χ_3, through the replacement rule

$$\begin{aligned}\mu_1 &= \chi_1 + \chi_2 - 4, \quad \mu_2 = 14 + 4\chi_1 - 4\chi_{13},\\ \mu_3 &= \chi_1 - \chi_2 + 1, \quad \mu_4 = \chi_{13} - 2\chi_1 - 2.\end{aligned} \tag{42}$$

in which $\chi_{13} = \sqrt{30}\sqrt{\chi_1 - \chi_3}$. The mass conservation condition (40) is identically satisfied by (42), which is why the number of free parameters can be cut by one. Conversely, if the μ_i are given and do satisfy (40), the χ_i can be computed from

$$\begin{aligned}\chi_1 &= \tfrac{1}{2}\,(3 + \mu_1 + \mu_3), \quad \chi_2 = \tfrac{1}{2}(5 + \mu_1 - \mu_3),\\ \chi_3 &= \frac{1}{480}\left[4\mu_1(40 + \mu_2 - 2\mu_3) + 40\,(8 + \mu_2 + 4\mu_3)\right.\\ &\quad \left. -4\mu_1^2 - (\mu_2 - 2\mu_3)^2\right].\end{aligned} \tag{43}$$

If $\mu_1 = \mu_2 = \mu_3 = 0$, this gives $\chi_1 = 3/2$, $\chi_2 = 5/2$ and $\chi_3 = 2/3$ for the CMM. On inserting (42) into (39) the so-called "χ-form" of the Bar3 mass template emerges:

$$\mathbf{M}^e_\chi = \frac{m^e}{30} \times \begin{bmatrix} \chi_1 + \chi_2 & \chi_1 - \chi_2 & -2\chi_1 + \chi_{13} \\ \chi_1 - \chi_2 & \chi_1 + \chi_2 & -2\chi_1 + \chi_{13} \\ -2\chi_1 + \chi_{13} & -2\chi_1 + \chi_{13} & 30 + 4\chi_1 - 4\chi_{13} \end{bmatrix} \tag{44}$$

An attractive feature of (44) is that mass matrix admissibility can be readily correlated to parameter values. Specifically, $\mathbf{M}^e_\chi$ is positive definite (PD) if and only if χ_1, χ_2 and χ_3 are positive. This can be proven from the following properties:

$$\begin{aligned}\lambda_1(\mathbf{M}^e_\chi) = \frac{m^e\,\chi_2}{15}, \quad \det(\mathbf{M}^e_\chi) = \frac{m^e\,\chi_2\,\chi_3}{225}, \quad \det(\mathbf{M}^e_{\chi\,2\times 2})\\ = \frac{m^e\,\chi_1\,\chi_2}{225},\end{aligned} \tag{45}$$

The first equality gives one eigenvalue of $\mathbf{M}^e_\chi$ (the other two have more complicated expressions), whence PD mandates $\chi_2 > 0$. The last equalities give the determinants of $\mathbf{M}^e_\chi$ and of its 2×2 upper principal minor, respectively. Accordingly, PD requires also $\chi_3 > 0$ and $\chi_1 > 0$. For $\mathbf{M}^e_\chi$ to be NND, simply change $>$ to $\geq$. Those conditions can be harked back to the μ_i of $\mathbf{M}^e_\mu$ using (43), but the expressions are noticeably messier. The second equality of (45) gives another nice feature: $\mathbf{M}^e_\chi$ becomes singular if and only if $\chi_2 = 0$, or $\chi_3 = 0$, or both.

The main advantage of $\mathbf{M}^e_\mu$ over $\mathbf{M}^e_\chi$ is the *linear dependence* of entries on the μ_i. This simplifies patch analysis as well as reparametrization for several template variants studied later.

5.4 Bar3 Patch Equations

To assess wave propagation and dispersion performance of the MS template defined by (39) and (41), we carry out the Fourier analysis of the infinite bar lattice shown in Fig. 7b. Extract a typical two node patch as illustrated. The patch has five nodes: three endpoints and two midpoints, which are assigned global numbers $j-2$, $j-1$, $\ldots$ $j+2$. The unforced semidiscrete dynamical equations of the patch are $\mathbf{M}_p\,\ddot{\mathbf{u}}_P + \mathbf{K}_p\,\mathbf{u}_P = \mathbf{0}$, in which

$$\mathbf{M}_p = \frac{m^e}{30} \times \begin{bmatrix} 4+\mu_1 & 2+\mu_4 & -1+\mu_3 & 0 & 0 \\ 2+\mu_4 & 16+\mu_2 & 2+\mu_4 & 0 & 0 \\ -1+\mu_3 & 2+\mu_4 & 2(4+\mu_1) & 2+\mu_4 & -1+\mu_3 \\ 0 & 0 & 2+\mu_4 & 16+\mu_2 & 2+\mu_4 \\ 0 & 0 & -1+\mu_3 & 2+\mu_4 & 4+\mu_1 \end{bmatrix},$$

$$\mathbf{K}_p = \frac{k^e}{3} \times \begin{bmatrix} 3+4\,\beta & -8\,\beta & -3+4\,\beta & 0 & 0 \\ -8\,\beta & 16\,\beta & -8\,\beta & 0 & 0 \\ -3+4\,\beta & -8\,\beta & 6+8\,\beta & -8\,\beta & -3+4\,\beta \\ 0 & 0 & -8\,\beta & 16\,\beta & -8\,\beta \\ 0 & 0 & -3+4\,\beta & -8\,\beta & 3+4\,\beta \end{bmatrix},$$

$$\mathbf{u}_P = \begin{bmatrix} u_{j-2} & u_{j-1} & u_j & u_{j+1} & u_{j+2} \end{bmatrix}^T. \tag{46}$$

Note that the element mass conservation constraint (40) is not preimposed as it would complicate intermediate expressions. It is enforced later. Keep the second and third equations, namely those for nodes $j-1$ and j. This selection picks the equations for a typical corner and midpoint node. Accordingly, the patch equations are

$$\widehat{\mathbf{M}}_p\ddot{\mathbf{u}}_P + \widehat{\mathbf{K}}_p\mathbf{u}_P = \mathbf{0}. \tag{47}$$

The 2×5 matrices $\widehat{\mathbf{M}}_p$ and $\widehat{\mathbf{K}}_p$ result on deleting rows 1,4,5 of $\mathbf{M}_p$ and $\mathbf{K}_p$, respectively.

5.5 Bar3 Fourier Analysis

We study the propagation of harmonic plane waves of wavelength λ, wavenumber $k = 2\pi/\lambda$, and circular frequency ω over the lattice of Fig. 7b. For convenience they are separated into corner and midpoint waves:

$$\begin{aligned}u_c(x,t) &= B_c\,\exp\left(j(kx - \omega t)\right),\\ u_m(x,t) &= B_m\,\exp\left(j(kx - \omega t)\right), \quad j = \sqrt{-1}.\end{aligned} \tag{48}$$

Wave $u_c(x,t)$ propagates only over corner nodes and vanishes at midpoints, whereas $u_m(x,t)$ propagates only over midpoints and vanishes at corner nodes. Both have the same

wavenumber and frequency but different amplitudes and phases. (The wave pair (48) can be combined to form a single waveform that propagates over all nodes. The combination has two components that propagate at the same speed but in opposite directions. This is useful when studying boundary conditions or transitions in finite lattices, but unecessary for a periodic infinite lattice.)

As in Sect. 4.5, we will work with the dimensionless frequency $\Omega = \omega\,\ell/c_0$ with $c_0 = \sqrt{E/\rho}$, and the dimensionless wavenumber $\kappa = k\ell$. Inserting (48) into (47), passing to dimensionless variables, removing scale factors, and requiring that solutions exist for any t yields the characteristic equation

$$\begin{bmatrix} \frac{1}{2}A_3(160\beta-(16+\mu_2)\Omega^2) & -A_1A_3(80\beta+(2+\mu_4)\Omega^2) \\ -A_1(80\beta+(2+\mu_4)\Omega^2) & 30+40\beta-(4+\mu_1)\Omega^2+A_1(-30+40\beta+(1-\mu_3)\Omega^2) \end{bmatrix} \begin{bmatrix} B_c \\ B_m \end{bmatrix} = \mathbf{0}. \tag{49}$$

in which $A_1 = \cos\kappa$, $A_2 = \cos(\kappa/2)$ and $A_3 = \cos(\kappa/2) - j\sin(\kappa/2)$. For nontrivial solutions the determinant of the characteristic matrix must vanish, which provides a quadratic equation in Ω^2. For each wavenumber κ, solving the equation gives two squared frequencies. Their expressions, found by *Mathematica*, are

$$\Omega_a^2 = 5\,\frac{P-\sqrt{Q}}{R}, \quad \Omega_o^2 = 5\,\frac{P+\sqrt{Q}}{R}, \tag{50}$$

in which coefficients P, Q, and R are given by

$$\begin{aligned}
P &= c_1 + 3\,c_2 + c_9\,\cos\kappa,\\
R &= c_5 - 4\,\mu_4 - \mu_4^2 + c_8\,\cos\kappa,\\
Q &= 192\,\beta\,(\cos\kappa - 1)\,(c_5 - c_3 + c_8\,\cos\kappa)\\
&\quad + (c_1 + 3\,c_2 + c_9\,\cos\kappa)^2,\\
c_1 &= 4\,\beta\,(40 + 4\,\mu_1 + \mu_2 + 4\,\mu_4), \quad c_2 = 16 + \mu_2,\\
c_3 &= \mu_4\,(4 + \mu_4),\\
c_4 &= 4\,(5 + \mu_3 + \mu_4), \quad c_5 = 60 + 4\,\mu_2 + \mu_1\,c_2,\\
c_6 &= 16\,\mu_3 - c_3,\\
c_7 &= 4\,\beta\,(\mu_2 + c_4), \quad c_8 = c_6 + \mu_2\,(\mu_3 - 1) - 20,\\
c_9 &= c_7 - 3\,c_2.
\end{aligned} \tag{51}$$

Subscripts a and o stand for *acoustic* and *optical* branches, respectively, a terminology explained in Sect. 5.1. If $\mathbf{M}^e$ is PD and the conservation condition (40) holds, the branch frequencies (50) have small κ (low frequency, long wavelength) Taylor series of the generic form

$$\begin{aligned}
\Omega_a^2 &= \kappa^2 + \frac{C_4\,\kappa^4}{4!} + \frac{C_6\,\kappa^6}{6!} + \frac{C_8\,\kappa^8}{8!} + \cdots,\\
\Omega_o^2 &= D_0 + \frac{D_2\,\kappa^2}{2!} + \frac{D_4\,\kappa^4}{4!} + \cdots,
\end{aligned} \tag{52}$$

Coefficients C_n and D_n were obtained through the *Mathematica* built-in `Series` function up to $n = 10$ and are displayed for some interesting instances below.

5.6 Bar3 Standard Template Instances

We start by considering two instances available in the FEM literature since the mid 1960s. The CMM instance $\mathbf{M}_C^e$ is obtained for $\mu_1 = \mu_2 = \mu_3 = \mu_4 = 0$. Using $\beta = 1$ for $\mathbf{K}^e$ we get $P = 208 + 32\,\cos\kappa$, $Q = 128\,(237 + 224\cos\kappa - 11\,\cos(2\kappa))$, and $R = 20\,(3 - \cos\kappa)$. The squared frequencies have the small-κ expansions

$$\begin{aligned}
\Omega_a^2 &= \kappa^2 + \frac{\kappa^6}{720} - \frac{11\,\kappa^8}{151200} + \cdots,\\
\Omega_o^2 &= 60 - 20\,\kappa^2 + \frac{19\,\kappa^4}{3} + \cdots.
\end{aligned} \tag{53}$$

The SLMM (Simpson-lumped diagonal mass matrix) instance derived in (146) of Appendix 3.1 results if $\mu_1 = 1$, $\mu_2 = 4$, $\mu_3 = 1$, and $\mu_4 = -2$. Using $\beta = 1$ in (41) gives $P = 220 + 20\cos\kappa$, $Q = 200\,(147 + 140 + \cos(2\kappa))$, and $R = 100$. The squared frequencies have the small-κ expansions

$$\Omega_a^2 = \kappa^2 - \frac{\kappa^6}{1440} - \frac{\kappa^8}{48384} + \cdots, \quad \Omega_o^2 = 24 - 2\kappa^2 + \frac{\kappa^4}{12} + \cdots. \tag{54}$$

For small κ, SLMM fits the continuum better than CMM. Dispersion diagrams for the foregoing instances are plotted in Fig. 9a, c. Corresponding group velocity diagrams are shown in Fig. 9b, d. As in the case of the two-node bar, the consistent mass overestimates the continuum frequency $\Omega = \kappa$ for $0 \le \kappa \le \pi$, whereas the lumped mass underestimates it.

5.7 Bar3 Low-Frequency Fitting

Inspection of the AB coefficient of κ^6 in (53) and (54) suggests combining one third of $\mathbf{M}_C^e$ with two thirds of $\mathbf{M}_L^e$ to cancel it. Setting

$$\mu_1 = 2/3, \quad \mu_2 = 8/3, \quad \mu_3 = -2/3, \quad \mu_4 = 4/3, \quad \beta = 1, \tag{55}$$

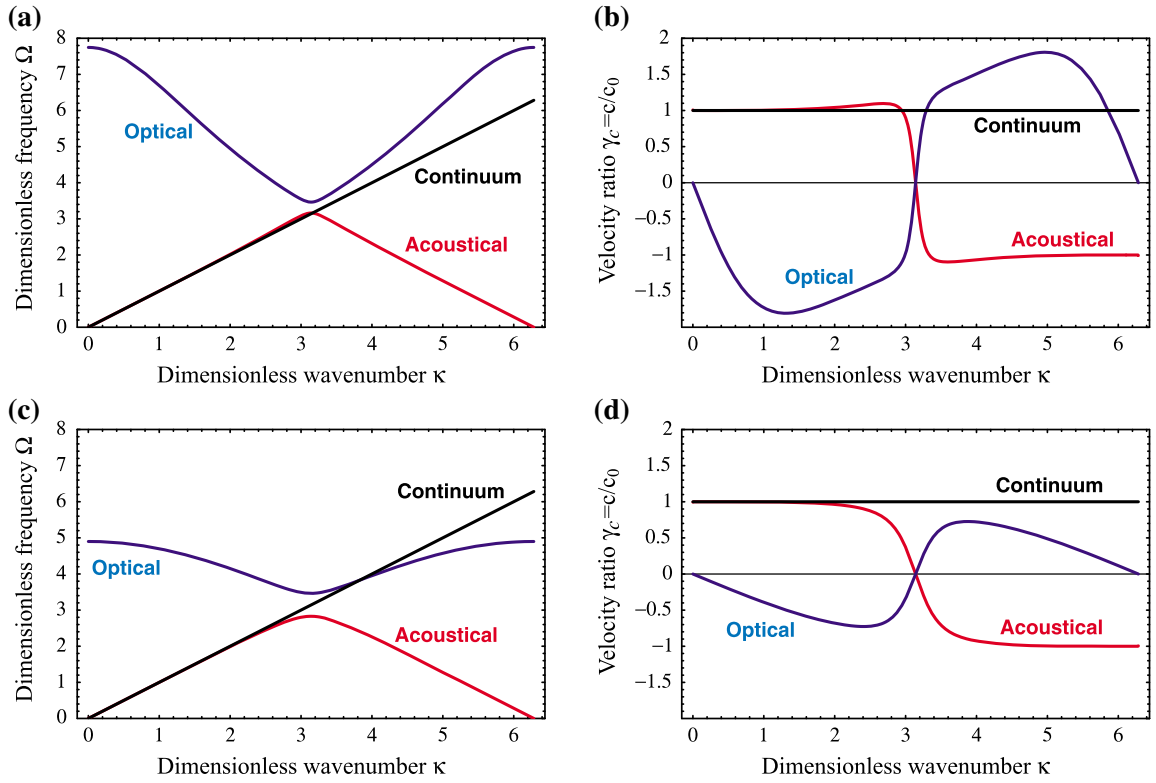

Fig. 9 DDD and DGVD plots for two Bar3 template instances treated in Sect. 5.6. **a**, **b** Diagrams for CMM instance, **c**, **d** diagrams for SLMM (Simpson DLMM) instance. Acoustic and optical branches shown in *red* and *blue*, respectively. Continuum case $\Omega = \kappa$ and $\gamma_c = 1$ shown in *black*. (Color figure online)

in (41) gives

$$\mathbf{M}^e_{BLCD} = \tfrac{1}{3}\,\mathbf{M}^e_C + \tfrac{2}{3}\,\mathbf{M}^e_L = \frac{\rho A\ell}{90}\begin{bmatrix} 14 & -1 & 2 \\ -1 & 14 & 2 \\ 2 & 2 & 56 \end{bmatrix}. \quad (56)$$

For this instance, labeled BLCD, $P = 24\,(9+\cos\kappa)$, $Q = 32\,(927{+}884\,\cos\kappa{-}11\,\cos 2\kappa)$, and $R = 20\,(13{-}\cos\kappa)/3$. It has the small κ expansions

$$\Omega_a^2 = \kappa^2 - \frac{\kappa^8}{37800} + \cdots, \quad \Omega_o^2 = 30 - \frac{15\,\kappa^2}{4} + \frac{11\,\kappa^4}{32} + \cdots. \quad (57)$$

Dispersion and group velocity diagrams are shown in Fig. 10a, b. Despite the $O(\kappa^8)$ accuracy achieved in the AB of BLCD, it is shown next that this instance is not optimal.

Considering next the general MS template (39) –(41), let us find the MS pair for which the AB Ω_a best matches the continuum $\Omega = \kappa$ for small κ. Given the expansion of Ω_a^2 in (52), the goal is to make as many coefficients beyond κ^2 vanish as possible, and to minimize the magnitude of the first surviving one. The analysis was actually performed using the χ-form (44) of the general mass template. Four free parameters are available: χ_1, χ_2, χ_3, and β. Only a procedural summary and final results are given.

It is possible to make $C_4 = C_6 = 0$ without difficulty, which permits elimination of χ_1 and χ_2. But all solutions of $C_8(\chi_3, \beta) = 0$ are imaginary, so the term in κ^8 cannot be cancelled. Extremization of C_8 with respect to χ_3 and β gives only one constraint: $160\beta^2 - 120\beta\chi_3 + 9\chi_3^2 = 0$, from which $\chi_3 = 4\,(5 \mp \sqrt{15}\beta)/3$. Both signs give the same C_8. Taking $\beta = 1$ for convenience, the $-$ sign in χ_3, and working back we get

$$\chi_1 = \frac{85}{6} - 2\sqrt{\frac{3}{5}} \mp 2\sqrt[4]{375}, \quad \chi_2 = 5 - \tfrac{1}{2}\sqrt{15},$$
$$\chi_3 = \frac{4}{3}\left(5 - \sqrt{15}\right), \quad \beta = 1. \quad (58)$$

The $-$ sign for χ_1 gives better conditioned mass matrices and still the same C_8, so we pick that one. The numeric values to 16 places are $\chi_1 = 2.7835604012611213$, $\chi_2 = 3.0635083268962915$, and $\chi_3 = 1.50268887172344$. The resulting minimum of $|C_8|$ is $C_{8best} = 64/3 - 28\sqrt{3/5} = -0.355373$. This is about 3 times smaller than the $C_8 =$

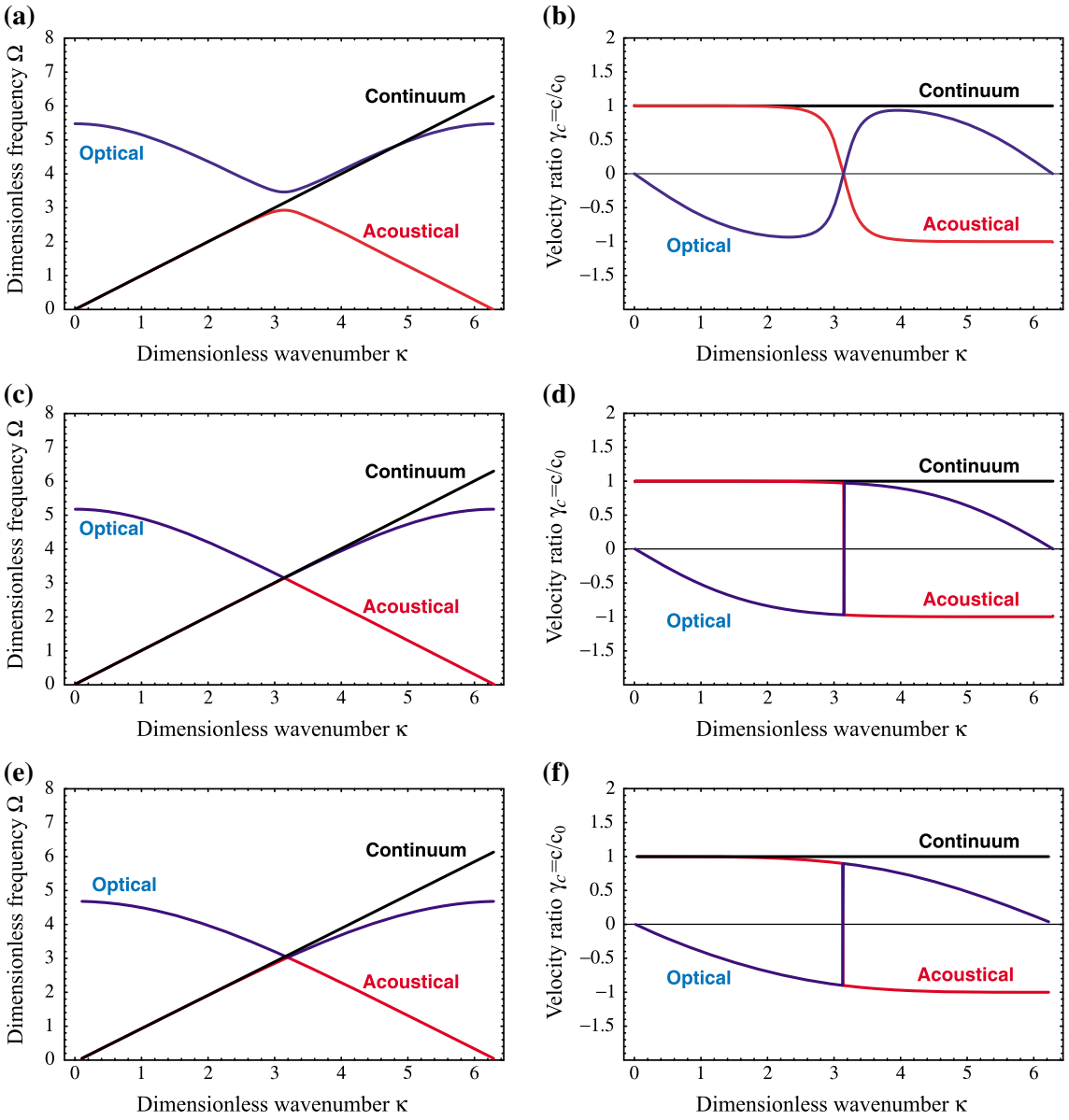

Fig. 10 DDD and DGVD plots for RHFP instances derived in Sect. 5.7 and Sect. 5.8. **a**, **b** Diagrams for the BLCD instance (56), **c**, **d** diagrams for the BLFM instance (60), **d**, **e** diagrams for the BLFD instance (66). Acoustic and optical branches shown in *red* and *blue*, respectively. Continuum case $\Omega = \kappa$ and $\gamma_c = c/c_0 = 1$ shown in *black*. (Color figure online)

$-8!/37800 = -16/15$ from (56). Converting to the μ_i parameters via (42) yields

$$\mu_1 = \frac{91-12\,a_1-7\,a_2}{6},\ \mu_2 = \frac{32-8\,a_2}{3},$$
$$\mu_3 = \frac{61-12\,a_1-a_2}{6},\ \mu_4 = \frac{-46+6\,a_1+4\,a_2}{3}, \tag{59}$$

in which $a_1 = 3^{1/4}\,5^{3/4} = \sqrt[4]{375}$ and $a_2 = \sqrt{15}$. Numerical values to 16 places are $\mu_1 = 1.8470687281574132$, $\mu_2 = 0.3387110767802213$, $\mu_3 = 0.7200520743648302$, and $\mu_4 = -1.3682381704561768$. The resulting mass matrix, labeled BLFM (for best low frequency match), given to 16 places, is

$$\mathbf{M}^e_{BLFM} = m^e \begin{bmatrix} 0.1949022909385804 & -0.0093315975211724 & 0.0210587276514608 \\ -0.0093315975211724 & 0.1949022909385804 & 0.0210587276514608 \\ 0.0210587276514608 & 0.0210587276514608 & 0.5446237025593408 \end{bmatrix}. \tag{60}$$

Its eigenvalues (to 6 places) are positive: 0.547077, 0.204234, and 0.183117 times $m^e = \rho A\,\ell$. Hence this mass matrix is admissible and well scaled. For this instance $P = 8\,(35 - 2\sqrt{15} - (5 - 2\sqrt{15})\cos\kappa)$, $Q = 1920\,(15 + 4\sqrt{15} + (15 - 4\sqrt{15})\cos\kappa)\cos(\kappa/2)^2$, and $R = 20\,(53 - 10\sqrt{15} + (7 - 2\sqrt{15})\cos\kappa)/3$. It has the small-$\kappa$ expansions

$$\Omega_a^2 = \kappa^2 + \frac{1127 - 291\sqrt{15}}{3024(5 - \sqrt{15})^3}\kappa^8 + \cdots$$
$$\Omega_o^2 = \frac{30}{5 - \sqrt{15}} - \frac{5(29 - 8\sqrt{15}))}{32(5 - \sqrt{15})^3}\kappa^2 - \cdots \tag{61}$$

Dispersion and group velocity diagrams are shown in Fig. 10c, d. Note that values at the folding (Nyquist) wavenumber $\kappa = \pi$ are identical: $\Omega_a^2(\pi) = \Omega_o^2(\pi) = 12(10 - \sqrt{15})/(23 - 4\sqrt{15}) = 9.792694126734647$, which is amazingly close to the continuum value of $\pi^2 = 9.86960440108935$ (in fact, the AB for $\kappa < \pi$ and the continuum are indistinguishable at plot resolution). There is no acoustoptical gap; instead we observe a bifurcation point.

5.8 Bar3 Lumped Mass Template Variant

Although DLMM plainly form a subset of the general template (39), their practical importance justifies the use of a more compact two-parameter form. This is done by taking

$$\mu_1 = \mu_{L1} + 1, \quad \mu_2 = \mu_{L2} + 4, \quad \mu_3 = 1, \quad \mu_4 = -2. \tag{62}$$

Replacing into (39) produces the *lumped mass template variant*

$$\mathbf{M}^e_L = \frac{\rho A\ell}{30}\begin{bmatrix} 5 + \mu_{L1} & 0 & 0 \\ 0 & 5 + \mu_{L1} & 0 \\ 0 & 0 & 20 + \mu_{L2} \end{bmatrix} = \mathbf{M}^e_{SLMM} + \frac{\rho A\ell}{30}\begin{bmatrix} \mu_{L1} & 0 & 0 \\ 0 & \mu_{L1} & 0 \\ 0 & 0 & \mu_{L2} \end{bmatrix}. \tag{63}$$

The baseline mass matrix is the DLMM (146) produced by Simpson's 3-point integration rule, and now labeled SLMM. The stiffness matrix template is still (41). Parameters μ_{L2} and β can be eliminated in favor of μ_{L1} through

$$2\mu_{L1} + \mu_{L2} = 0, \qquad \beta = \frac{(10 - \mu_{L1})^2}{20\,(5 - \mu_{L1})}. \tag{64}$$

The first constraint expresses element mass conservation while the second one enforces $C_4 = 0$ and makes the AB agree with the continuum through κ^4 in the expansion (52) (this agreement is considered essential as otherwise there would be no advantage in using this element instead of Bar2). As only one parameter remains, customization is straightforward. The admissible range in μ_{L1} for PD mass is $-5 < \mu_{L1} < 10$, but if $\mu_{L1} > 5$, $\beta < 0$ and $\mathbf{K}^e$ becomes indefinite.

On applying (64), the first nonzero term in the ABTS beyond κ^2 is $C_6\kappa^6/6!$, in which $C_6 = (5 - 3\mu_{L1} + \mu_{L1}^2)/(\mu_{L1} - 10)$. Trying to attain $O(\kappa^6)$ accuracy by setting $C_6 = 0$ is futile since the μ_{L1} roots are complex conjugate. Solving $\partial C6/\partial\mu_{L1} = 0$ gives two real solutions: $\mu_{L1} = 5(2 \pm \sqrt{3})$. Of these only the one with $-\sqrt{3}$ keeps $\mathbf{M}^e$ admissible. Replacing into (64) gives the signature

$$\mu_{L1} = 5(2 - \sqrt{3}), \quad \mu_{L2} = -2 \quad \mu_{L1} = -10(2 - \sqrt{3}), \qquad \beta = \frac{3}{4(\sqrt{3} - 1)}. \tag{65}$$

Numerical values to 16 places are $\mu_{L1} = 1.339745962155614$, $\mu_{L2} = -2.679491924311228$, and $\beta = 1.024519052838329$. The κ^6 term in the AB is about 36 % smaller than that of SLMM: $\approx -\kappa^6/2246$ versus $-\kappa^6/1440$. The template instance, labeled BLFD, is

$$\mathbf{M}^e_{BLFD} = \frac{\rho A\ell}{30}\begin{bmatrix} 5\sqrt{3} - 5 & 0 & 0 \\ 0 & 5\sqrt{3} - 5 & 0 \\ 0 & 0 & 20 - 10\sqrt{3} \end{bmatrix},$$
$$\mathbf{K}^e_{BLFD} = \frac{EA}{\ell}\begin{bmatrix} 1 & -1 & 0 \\ -1 & 1 & 0 \\ 0 & 0 & 0 \end{bmatrix} + \frac{4EA}{\ell\,(\sqrt{3} - 1)}\begin{bmatrix} 1 & 1 & -2 \\ 1 & 1 & -2 \\ -2 & -2 & 4 \end{bmatrix}. \tag{66}$$

The Taylor series of the dispersion branches are

$$\Omega_a^2 = \kappa^2 - \frac{10\sqrt{3} - 10}{720}\kappa^6 - \cdots,$$
$$\Omega_o^2 = \frac{12}{(\sqrt{3} - 1)^2} - \frac{\sqrt{3}}{4\sqrt{3} - 6}\kappa^2 - \cdots \tag{67}$$

The DDD and DGVD are shown in Fig. 10e, f. As in the case of the BLFM, pictured in (c,d) of that figure, the branches intersect at $\kappa = \pi$, where $\Omega_{af}^2 = \Omega_{of}^2 = (6 - 2\sqrt{3})/(2 - \sqrt{3}) \approx 9.4641$.

5.9 Bar3 Maximum Stable Time Step Customization

Since DLMM are often used in explicit DTI, it is of some interest to find whether the stable time stepsize can be maximized while still satisfying $O(\kappa^4)$ accuracy. This goal pertains to the MSTS customization of Table 1. Let Ω_{max} be the maximum of Ω_a and Ω_o over the Brillouin zone $\kappa \in [0, 2\pi]$. To maximize the stable time step, one minimizes Ω_{max} over free parameters, while trying to keep both mass and stiffness admissible. This procedure can be streamlined by assuming a DDD configured as in Fig. 8, whence only frequency values at $\kappa = 0$ and $\kappa = \pi$ need to be considered. Since $\Omega_a|_{\kappa=0} = 0$, the search only involves Ω_{oc}, Ω_{af} and Ω_{of}, or (for convenience) their squares. For the DLMM template variant (63) under the accuracy constraints (64) the process boils down to solving the max-min problem in one variable:

$$\min_{\mu_{L1}} \max \left(\Omega_{oc}^2, \Omega_{af}^2, \Omega_{of}^2\right) = \min_{\mu_{L1}} \max \left(\frac{60(10-\mu_{L1})}{25-\mu_{L1}^2}, \frac{4(10-\mu_{L1})}{\mu_{L1}-5}, \frac{60}{5+\mu_{L1}}\right). \tag{68}$$

A simple plot shows that the cutoff frequency dominates for admissible $\mu_{L1} \in (-5, 5)$, so it is sufficient to minimize with respect to Ω_{oc}^2. This again leads to the solution (65). Consequently the BLFD instance also maximizes the explicit DTI time step. The reward, however, is marginal with respect to SLMM: only about a 3.5 % gain.

To get a more significant improvement, it is necessary to keep β free, and accept that $O(\kappa^4)$ accuracy is lost. It may be verified that the largest possible stable timestep is produced by the signature

$$\mu_{L1} = 5/2, \quad \mu_{L2} = -2\mu_{L1} = -5, \quad \beta = 3/8. \tag{69}$$

which apportions nodal masses as 1:1:2, while substantially modifying the stiffness matrix. Setting (69) gives an instance with a COB $\Omega_o^2 = 8$. Its stable stepsize is 1.673 times that of BLFD. But its LF performance is exactly the same as that of the lumped-mass Bar2, which does not have an OB. So it is largely a curiosity.

5.10 Reducing High Frequency Pollution

The presence of the OB does not affect vibration calculations in structural dynamics. One simply ignores those eigenfrequencies as nonphysical. However, the OB may become a nuisance in direct time integration (DTI) for problems that involve discontinuities, such as pulse propagation, or contact-impact, because it may feed spurious noise. To alleviate this problem three approaches may be tried at the template level:

1. *Singular Mass Matrix* If $\mathbf{M}^e$ is made singular with an appropriate null eigenvector, the OB is raised. In fact it becomes infinite at $\kappa = 0$. The net effect is that the acoustoptical gap is increased at low wavenumbers. This heps to filter out frequencies that fall in the gap, since they will decay exponentially. One drawback of singularity is that explicit DTI is excluded, even if $\mathbf{M}^e$ is diagonal.
2. *SMS* A scaled stiffness matrix is added to the mass. As discussed in Sect. 3.5, eigenvectors are unchanged but higher natural frequencies are effectively reduced. The effect is similar to that of adding stiffness proportional damping, but without altering vibration modes. It may be done at the element or assembly (master) level. In the study of Sect. 5.12 it is done at the element level.
3. *COB* A constant optical branch (COB) is one independent of wavenumber. It stays at a constant frequency $\Omega_o = \Omega_{oc}$ over the entire Brillouin zone, and has zero group velocity since $\partial\Omega_{oc}/\partial\kappa = 0$. To be effective in cutting noise pollution, $\Omega_{oc} \geq \Omega_{af}$, in which Ω_{af} is the folding acoustic frequency. If that holds, the stopping band above Ω_{af} is effectively maximized (even if a mesh frequency hits Ω_{oc} exactly, it will not propagate since its group velocity vanishes). A COB template is one that possesses that property (for each OB in case there are multiple ones).

The three foregoing approaches are studied below for the Bar3 element.

5.11 Bar3 Spectral Mass Variant

Making $\mathbf{M}^e$ singular is not sufficient. It is important to have the correct null eigenvector. To achieve that it is convenient to use the SP outlined in Sect. 3.2. Select three generalized coordinates: g_0, g_1 and g_2 as amplitudes of three physically transparent eigenmotions:

g_0 Amplitude of rigid body motion: $\mathbf{v}_0 = [\,1 \quad 1 \quad 1\,]^T$.
g_1 Amplitude of acoustic bar motion:: $\mathbf{v}_1 = [\,-1 \quad 1 \quad 0\,]^T$.
g_2 Amplitude of optical bar motion: : $\mathbf{v}_2 = [\,1 \quad 1 \quad -2\,]^T$.

Those three vectors are mutually orthogonal. To make them orthonormal, divide by $\sqrt{3}$, $\sqrt{2}$ and $\sqrt{6}$, respectively. Stacking the orthonormalized vectors as columns, the linkage between physical and generalized coordinates can be expressed as

$$\mathbf{u}^e = \begin{bmatrix} u_1 & u_2 & u_3 \end{bmatrix} = \begin{bmatrix} 1/\sqrt{3} & -1/\sqrt{2} & 1/\sqrt{6} \\ 1/\sqrt{3} & 1/\sqrt{2} & 1/\sqrt{6} \\ 1/\sqrt{3} & 0 & -2/\sqrt{6} \end{bmatrix} = \begin{bmatrix} g_0 \\ g_1 \\ g_2 \end{bmatrix} = \mathbf{H}^T\mathbf{g}. \tag{70}$$

The inverse relation is $\mathbf{g} = \mathbf{H}\,\mathbf{u}^e$ because $\mathbf{H}$ is orthogonal by construction, and thus $\mathbf{H}^{-1} = \mathbf{H}^T$. As mass matrix in generalized coordinates we stipulate the 3×3 diagonal matrix $\mathbf{D}_\mu$ of entries $m^e\mu_{S0}/3$, $m^e\mu_{S1}/45$, and $m^e\mu_{S2}/15$, in which $m^e = \rho\,A\,\ell$, and the scaling factors were chosen for convenience in cleaning up downstream expressions. Element mass conservation will require $\mu_{S0} = 1$, so the first entry is simply $m^e/3$. Transforming to physical coordinates yields the *spectral mass template variant*

$$\mathbf{M}^e_S = \frac{m^e}{45}\mathbf{H}^T\begin{bmatrix}15 & 0 & 0\\ 0 & \mu_{S1} & 0\\ 0 & 0 & 3\mu_{S2}\end{bmatrix}$$
$$\mathbf{H} = \frac{m^e}{90}\begin{bmatrix}10+\mu_{S1}+\mu_{S2} & 10-\mu_{S1}+\mu_{S2} & 10-2\,\mu_{S2}\\ 10-\mu_{S1}+\mu_{S2} & 10+\mu_{S1}+\mu_{S2} & 10-2\,\mu_{S2}\\ 10-2\,\mu_{S2} & 10-2\,\mu_{S2} & 10+4\,\mu_{S2}\end{bmatrix}. \tag{71}$$

The variant (71) is a subset of the general template (39) that results by taking

$$\mu_1 = \tfrac{1}{3}(\mu_{S1}+\mu_{S2}-2),\ \ \mu_2 = \tfrac{1}{3}(4\,\mu_{S2}-38),$$
$$\mu_3 = \tfrac{1}{3}(13-\mu_{S1}+\mu_{S2}),\ \ \mu_4 = \tfrac{1}{3}(4-2\,\mu_{S2}). \tag{72}$$

By construction, the eigenvalues of (71) are $m^e/3, m^e\mu_{S1}/45$ and $m^e\,\mu_{S2}/15$, whence the nonnegativity condition is fulfilled if μ_{S1} and μ_{S2} are nonnegative. To make $\mathbf{M}^e_S$ singular, set $\mu_{S2} = 0$, which produces

$$\mathbf{M}^e_S = \mathbf{H}^T\,\mathbf{D}_\mu\,\mathbf{H} = \frac{m^e}{90}\begin{bmatrix}10+\mu_{S1} & 10-\mu_{S1} & 10\\ 10-\mu_{S1} & 10+\mu_{S1} & 10\\ 10 & 10 & 10\end{bmatrix}. \tag{73}$$

Solving $C_4 = 0$ and $C_6 = 0$ yields two solutions for β and μ_{S1}, of which we pick that with larger μ_{S1} (to get a better conditioned nonsingular subspace). This gives

$$\mu_{S1} = \frac{3(5+\sqrt{10})}{2} = 12.24341649025257,$$
$$\beta = \frac{5+\sqrt{10}}{12} = 0.6801898050140316, \tag{74}$$

in addition to $\mu_{S2} = 0$. Inserting into (76) gives the instance labeled `BSSM` for Best Singular Spectral Mass. The mass matrix, with numerical values given to 6 places, is

$$\mathbf{M}^e_{BSSM} = \frac{m^e}{180}\begin{bmatrix}M_{11} & M_{12} & M_{13}\\ M_{12} & M_{22} & M_{23}\\ M_{13} & M_{23} & M_{33}\end{bmatrix}$$
$$\approx m^e\begin{bmatrix}0.247149 & -0.024927 & 0.111111\\ -0.024927 & 0.247149 & 0.111111\\ 0.111111 & 0.111111 & 0.111111\end{bmatrix}. \tag{75}$$

in which $M_{11} = M_{22} = 35+\sqrt{10}$, $M_{12} = 5-3\sqrt{10}$, and $M_{13} = M_{23} = M_{33} = 20$. The associated stiffness matrix, with numerical values given to 6 places, is

$$\mathbf{K}^e_{BSSM} = \frac{k^e}{9}\begin{bmatrix}K_{11} & K_{12} & K_{13}\\ K_{12} & K_{22} & K_{23}\\ K_{13} & K_{23} & K_{33}\end{bmatrix}$$
$$\approx k^e\begin{bmatrix}1.906920 & -0.093080 & -1.813839\\ -0.093080 & 1.906920 & -1.813839\\ -1.813839 & -1.813839 & 3.627679\end{bmatrix}. \tag{76}$$

in which $k^e = E\,A/\ell$, $K_{11} = K_{22} = 14+\sqrt{10}$, $K_{12} = -4+\sqrt{10}$, $K_{13} = K_{23} = -10-2\sqrt{10}$ and $K_{33} = 20+4\sqrt{10}$. Dispersion and group velocity diagrams are shown in Fig. 11a, b. The Taylor series of the dispersion branches are

$$\Omega_a^2 = \kappa^2 - \frac{\kappa^8}{6048} - \cdots, \qquad \Omega_o^2 = 240\,\kappa^{-2} + \frac{5\kappa^4}{126} + \cdots \tag{77}$$

The $O(\kappa^8)$ AB accuracy of this element is comparable to that of BLCD and BLFM, but its OB gets out of the way. Is this the template instance for all seasons? Only future experimentation in DTI will tell.

5.12 Bar3 Selective Mass Scaling Variant

In the SMS approach outlined in Sect. 3.5, the mass matrix is modified by adding a scaled version of the stiffness matrix:

$$\mathbf{M}^e_K = \mathbf{M}^e_u + c_K\,\mathbf{K}^e. \tag{78}$$

Here $\mathbf{M}^e$ is an unmodified mass matrix, and c_K a scaling coefficient with appropriate physical dimensions. Both $\mathbf{M}^e$ and $\mathbf{K}^e$ may be template forms. Since $\mathbf{M}^e$ and $\mathbf{K}^e$ have different physical dimensions, it is convenient to change the raw expression (78) to

$$\mathbf{M}^e_K = \mathbf{M}^e_u + \mu_K\,s^e\,\mathbf{K}^e, \tag{79}$$

in which s^e is a scaling coefficient with dimension of mass-over-stiffness (equivalently, $1/s^e$ has dimensions of squared physical frequency) while μ_K is a dimensionless free parameter. For the Bar3 element we take $s^e = (\rho\,A\,\ell)/(E\,A/\ell) = \rho\,\ell^2/E$. This can be maneuvered to the following equivalent form, which is convenient for implementation:

$$\mathbf{M}^e_K = \mathbf{M}^e_u + \mu_K\,m^e\,\widehat{\mathbf{K}}^e. \tag{80}$$

Here $m^e = \rho A\ell$ is (as usual) the element mass, whereas $\widehat{\mathbf{K}}^e_u$ is a *dimensionless stiffness matrix* obtained by setting $E = 1$, $A = 1$ and $\ell = 1$. To reduce the overall number of parameters, we pick $\mathbf{M}^e_u$ to be the diagonally lumped template subset (63); this agrees with the common use of SMS in

explicit DTI. The general stiffness template (41) with unit E, A and ℓ is used for $\widehat{\mathbf{K}}^e$. Hence

$$\mathbf{M}_K^e = m^e \left(\frac{1}{30} \begin{bmatrix} 5+\mu_{L1} & 0 & 0 \\ 0 & 5+\mu_{L1} & 0 \\ 0 & 0 & 20+\mu_{L2} \end{bmatrix} + \frac{4\beta\,\mu_K}{3\,\ell} \begin{bmatrix} 1 & 1 & -2 \\ 1 & 1 & -2 \\ -2 & -2 & 4 \end{bmatrix} \right). \tag{81}$$

Mass conservation is enforced if $\mu_{L2} = -2\mu_{L1}$. Inserting this in (81) we have three free parameters: μ_{L1}, μ_K and β. This $\mathbf{M}_K^e$ with $\mu_{L2} = -2\mu_{L1}$ is a particular case of the general mass template if

$$\begin{aligned} \mu_1 &= 1 + \mu_{L1} + 10\,(4\beta+3)\mu_K, \\ \mu_2 &= 4 - 2\mu_{L1} + 160\,\beta\mu_K, \\ \mu_3 &= 1 + 10\,(4\beta-3)\mu_K, \quad \mu_4 = -2 - 80\,\beta\mu_K. \end{aligned} \tag{82}$$

Unlike previous variants, now β appears in the mass template. The linkage (82) becomes linear if β is preset, for example to 1, and nonlinear otherwise.

Further experimentation with the SMS template variant (81) was confined to $\mu_{L1} = \mu_{L2} = 0$, which takes SLMM as original mass matrix. That leaves out two free parameters: μ_K and β. Suppose μ_K is chosen. Then $O(\kappa^4)$ AB accuracy can be maintained by taking

$$\beta = \frac{1}{1-12\mu_K}. \tag{83}$$

If $\mu_K > 1/12$, $\beta < 0$ and $\mathbf{K}^e$ becomes indefinite. But setting $0 \le \mu_K \le 1/12$ hardly change the higher frequencies. For that one needs a much larger μ_K; say $\mu_K = O(1)$. If so, adjusting $\mathbf{K}^e$ as per (83) is precluded: the cure is worst than the disease. One may as well set $\beta = 1$. The high frequencies are cut down, but LF accuracy is seriously lost.

This tradeoff is vividly displayed in the vibration benchmarks reported in Sect. 5.14. Three instances labeled SMS1, SMS2 and SMS3, are tested there. Their signatures are $\{\mu_K = 1/24, \beta = 2\}$, $\{\mu_K = 1/2, \beta = 1\}$, and $\{\mu_K = 2, \beta = 1\}$, respectively. Dispersion and group velocity diagrams for SMS2 are shown in Fig. 11c, d. The poor LF fit is obvious.

5.13 Bar3 Constant Optical Branch Variant

The investigation of the general Bar3 template (39)–(41) for COB instances was done under two preset conditions: $C_4 = 0$, which enforces order $O(\kappa^4)$ accuracy in the AB (AB), and $\beta = 1$ in the stiffness template (41). Several one-parameter families satisfying these conditions were found. The two that produced simpler mass matrices were retained, reparametrized, and labeled COBA and COBB. Associated mass matrices are subscripted accordingly.

The COBA family is defined by

$$\mathbf{M}_{COBA}^e = \frac{m^e}{12} \begin{bmatrix} 6-\nu_A & 2-\nu_A & -2+2\nu_A \\ 2-\nu_A & 6-\nu_A & -2+2\nu_A \\ -2+2\nu_A & -2+2\nu_A & 4-4\nu_A \end{bmatrix}. \tag{84}$$

in which $m^e = \rho\,A\,\ell$. The determinant is $(1-\nu_A)/18$. $\mathbf{M}_{COBA}$ is PD if $\nu_A < 1$. Parameter ν_A is linked to those of the general template (39) by

$$\begin{aligned} &\mu_1 = 11 - \frac{5\nu_A}{2}, \quad \mu_2 = -2(3+5\nu_A), \quad \mu_3 = 6 - \frac{5\nu_A}{2}, \\ &\mu_4 = -7 + 5\nu_A. \end{aligned} \tag{85}$$

The COBB family is defined by

$$\mathbf{M}_{COBB}^e = \frac{m^e}{432} \begin{bmatrix} 96-36\nu_B-\nu_B^2 & 24-12\nu_B+\nu_B^2 & -48+24\nu_B \\ 24-12\nu_B+\nu_B^2 & 96-36\nu_B-\nu_B^2 & -48+24\nu_B \\ -48+24\nu_B & -48+24\nu_B & 384 \end{bmatrix}. \tag{86}$$

The determinant is $(36-12\nu_B-\nu_B^2)^2/34992$. $\mathbf{M}_{COBB}$ is PD if $-6(\sqrt{2}+1) < \nu_B < 6(\sqrt{2}-1)$. Parameter ν_B is linked to those of the general template (39) by

$$\begin{aligned} &\mu_1 = \frac{8}{3} - \frac{5\nu_B}{2} - \frac{5\nu_B^2}{72}, \quad \mu_2 = \frac{32}{3}, \\ &\mu_3 = \frac{8}{3} - \frac{5\nu_B}{6} + \frac{5\nu_B^2}{72}, \quad \mu_4 = \frac{-16+5\nu_B}{3}. \end{aligned} \tag{87}$$

These two families are taken to collectively define the Bar3 template variant identified as COB. They coalesce only for $\nu_A = -5/3$ and $\nu_B = -6$, which produces an instance discussed below. An interesting result is that the AB is *identical* for all COB instances:

$$\Omega_a^2 = \frac{12(1-\cos\kappa)}{5+\cos\kappa} = \kappa^2 - \frac{\kappa^6}{240} - \frac{\kappa^8}{6048} - \cdots \tag{88}$$

whereas the constant OB value is family and parameter dependent:

$$\Omega_{ocA}^2 = \frac{16}{1-\nu_A}, \qquad \Omega_{ocB}^2 = \frac{432}{36-12\nu_B-\nu_B^2}. \tag{89}$$

It follows that the only role played by ν_A and ν_B is to adjust the "OB height" along the vertical DDD axis. As noted in Sect. 5.10, it should equal or exceed the folding acoustic frequency $\Omega_{af}^2 = 6$, which is the same for all COB instances on account of (88). This requires $\nu_A \ge -5/3$ and $\nu_B \ge -6$. As $\nu_A \to 1$ and $\nu_B \to 12$ the OB moves to ∞ and the mass

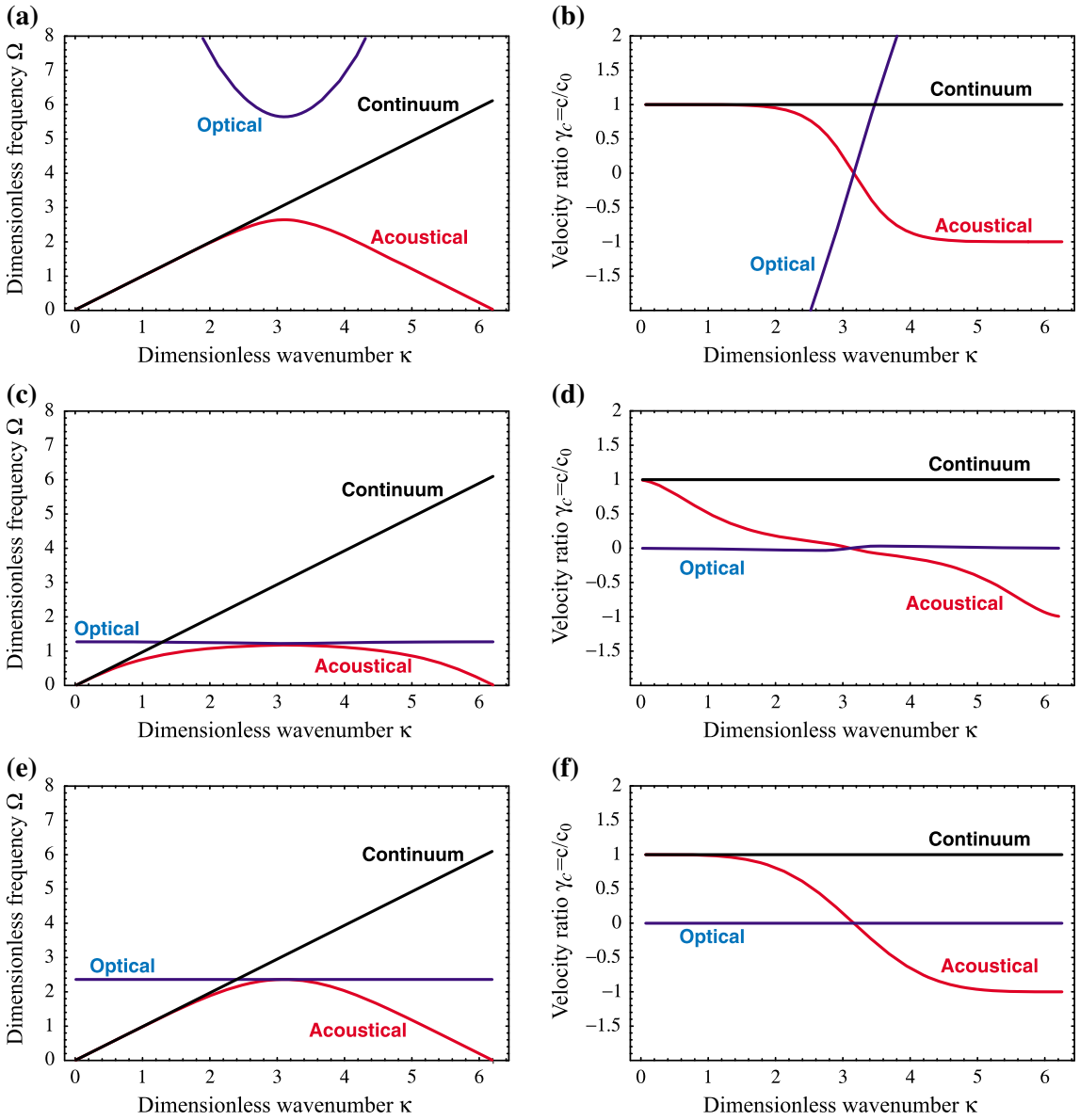

Fig. 11 DDD and DGVD plots for three RHFP instances derived in Sects. 5.11–5.13. **a**, **b** Diagrams for the BSSM instance (56), **c**, **d** diagrams for the SMS2 instance (60), **e**, **f** diagrams for the COB0 instance: first of (90). Acoustic and optical branches shown in *red* and *blue*, respectively. Continuum case $\Omega = \kappa$ and $\gamma_c = c/c_0 = 1$ shown in *black*. (Color figure online)

matrices assume different limits. For COBA, $\mathbf{M}^e_{COBA}\big|_{\nu_A\to 1}$ is the optimal Bar2 matrix (22), which is PD. On the other hand the limit $\mathbf{M}^e_{COBB}\big|_{\nu_B\to 12}$ falls in the indefinite range. Three noteworthy instances of the mass matrices produced by these two families are

$$\mathbf{M}^e_{COB0} = \frac{m^e}{36}\begin{bmatrix} 23 & 11 & -16 \\ 11 & 23 & -16 \\ -16 & -16 & 32 \end{bmatrix},$$

$$\mathbf{M}^e_{COB1} = \frac{m^e}{6}\begin{bmatrix} 3 & 1 & -1 \\ 1 & 3 & -1 \\ -1 & -1 & 2 \end{bmatrix},$$

$$\mathbf{M}^e_{COB2} = \frac{m^e}{18}\begin{bmatrix} 4 & 1 & -2 \\ 1 & 4 & -2 \\ -2 & -2 & 16 \end{bmatrix}. \tag{90}$$

$\mathbf{M}^e_{COB0}$ is the unique mass matrix for which $\Omega^2_{oc} = \Omega^2_a = 6$; that is, the COB passes through the folding (Nyquist) frequency. It emerges by setting either $\nu_A = -5/3$ in (84) or $\nu_B = -6$ in (86). $\mathbf{M}^e_{COB1}$ which gives $\Omega^2_{ocA} = 16$, is the simplest mass matrix that produces a COB. It is obtained by setting $\nu_A = 0$ in (84). Finally $\mathbf{M}_{COB2}$, which yields $\Omega^2_{ocB} = 12$, was the first COB instance discovered, as noted in Appendix Sect. 1.7. It is obtained by setting $\nu_B = 0$ in (86).

Table 10 Bar3 instances compared in fixed-free bar vibrations tests

Instance name	Variant ref. Eqs.	Full or diag $\mathbf{M}^e$	Signature	First NCT in ABTS[a]	Cutoff & folding fr.[b]		
					Ω_{oc}	Ω_{af}	Ω_{of}
CMM	(39)	F	β=1, μ_1=μ_2=μ_3=μ_4=0	$+\kappa^6/720$	7.746	3.162	3.464
SLMM	(63)	D	β=1, μ_{L1}=μ_{L2}=0	$-\kappa^6/1440$	4.899	2.828	3.464
BLCD	(39)	F	See (55)	$-\kappa^8/37800$	5.477	2.928	3.464
BLFM	(39)	F	See (59)	$-\kappa^8/113458$	5.159	3.129	3.129
BLFD	(63)	D	See (65)	$-\kappa^6/2246$	4.732	3.076	3.076
BSSM	(71)	F	See (74)	$-\kappa^8/6048$	∞	2.711	5.714
SMS1	(81)	F	β=2, μ_K=1/24	$-\kappa^6/640$	4.000	2.828	3.098
SMS2	(81)	F	β=1, μ_K=1/2	$-\kappa^4/2$	1.359	1.265	1.309
SMS3	(81)	F	β=1, $\mu_K = 2$	$-2\kappa^4$	0.700	0.686	0.692
COB0	(84)	F	β=1, $\nu_A = -5/3$	$-\kappa^6/240$	2.449	2.449	2.449

[a] *NCT* non-continuum term, *ABTS* AB Taylor series of Ω_a^2 wrt κ, centered at $\kappa = 0$
[b] Ω_{oc} : Ω_o at $\kappa = 0$; Ω_{af} : Ω_a at $\kappa = \pi$; Ω_{of} : Ω_o at $\kappa = \pi$

Dispersion and group velocity diagrams for COB0 are shown in Fig. 11e, f. The DDD for COB1 and COB2 would possess an identical AB branch but the flat OB would appear higher, whereas the DGVD would be identical. Those four diagrams are omitted to save space.

5.14 Bar3 Test: Vibrations of a Fixed-Free Bar Member

The natural frequency benchmark test presented in Sect. 4.9 for three Bar2 discretizations is repeated for the ten Bar3 template instances listed in Table 10. The fixed-free bar member is pictured in Fig. 5b. It is prismatic, with constant $E = 1$, $A = 1$ $\rho = 1$. The total member length is $L = \pi/2$. With those numerical properties, the continuum eigenfrequencies ω_{0i} are given by (24). The member is divided into N_e identical elements, with $N_e = 1, 2, \ldots 16$.

To reduce cluttering the instances in Table 10 are divided into two groups of five each. Results are presented in number of correct digits versus number of elements for the first three frequencies, exactly as described for the Bar2 test in Sect. 4.9. Group 1 include CMM and SLMM as well as instances constructed with optimal LFF customization in mind: BLCD, BLFM and BLFD. Results are displayed in Fig. 12a–c. Group 2 includes instances derived with RHFP in mind: BSSM, SMSx ($x = 1, 2, 3$) and COB0. Results are displayed in Fig. 12d–f.

BLFM is the clear winner in the first group, with BLCD close behind, while the others, with only $O(\kappa^4)$ AB accuracy, lag appreciably. In the second group, BSSM is the clear winner, with performance comparable to BLFM and BLCD of the first group. SMS1 and COB0 are way behind, while SMS2 and SMS3 are highly inaccurate (as observed in Sect. 5.12, SMS1 would hardly effect any HF reduction, so its reasonable LF accuracy is misleading).

6 The Bernoulli–Euler Plane Beam Element

This Section and the next one study templates for two-node plane beam elements constructed from the Bernoulli–Euler (BE) and Timoshenko models, respectively. To keep the material relatively compact, two restrictions are observed:

- Only mass matrix templates are developed.
- The only customization is LFCF

To enforce the first one, the optimal stiffness matrix for statics ("optimal" means that it satisfies the homogeneous static equilibrium equations over the element) is chosen and kept fixed. Simultaneous adjustment of the mass and stiffness templates to form MS pairs is relegated to future research. Prior experience in this regard, cited in Appendix Sect. 1.7, suggests that the improvement is marginal.

6.1 The BE Beam Mass Template

The BE beam model is a special case of the Timoshenko model treated in Sect. 7. Nevertheless it is useful to build its mass template separately, since results provide a valuable cross check with the more complicated Timoshenko beam. The well known CMM of this element is derived in Appendix Sect. 3.2, to which the reader is referred for notation; the derivation assumes a prismatic two-node element with four nodal DOF with the standard cubic shape functions. This matrix is augmented to produce the following EW template:

$$\mathbf{M}^e_\mu = m^e \begin{bmatrix} \frac{13}{35}+\mu_{11} & \left(\frac{11}{210}+\mu_{12}\right)\ell & \frac{9}{70}+\mu_{13} & -\left(\frac{13}{420}+\mu_{14}\right)\ell \\ & \left(\frac{1}{105}+\mu_{22}\right)\ell^2 & \left(\frac{13}{420}+\mu_{23}\right)\ell & -\left(\frac{1}{140}+\mu_{24}\right)\ell^2 \\ & & \frac{13}{35}+\mu_{11} & -\left(\frac{11}{210}+\mu_{12}\right)\ell \\ \text{symm} & & & \left(\frac{1}{105}+\mu_{22}\right)\ell^2 \end{bmatrix} \tag{91}$$

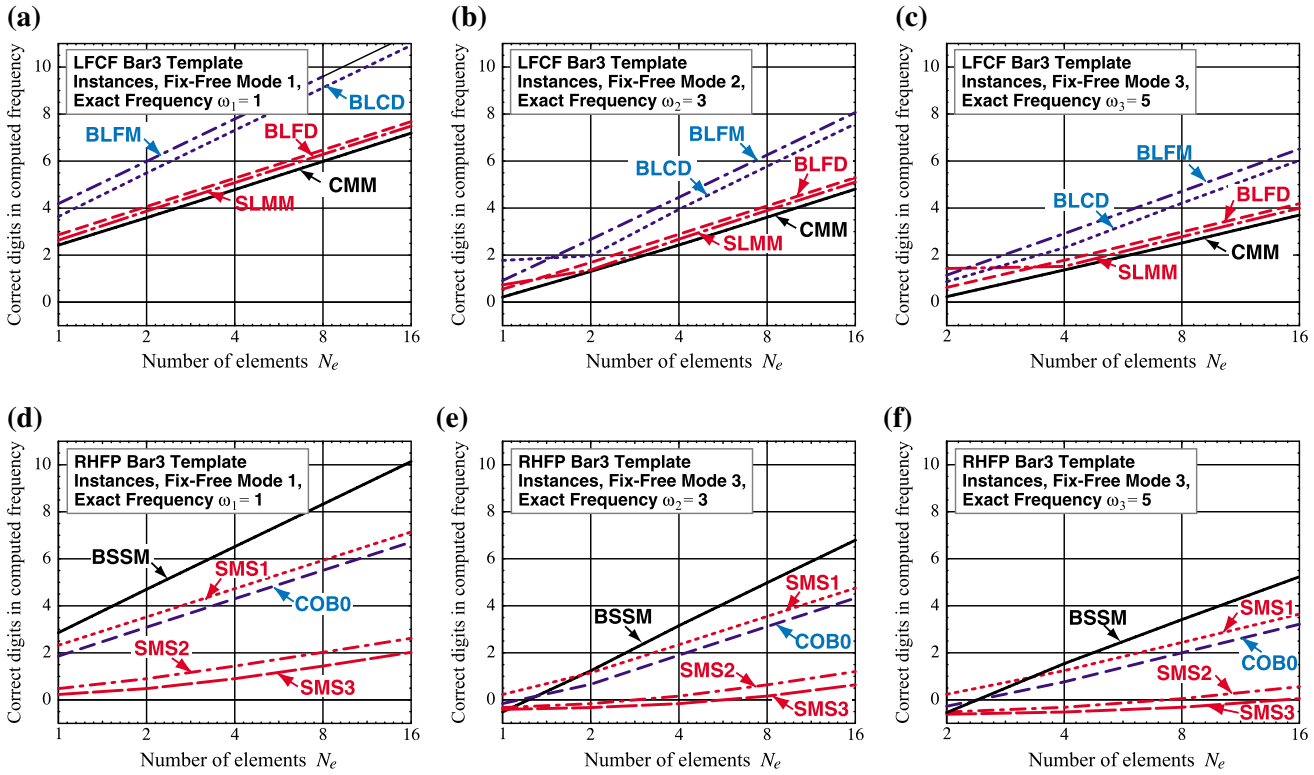

Fig. 12 Performance of ten Bar3 template instances in predicting the first three natural frequencies ω_i, $i = 1, 2, 3$ of the fixed-free prismatic homogeneous bar shown in Fig. 5b. See text in Sect. 4.9 for a detailed description of the log-log plots

in which $m^e = \rho\, A\, \ell$. The parameters in (91) are μ_{ij}, in which ij identifies the mass matrix entry. The template (91) accounts for matrix symmetry and some physical symmetries. Three more conditions can be imposed right away:

$$\mu_{14} = \mu_{23}, \quad \mu_{13} = -\mu_{11},$$
$$2\mu_{12} = \mu_{11} + 2\mu_{22} + 2\mu_{23} - 2\mu_{24}. \tag{92}$$

The first comes from prismatic fabrication, and the others from conservation of total translational mass and angular momentum, respectively. Four free parameters remain: $\{\mu_{11}, \mu_{22}, \mu_{23}, \mu_{24}\}$. For the stiffness matrix we take the well known one for a plane prismatic homogeneous BE beam element

$$\mathbf{K}^e = \frac{EI}{\ell^3}\begin{bmatrix} 12 & 6\ell & -12 & 6\ell \\ & 4\ell^2 & -6\ell & 2\ell^2 \\ & & 12 & -6\ell \\ \text{symm} & & & 4\ell^2 \end{bmatrix} \tag{93}$$

in which $I = I_{zz}$ is the second moment of inertial of the cross section with the respect to z, which is chosen to go along the neutral axis. If the FEM model contains only prismatic beams, this $\mathbf{K}^e$ is nodally exact, and consequently statically optimal (it can also be derived from the equilibrium equations). This stiffness is kept fixed throughout the Fourier analysis.

6.2 BE Beam Template Fourier Analysis

The Fourier analysis procedure should be by now familiar to the reader. An infinite lattice of identical beam elements of length ℓ is set up. This will look like Fig. 2b–d, except that the member is now a plane beam. Plane waves of wavenumber k and frequency ω propagating over the lattice are represented by

$$\begin{aligned} v(x,t) &= B_v\, \exp\big(j(kx - \omega t\big), \quad \theta(x,t) \\ &= B_\theta\, \exp\big(j(kx - \omega t\big), \quad j = \sqrt{-1}. \end{aligned} \tag{94}$$

At a typical lattice node j there are two DOF: v_j and θ_j. Two patch equations are extracted, and converted to dimensionless form on defining $\kappa = k\ell$ and $\Omega = \omega c_0/\ell$, in which $c_0 = EI/(\rho A \ell^4)$ is a reference phase velocity. The condition for wave propagation gives the characteristic matrix equation

$$\det\begin{bmatrix} C_{vv} & C_{v\theta} \\ C_{\theta v} & C_{\theta\theta} \end{bmatrix} = C_{vv}C_{\theta\theta} - C_{v\theta}C_{\theta v} = 0, \tag{95}$$

in which

$$\begin{aligned} C_{vv} &= \big(840 - 2(13+35\mu_{11})\Omega^2 \\ &\quad - (840 + (9 - 70\mu_{11})\Omega^2)\cos\kappa\big)/35, \\ -C_{\theta v} &= C_{v\theta} = j\big(2520 + (13+420\mu_{23})\Omega^2\big)\sin\kappa/210, \end{aligned}$$

$$C_{\theta\theta} = \big(1680 - 4(1{+}105\mu_{22})\Omega^2 + (840 + 3(1{+}140\mu_{24})\Omega^2)\cos\kappa\big)/210. \tag{96}$$

The condition (95) gives a quadratic equation in Ω^2 that provides two dispersion solutions: AB $\Omega_a^2(\kappa)$ and OB $\Omega_o^2(\kappa)$. The AB represent genuine flexural modes, whereas the OB is a spurious byproduct of the FEM discretization. The small-κ (low frequency, long wavelength) expansions of these roots are

$$\Omega_a^2 = \kappa^4 + C_6\kappa^6 + C_8\kappa^8 + C_{10}\kappa^{10} + C_{12}\kappa^{12} + \cdots,$$
$$\Omega_o^2 = D_0 + D_2\kappa^2 + D_4\kappa^4 + \cdots, \tag{97}$$

in which $C_6 = -\mu_{11} - 2\mu_{22} - 4\mu_{23} + 2\mu_{24}$, $C_8 = 1/720 + \mu_{11}^2 + 4\mu_{22}^2 + 2\mu_{23}/3 + 16\mu_{22}\mu_{23} + 16\mu_{23}^2 + \mu_{11}(1/12 + 4\mu_{22} + 8\mu_{23} - 4\mu_{24}) - \mu_{24} - 8\mu_{22}\mu_{24} - 16\mu_{23}\mu_{24} + 4\mu_{24}^2$, etc.; and $D_0 = 2520/(1 + 420\mu_{22} - 420\mu_{24})$, etc. *Mathematica* calculated these series up to C_{14} and D_4.

The continuum dispersion curve is $\Omega^2 = \kappa^4$, which automatically matches Ω_a^2 as $\kappa \to 0$. Thus four free parameters offer the opportunity to match coefficients of four powers: $\{\kappa^6, \kappa^8, \kappa^{10}, \kappa^{12}\}$. But it will be seen that the last match is unfeasible if $\mathbf{M}^e$ is to stay nonnegative. We settle for a scheme that agrees up to κ^{10}. Setting $C_6 = C_8 = C_{10} = 0$ while keeping μ_{22} free yields two sets of solutions, of which the most useful one is

$$\mu_{11} = 4\mu_{22} - 67/540 - (4/27)\sqrt{38/35 - 108\mu_{22}},$$
$$\mu_{23} = 43/1080 - 2\mu_{22} + \sqrt{95/14 - 675\mu_{22}}/54,$$
$$\mu_{24} = 19/1080 - \mu_{22} + \sqrt{19/70 - 27\mu_{22}}/27. \tag{98}$$

The positivity behavior of $\mathbf{M}_\mu^e$ as μ_{22} is varied is shown in Fig. 13a. $\mathbf{M}^{(e)}$ is indefinite for $\mu_{22} < \mu_{22}^{min} = (27 - 4\sqrt{35})/5040 = 0.0006618414419844316$. At the other extreme the solutions of (98) become complex if $\mu_{22} > \mu_{22}^{max} = 19/1890 = 0.010052910052910053$.

Figure 13b plots $C_{12}(\mu_{22}) = (-111545 - 3008\psi + 15120(525 + 4\psi)\mu_{22})/685843200$, with $\psi = \sqrt{70\sqrt{19 - 1890\mu_{22}}}$. This has one real root $\mu_{22}^z = -0.02830257472322391$, but that gives an indefinite mass matrix. For μ_{22} in the legal range $[\mu_{22}^{min}, \mu_{22}^{max}]$, C_{12} is minimized for $\mu_{22}^b = (25\sqrt{105} - 171)/30240 = 0.0028165928951385567$, which substituted gives the optimal mass matrix:

$$\mathbf{M}^e_{LFFO} = \frac{m^e}{30240}\begin{bmatrix} a_{11} & 1788\ell & a_{13} & -732\ell \\ & a_{22}\ell^2 & 732\ell & a_{24}\ell^2 \\ & & a_{33} & 1788\ell \\ \text{symm} & & & a_{44}\ell^2 \end{bmatrix}$$
$$= m^e\begin{bmatrix} 0.389589 & 0.059127\ell & 0.110410 & -0.024206\ell \\ & 0.012340\ell^2 & 0.024206\ell & -0.005548\ell^2 \\ & & 0.389589 & -0.059127\ell \\ & & & 0.012340\ell^2 \end{bmatrix}. \tag{99}$$

in which $a_{11} = a_{33} = 12396 - 60\sqrt{105}$, $a_{13} = 2724 + 60\sqrt{105}$, $a_{22} = a_{44} = 117 + 25\sqrt{105}$ and $a_{24} = -219 + 5\sqrt{105}$. For this set, $C_{12} = (25\sqrt{105} - 441)/91445760 = -2.021\,10^{-6}$. Another interesting value is $\mu_{22} = 13/3150 = 0.004126984126984127$, which substituted in (98) yields rational values for the other parameters: $\mu_{11} = -\mu_{13} = 23/2100$, $\mu_{12} = -\mu_{14} = -\mu_{23} = 23/4200$, $\mu_{24} = 23/4200$ and $\mu_{24} = -17/12600$. Substitution into (91) gives

$$\mathbf{M}^e_{BLFM} = \frac{m^e}{12600}\begin{bmatrix} 4818 & 729\ell & 1482 & -321\ell \\ & 172\ell^2 & 321\ell & -73\ell^2 \\ & & 4818 & -729\ell \\ \text{symm} & & & 172\ell^2 \end{bmatrix}$$
$$= m^e\begin{bmatrix} 0.382381 & 0.057857\ell & 0.117619 & -0.025476\ell \\ & 0.013651\ell^2 & 0.025476\ell & -0.005794\ell^2 \\ & & 0.382381 & -0.057857\ell \\ \text{symm} & & & 0.013651\ell^2 \end{bmatrix}. \tag{100}$$

For this matrix, $C_{12} = -41/18144000 = -2.26\,10^{-6}$. Its magnitude is only about 10 % higher than for the truly LFF optimal (99). Since its entries are simpler, (100) is adopted as BLFM matrix for the BE element, and used as a baseline for the Timoshenko beam element investigated in Sect. 7.

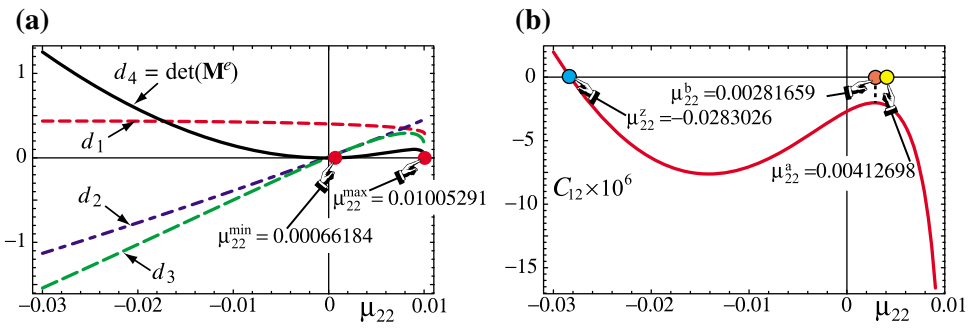

Fig. 13 Behavior of $\mathbf{M}_\mu^e$ as function of μ_{22} with other parameters given by (98): **a** determinants d_k of principal minors of order k of $\mathbf{M}_\mu^e$, showing legal positivity range $\{\mu_{22}^{min}, \mu_{22}^{max}\}$, **b** coefficient C_{12} of κ^{12} in ABTS series

7 The Timoshenko Plane Beam Element

This last example is far more elaborate than the previous ones. The goal is to construct a mass template for the prismatic, plane beam Timoshenko model, a name often abbreviated to *Ti-beam*. It includes the BE model as special case; consequently results can be crosschecked with those of Sect. 6.2. One interesting feature of this model is that the continuum dispersion diagram has *two branches*, both of which are *physical*.

The "acoustical-like branch", which has zero frequency at zero wavenumber, corresponds to lower-frequency bending oscillations in which the beam displaces transversely. The "optical-like branch", which exhibits a nonzero cutoff frequency, corresponds to higher frequency shear oscillations. Because of these interpretations, they are called the *flexural frequency branch* (FFB) and the *shear frequency branch* (SFB), respectively. They are identified by subscripts f and s, respectively, for the continuum model, while a and o are reused for the FEM discretization. Both branches are dispersive, meaning that group velocity depends on wavenumber. Those velocities tend to finite values, except in the BE limit.

The upshoot of these complications is that LFCF customization, which was so clear-cut with Bar3, becomes ambiguous: do we want to fit the FFB or the SSB? For thin beams, (as well as in the BE limit, in which case the SSB moves to ∞) the FFB is dominant. But as the beam becomes progressively thicker (as measured by a slenderness coefficient introduced in Sect. 7.1) the situation is less clear: for an extremely thick beam the shear oscillations may well dominate (of course in that case the Timoshenko model is questionable).

The continuum model is first studied in some detail, since frequency expansion formulas applicable to template customization by characteristic root fitting are not available in the literature.

7.1 Ti-Beam Continuum Elastodynamic Analysis

Consider a structural beam member modeled as a shear-flexible Timoshenko plane beam (Ti-beam), as illustrated in Fig. 14. This figure provides the notation used below. Section properties $\{\rho, E, A, A_s, I, I_R\}$ are constant along x. The beam is transversally loaded by line load $q(x,t)$ (not shown in figure), with dimension of force per length. The primary kinematic variables are the transverse deflection $v(x,t)$ and the total cross-section rotation $\theta(x,t) = v'(x,t) + \gamma(x,t)$, where $\gamma = V/(GA_s)$ is the mean shear rotation. The kinetic and potential energies in terms of those variables are

$$T[v,\theta] = \tfrac{1}{2}\int_0^L \left(\rho A\,\dot{v}^2 + \rho I_R\,\dot{\theta}^2\right) dx,\quad \Pi[v,\theta] = \int_0^L \left(\tfrac{1}{2}EI\,(v'')^2 + \tfrac{1}{2}GA_s(\theta - v')^2 - qv\right) dx. \tag{101}$$

where superposed dots denote time derivatives. The equations of motion (EOM) follow on forming the Euler equations from the Lagrangian $L = T - \Pi$:

$$\frac{\delta L}{\delta v} = 0 \to GA_s\,(\theta' - v'') + \rho A\ddot{v} = q,\quad \frac{\delta L}{\delta \theta} = 0 \to EI\,\theta'' + GA_s\,(v' - \theta) - \rho I_R\,\ddot{\theta} = 0. \tag{102}$$

An expedient way to eliminate θ is to rewrite the coupled equations (102) in transform space:

$$\begin{bmatrix} \rho A s^2 - GA_s\,p^2 & GA_s\,p \\ GA_s\,p & EI\,p^2 - GA_s - \rho\,I_R\,s^2 \end{bmatrix} \begin{bmatrix} \tilde{v} \\ \tilde{\theta} \end{bmatrix} = \begin{bmatrix} \tilde{q} \\ 0 \end{bmatrix}, \tag{103}$$

in which $\{p, s, \tilde{v}, \tilde{\theta}, \tilde{q}\}$ denote transforms of $\{d/dx, d/dt, v, \theta, q\}$, respectively (Fourier in x and Laplace in t). Eliminat-

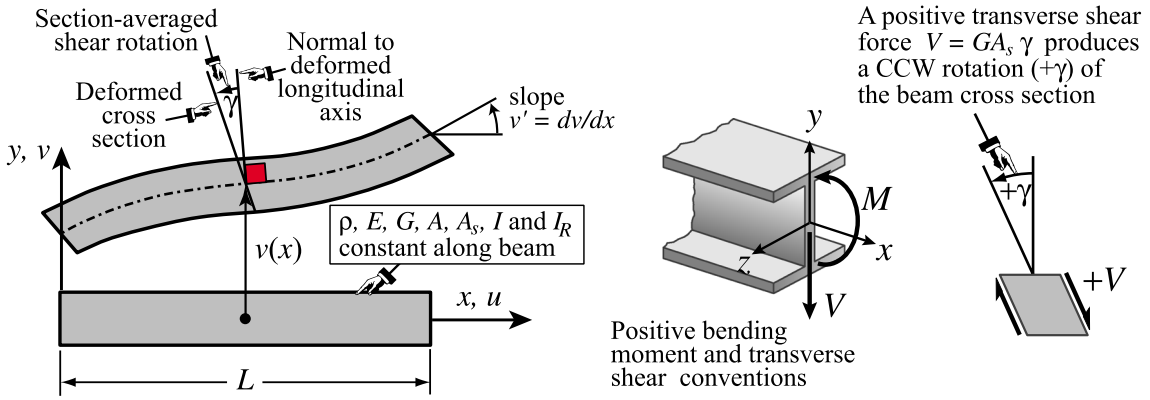

Fig. 14 Plane beam member modeled as Ti-beam, illustrating notation followed in Sect. 7.1. Transverse load $q(x)$ not shown to reduce clutter. Infinitesimal deflections and deformations grossly exaggerated for visibility

ing $\tilde{\theta}$ and returning to the physical domain yields

$$EI\,v'''' + \rho A\ddot{v} - \left(\rho I_R + \frac{\rho AEI}{GA_s}\right)\ddot{v}'' + \frac{\rho^2 AI_R}{GA_s}\ddddot{v} = q - \frac{EI}{GA_s}q'' + \frac{\rho I_R}{GA_s}\ddot{q}. \tag{104}$$

This derivation does not preset $I \equiv I_R$, as usually done in textbooks. For the unforced case $q = 0$, (104) has plane wave solutions $v = B\,\exp\big(i\,(k_0\,x - \omega_0\,t)\big)$. The propagation condition yields a characteristic equation relating k_0 and ω_0. To render it dimensionless, introduce a reference phase velocity $c_0^2 = EI/(\rho AL^4)$ so that $k_0 = \omega_0/c_0 = 2\pi/\lambda_0$, a dimensionless frequency $\Omega = \omega_0 L/c_0$ and a dimensionless wavenumber $\kappa = k_0 L$.

As dimensionless measures of relative bending-to-shear rigidities and rotary inertia take

$$\Phi_0 = 12EI/(GA_sL^2), \qquad r_R^2 = I_R/A, \qquad \Psi_0 = r_R/L. \tag{105}$$

The resulting dimensionless characteristic equation is

$$\kappa^4 - \Omega^2 - (\tfrac{1}{12}\Phi_0 + \Psi_0^2)\,\kappa^2\,\Omega^2 + \tfrac{1}{12}\Phi_0\,\Psi_0^2\,\Omega^4 = 0. \tag{106}$$

This is quadratic in Ω^2. Its solution yields two kinds of squared-frequencies, which will be denoted by Ω_f^2 and Ω_s^2 in which $P = 1+\kappa^2(\Psi_0^2+\frac{1}{12}\Phi_0)$ and $Q = P^2 - \frac{1}{3}\kappa^4\Phi_0\Psi_0^2$. The dispersion relation $\Omega_f^2(\kappa)$ defines the *flexural frequency branch* (FFB) whereas $\Omega_s^2(\kappa)$ defines the *shear frequency branch* (SFB). If $\Phi_0 \to 0$ and $\Psi_0 \to 0$, which reduces the the Ti model to BE, (106) collapses to $\Omega^2 = \kappa^4$ or (in principal value) $\Omega = \kappa^2$. This surviving branch pertains to flexural motions whereas the shear branch disappears; more precisely, $\Omega_s^2(\kappa) \to \infty$.

It is easily shown that the radicand Q in the exact expressions is strictly positive for any $\{\Phi_0 > 0, \Psi_0 > 0, \kappa \geq 0\}$. Thus for any such triple, Ω_f^2 and Ω_s^2 are real, finite and distinct with $\Omega_f^2(\kappa) < \Omega_s^2(\kappa)$. Further $\{\Omega_f^2, \Omega_s^2\}$ increase indefinitely as $\kappa \to \infty$. Following the dispersion-diagram nomenclature introduced in Fig. 8, the value Ω_s at $\kappa = 0$ is called the *cutoff frequency*.

To see what branches look like, consider a beam of narrow rectangular cross section of width b and height h, fabricated of isotropic material with Poisson's ratio ν. Accordingly $E/G = 2(1+\nu)$ and $A_s/A \approx 5/6$ (actually a more refined A_s/A ratio would be $10(1+\nu)/(12+11\nu)$, but that makes little difference in the results). We have $A = bh$, $I = I_R = bh^3/12$, $r_R^2 = I_R/A = h^2/12$, $\Psi_0^2 = r_R^2/L^2 = \frac{1}{12}h^2/L^2$ and $\Phi_0 = 12EI/(GA_sL^2) = 12(1+\nu)h^2/(5L^2)$. Since $\Phi_0/12 = 12(1+\nu)\,\Psi_0^2/5$, the first-order effect of shear on Ω_f^2, as measured by the κ^6 term in (107), is 2.4 to 3.6 times that from rotary inertia, depending on ν. Replacing into (107) and (108) yields

$$\left.\begin{matrix}\Omega_f^2\\ \Omega_s^2\end{matrix}\right\} = \frac{60+\kappa^2(17+12\nu)\Lambda^2 \mp \sqrt{\big(60+\kappa^2(17+12\nu)\Lambda^2\big)^2 - 240\kappa^4(1+\nu)\Lambda^4}}{2(1+\nu)\Lambda^4} = \begin{cases}\kappa^4 - \frac{1}{60}(17+12\nu)\Lambda^2\kappa^6 + \frac{1}{3600}(349+468\nu+144\nu^2)\Lambda^4\kappa^8 + \cdots\\ \dfrac{60+(17+12\nu)\Lambda^2\kappa^2 - (1+\nu)\Lambda^4\kappa^4 + \ldots}{(1+\nu)\Lambda^4}\end{cases} \tag{109}$$

because they are associated with flexural and shear modes, respectively. Their expressions are listed below along with their small-κ (long wavelength) Taylor series:

$$\Omega_f^2 = 6\frac{P-\sqrt{Q}}{\Phi_0\Psi_0^2} = \kappa^4 - (\tfrac{1}{12}\Phi_0 + \Psi_0^2)\,\kappa^6 + \left(\frac{1}{144}\Phi_0^2 + \tfrac{1}{4}\Phi_0\Psi_0^2 + \Psi_0^4\right)\kappa^8 - (\frac{1}{1728}\Phi_0^3 + \frac{1}{24}\Phi_0^2\Psi_0^2 + \tfrac{1}{2}\Phi_0\Psi_0^4 + \Psi_0^6)\,\kappa^{10} + \cdots = A_4\kappa^4 + A_6\kappa^6 + A_8\kappa^8 + \cdots. \tag{107}$$

$$\Omega_s^2 = 6\frac{P+\sqrt{Q}}{\Phi_0\Psi_0^2} = \frac{12}{\Phi_0\Psi_0^2} + \left(\frac{12}{\Phi_0} + \frac{1}{\Psi_0^2}\right)\kappa^2 - \kappa^4 + (\tfrac{1}{12}\Phi_0 + \Psi_0^2)\kappa^6 + \cdots = B_0 + B_2\kappa^2 + \cdots, \tag{108}$$

in which $\Lambda = h/L$. Dispersion curves $\Omega(\kappa)$ for $\Lambda = h/L = \frac{1}{4}$ and $\nu = \{0, \frac{1}{2}\}$ are plotted in Fig. 15a. Phase velocities Ω/κ are shown in Fig. 15b. The figure also shows the flexural branch of the BE model. The phase velocities of the Timoshenko model tend to finite values in the shortwave, high-frequency limit $\kappa \to \infty$, which is physically correct. The BE model is physically wrong in that limit because it predicts an infinite propagation speed.

7.2 Ti-Beam Element

The shear-flexible plane beam member of Fig. 14 is discretized by two-node elements. An individual element of this type is shown in Fig. 16, which illustrates its kinematics. The element has four nodal freedoms arranged as

$$\mathbf{u}^e = \begin{bmatrix} v_1 & \theta_1 & v_2 & \theta_2 \end{bmatrix}^T \tag{110}$$

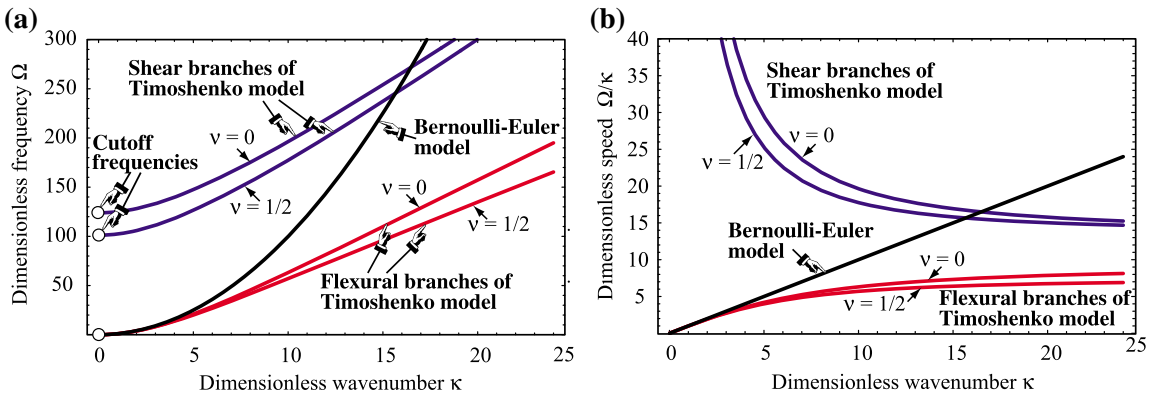

Fig. 15 Spectral behavior of continuum Ti-beam model for a narrow $b \times h$ rectangular cross section. **a** Dispersion curves $\Omega(\kappa)$ for $\Lambda = h/\ell = 1/4$ and two Poisson's ratios; Timoshenko flexural and shear branches in *red* and *blue*, respectively; BE curve $\Omega = \kappa^2$ in *black*, **b** Wavespeed $\partial\Omega/\partial\kappa$. (Color figure online)

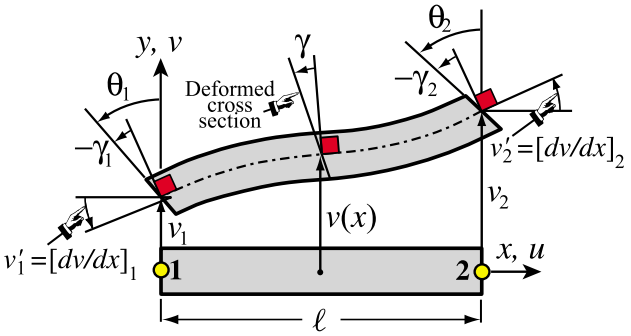

Fig. 16 Two-node element for Timoshenko plane beam, illustrating kinematics

Here $\theta_1 = v_1 + \gamma_1$ and $\theta_2 = v_2 + \gamma_2$ are the *total cross section rotations* evaluated at the end nodes. The dimensionless properties (105) that characterize relative shear rigidity and rotary inertia are redefined using the element length:

$$\Phi = 12EI/(GA_s\ell^2), \qquad r_R^2 = I_R/A, \qquad \Psi = r_R/\ell. \tag{111}$$

If the beam member is divided into N_e elements of equal length, $\ell = L/N_e$ whence $\Phi = \Phi_0 N_e^2$ and $\Psi = \Psi_0 N_e$. Thus even if Φ_0 and Ψ_0 are small with respect to one, they can grow without bound as the mesh is refined. For example if $\Phi_0 = 1/4$ and $\Psi_0^2 = 1/100$, which are typical values for a moderately thick beam, and we take $N_e = 32$, then $\Phi \approx 250$ and $\Psi^2 \approx 10$. Those are no longer small numbers, a fact that will impact performance as N_e increases. The stiffness matrix to be paired with the mass template is taken to be that of the equilibrium element:

$$\mathbf{K}^e = \frac{EI}{\ell^3(1+\Phi)}\begin{bmatrix} 12 & 6\ell & -12 & 6\ell \\ 6\ell & \ell^2(4+\Phi) & -6\ell & \ell^2(2-\Phi) \\ -12 & -6\ell & 12 & -6\ell \\ 6\ell & \ell^2(2-\Phi) & -6\ell & \ell^2(4+\Phi) \end{bmatrix}. \tag{112}$$

This is known to be optimal in static analysis for a prismatic beam member. It will be kept fixed in the ensuing derivations. It reduces to the stiffness matrix (93) of the BE model if $\Phi = 0$.

7.3 The Ti-Beam Mass Template

FEM derivations usually split the 4×4 mass matrix of this element into $\mathbf{M}^e = \mathbf{M}^e_v + \mathbf{M}^e_\theta$, where $\mathbf{M}^e_v$ and $\mathbf{M}^e_\theta$ come from the translational inertia and rotary inertia terms, respectively, of the kinetic energy functional $T[v, \theta]$ of (101). The most general mass template would result from applying a EW parametrization of those two matrices. This would require a set of 20 parameters (10 in each matrix), reducible to 9 through 11 on account of invariance and conservation conditions. Attacking the problem this way, however, leads to unwieldy algebraic equations even with the help of a CAS, while concealing the underlying physics. A divide and conquer approach works better. This is briefly outlined next and covered in more detail in the next subsections.

(I) Express $\mathbf{M}^e$ as the one-parameter matrix-weighted form $\mathbf{M}^e = (1-\mu_0)\,\mathbf{M}^e_F + \mu_0\,\mathbf{M}^e_D$. Here $\mathbf{M}^e_F$ is full and includes the CMM as instance, whereas $\mathbf{M}^e_D$ is 2×2 block diagonal and includes the DLMM as instance. This is plainly a generalization of the LC linear combination (2).

(II) Decompose the foregoing mass components as $\mathbf{M}^e_F = \mathbf{M}^e_{FT} + \mathbf{M}_{FR}$ and $\mathbf{M}^e_D = \mathbf{M}^e_{DT} + \mathbf{M}^e_{DR}$, where T and R subscripts identify their source in the kinetic energy functional: T if coming from the translational inertia term $\frac{1}{2}\rho A\,\dot{v}^2$ and R from the rotary inertia term $\frac{1}{2}\rho I_R\,\dot{\theta}^2$.

(III) Both components of $\mathbf{M}^e_F$ are expressed as parametrized spectral forms, whereas those of $\mathbf{M}^e_D$ are expressed as EW. The main reasons for choosing spectral forms for the full matrix are reduction of parameters and physical transparency. No such concerns apply to $\mathbf{M}^e_D$.

The analysis follows a "bottom up" sequence, in order (III)–(II)–(I). This has the advantage that if a satisfactory

custom mass matrix for a target application emerges during (III), stages (II) and (I) need not be carried out, and that matrix directly used by setting the remaining parameters to zero.

7.4 Ti-Beam Full Mass Parametrization

As noted above, one starts with full-matrix spectral forms. Let ξ denote the natural iso-P coordinate that varies from -1 at node 1 to $+1$ at node 2. Two element transverse displacement expansions in generalized coordinates are introduced:

$$\begin{aligned} v_T(\xi) &= L_1(\xi)\, c_{T1} + L_2(\xi)\, c_{T2} + L_3(\xi)\, c_{T3} \\ &\quad + L_4(\xi)\, c_{T4} = \mathbf{L}_T\, \mathbf{c}_T, \\ v_R(\xi) &= L_1(\xi)\, c_{R1} + L_2(\xi)\, c_{R2} + L_3(\xi)\, c_{R3} \\ &\quad + \widehat{L}_4(\xi)\, c_{R4} = \mathbf{L}_R\, \mathbf{c}_R, \\ L_1(\xi) &= 1,\ L_2(\xi) = \xi,\ L_3(\xi) = \tfrac{1}{2}(3\xi^2 - 1), \\ L_4(\xi) &= \tfrac{1}{2}(5\xi^3 - 3\xi), \\ \widehat{L}_4(\xi) &= \tfrac{1}{2}\big(5\xi^3 - (5 + 10\Phi)\xi\big) = L_4(\xi) - (1 + 5\Phi)\xi. \end{aligned} \tag{113}$$

The v_T and v_R expansions are used for the translational and rotational parts of the kinetic energy, respectively. The interpolation function set $\{L_i\}$ used for v_T is formed by the first four Legendre polynomials over $\xi = [-1, 1]$. The set used for v_R is the same except that L_4 is adjusted to $\widehat{L}_4$ to produce a diagonal rotational mass matrix. All amplitudes c_{Ti} and c_{Ri} have dimension of length.

Unlike the usual Hermite cubic shape functions, the polynomials in (113) have a direct physical interpretation. L_1: translational rigid mode; L_2: rotational rigid mode; L_3: pure-bending mode symmetric about $\xi = 0$; L_4 and $\widehat{L}_4$: bending-with-shear mode antisymmetric about $\xi = 0$.

With the abbreviation $(.)' \equiv d(.)/dx = (2/\ell)d(.)/d\xi$, the associated cross section rotations are compactly expressed as

$$\theta_T = v_T' + \gamma_T = \mathbf{L}_T' \mathbf{c}_T + \gamma_T, \quad \theta_R = v_R' + \gamma_R = \mathbf{L}_R' \mathbf{c}_R + \gamma_R, \tag{114}$$

in which the mean shear distortions are constant over the element:

$$\gamma_T = \frac{\Phi \ell^2}{12} v_T''' = \frac{10\Phi}{\ell} c_{T4}, \quad \gamma_R = \frac{\Phi \ell^2}{12} v_R''' = \frac{10\Phi}{\ell} c_{R4}. \tag{115}$$

The kinetic energy of the element in generalized coordinates is

$$\begin{aligned} T^e &= \tfrac{1}{2} \int_0^\ell \big(\rho A\, \dot{v}_T^2 + \rho I_R\, \dot{\theta}_R^2\big)\, dx \\ &= \frac{\ell}{4} \int_{-1}^{1} \big(\rho A\, \dot{v}_T^2 + \rho I_R\, \dot{\theta}_R^2\big)\, d\xi \\ &= \tfrac{1}{2} \dot{\mathbf{c}}_T^T\, \mathbf{D}_T\, \dot{\mathbf{c}}_T + \tfrac{1}{2} \dot{\mathbf{c}}_R^T\, \mathbf{D}_R\, \dot{\mathbf{c}}_R, \end{aligned} \tag{116}$$

Both generalized mass matrices turn out to be diagonal as expected:

$$\begin{aligned} \mathbf{D}_T &= m^e\, \mathbf{diag}\big[\,1 \quad \tfrac{1}{3} \quad \tfrac{1}{5} \quad \tfrac{1}{7}\,\big], \\ \mathbf{D}_R &= 4m^e\, \Psi^2\, \mathbf{diag}\big[\,0 \quad 1 \quad 3 \quad 5\,\big], \end{aligned} \tag{117}$$

in which as usual $m^e = \rho\, A\, \ell$. To convert $\mathbf{D}_T$ and $\mathbf{D}_R$ to physical coordinates (110), v_T, v_R, θ_T and θ_R are evaluated at the nodes by setting $\xi = \pm 1$. This establishes the transformations $\mathbf{u}^e = \mathbf{G}_T\, \mathbf{c}_T$ and $\mathbf{u}^e = \mathbf{G}_R\, \mathbf{c}_R$. Inverting: $\mathbf{c}_T = \mathbf{H}_T\, \mathbf{u}^e$ and $\mathbf{c}_R = \mathbf{H}_R\, \mathbf{u}^e$ with $\mathbf{H}_T = \mathbf{G}_T^{-1}$ and $\mathbf{H}_R = \mathbf{G}_R^{-1}$. A symbolic calculation yields for $\mathbf{H}_T$:

$$\mathbf{H}_T = \frac{1}{60(1+\Phi)} \begin{bmatrix} 30(1+\Phi) & 5\ell(1+\Phi) & 30(1+\Phi) & -5\ell(1+\Phi) \\ -36-30\Phi & -3\ell & 36+30\Phi & -3\ell \\ 0 & -5\ell(1+\Phi) & 0 & 5\ell(1+\Phi) \\ 6 & 3\ell & -6 & 3\ell \end{bmatrix}. \tag{118}$$

Matrix $\mathbf{H}_R$ differs only in the second row:

$$\mathbf{H}_R = \frac{1}{60(1+\Phi)} \begin{bmatrix} 30(1+\Phi) & 5\ell(1+\Phi) & 30(1+\Phi) & -5\ell(1+\Phi) \\ -30 & 15\ell\Phi & 30 & 15\ell\Phi \\ 0 & -5\ell(1+\Phi) & 0 & 5\ell(1+\Phi) \\ 6 & 3\ell & -6 & 3\ell \end{bmatrix}. \tag{119}$$

The difference comes from adjusting L_4 to $\widehat{L}_4$ in (113). To map this into a spectral template, inject six free parameters in the generalized masses while moving $4\Psi^2$ inside $\mathbf{D}_{R\mu}$:

$$\begin{aligned} \mathbf{D}_{T\mu} &= m^e\, \mathbf{diag}\big[\,1 \quad \tfrac{1}{3}\mu_{T1} \quad \tfrac{1}{5}\mu_{T2} \quad \tfrac{1}{7}\mu_{T3}\,\big], \quad \mathbf{D}_{R\mu} \\ &= m^e\, \mathbf{diag}\big[\,0 \quad \mu_{R1} \quad 3\mu_{R2} \quad 5\mu_{R3}\,\big]. \end{aligned} \tag{120}$$

The transformation matrices (118) and (119) can be reused without change to produce $\mathbf{M}_F^e = \mathbf{H}_T^T \mathbf{D}_{T\mu} \mathbf{H}_T + \mathbf{H}_R^T \mathbf{D}_{R\mu} \mathbf{H}_R$. If $\mu_{T1} = \mu_{T2} = \mu_{T3} = 1$ and $\mu_{R1} = \mu_{R2} = \mu_{R3} = 4\Psi^2$ one obtains the well known CMM as a valuable check. The configuration (120) already accounts for linear momentum conservation, which is why the upper diagonal entries are not parametrized. Enforcing also angular momentum conservation requires $\mu_{T1} = 1$ and $\mu_{R1} = 4\Psi^2$, whence the template is reduced to four parameters:

$$\mathbf{M}_F^e = m^e\,\mathbf{H}_T^T \begin{bmatrix} 1 & 0 & 0 & 0 \\ 0 & \frac{1}{3} & 0 & 0 \\ 0 & 0 & \frac{1}{5}\mu_{T2} & 0 \\ 0 & 0 & 0 & \frac{1}{7}\mu_{T3} \end{bmatrix} \mathbf{H}_T + m^e\,\mathbf{H}_R^T \begin{bmatrix} 0 & 0 & 0 & 0 \\ 0 & 4\Psi^2 & 0 & 0 \\ 0 & 0 & 3\mu_{R2} & 0 \\ 0 & 0 & 0 & 5\mu_{R3} \end{bmatrix} \mathbf{H}_R. \quad (121)$$

Since both $\mathbf{H}_T$ and $\mathbf{H}_R$ are nonsingular, choosing all parameters in (121) to be nonnegative guarantees that $\mathbf{M}_F^e$ is nonnegative. This property eliminates lengthy *a posteriori* checks.

Setting $\mu_{T2} = \mu_{T3} = \mu_{R2} = \mu_{R3} = 0$ and $\Phi = 0$ yields the correct mass matrix for a *rigid* beam, including rotary inertia. This simple result highlights the physical transparency of spectral forms.

7.5 Ti-Beam Block-Diagonal Mass Parametrization

Template (121) has a flaw: it does not include the DLMM. To remedy the omission, a block diagonal form, with four free parameters: ν_{T1}, ν_{T2}, ν_{R1}, and ν_{R2} is separately constructed:

$$\mathbf{M}_D^e = m^e \begin{bmatrix} \frac{1}{2} & \nu_{T1}\ell & 0 & 0 \\ \nu_{T1}\ell & \nu_{T2}\ell^2 & 0 & 0 \\ 0 & 0 & \frac{1}{2} & -\nu_{T1}\ell \\ 0 & 0 & -\nu_{T1}\ell & \nu_{T2}\ell^2 \end{bmatrix} + m^e \begin{bmatrix} 0 & \nu_{R1}\ell & 0 & 0 \\ \nu_{R1}\ell & \nu_{R2}\ell^2 & 0 & 0 \\ 0 & 0 & 0 & -\nu_{R1}\ell \\ 0 & 0 & -\nu_{R1}\ell & \nu_{R2}\ell^2 \end{bmatrix}. \quad (122)$$

Four parameters can be merged into two by adding the foregoing matrices:

$$\mathbf{M}_D^e = m^e \begin{bmatrix} \frac{1}{2} & \nu_1\ell & 0 & 0 \\ \nu_1\ell & \nu_2\ell^2 & 0 & 0 \\ 0 & 0 & \frac{1}{2} & -\nu_1\ell \\ 0 & 0 & -\nu_1\ell & \nu_2\ell^2 \end{bmatrix}. \quad (123)$$

in which $\nu_1 = \nu_{T1} + \nu_{R1}$ and $\nu_2 = \nu_{T2} + \nu_{R2}$. Sometimes it is convenient to use the split form (122), for example in lattices with varying beam properties or lengths, a topic not considered there. Otherwise (123) suffices. If $\nu_1 = 0$, $\mathbf{M}_D^e$ is diagonal. However for computational purposes a block diagonal form is just as good and provides additional customization power. Terms in the (1,1) and (3,3) positions must be as shown to satisfy linear momentum conservation. If angular momentum conservation is imposed *a priori* it is necessary to set $\nu_2 = \frac{1}{2}\Psi^2$, and only one parameter: ν_1, remains.

The general template is obtained as a linear combination of $\mathbf{M}_F^e$ and $\mathbf{M}_D^e$:

$$\mathbf{M}^e = (1-\mu_0)\mathbf{M}_F^e + \mu_0\mathbf{M}_D^e \quad (124)$$

In summary, there is a total of 7 parameters to play with: 4 in $\mathbf{M}_F^e$, 2 in $\mathbf{M}_D^e$, plus μ_0. This is less that the 9-to-11 count that would result from a full EW parametrization, so not all possible mass matrices for this element are included by (124).

7.6 Ti-Beam Fourier Analysis

An infinite lattice of identical Ti-beam elements of length ℓ is set up in th usual manner. As in Sect. 6.2, plane waves of wavenumber k and frequency ω propagating over the lattice are represented by

$$v(x,t) = B_v\,\exp\big(i(kx-\omega t\big), \quad \theta(x,t) = B_\theta\,\exp\big(i(kx-\omega t\big). \quad (125)$$

At each typical lattice node j there are two freedoms: v_j and θ_j. Two patch equations are extracted, and converted to dimensionless form on defining $\kappa = k\ell$ and $\Omega = \omega\, c/\ell$, in which $c = EI/(\rho A\ell^4)$ is a reference phase velocity (these should not be confused with c_0). The condition for wave propagation gives the characteristic matrix equation

$$\det \begin{bmatrix} C_{vv} & C_{v\theta} \\ C_{\theta v} & C_{\theta\theta} \end{bmatrix} = C_{vv}C_{\theta\theta} - C_{v\theta}C_{\theta v} = 0, \quad (126)$$

in which the coefficients are complicated functions computed by *Mathematica* and omitted for brevity. Solving the equation provides two equations: Ω_a^2 and Ω_o^2, where a and o denote acoustic and OB, respectively. These are expanded in powers of κ for matching to the continuum. For the full mass matrix one obtains

$$\overset{2}{\Omega}_a = \kappa^4 + C_6\kappa^6 + C_8\kappa^8 + C_{10}\kappa^{10} + \cdots, \quad \Omega_o^2 = D_0 + D_2\kappa^2 + \cdots \quad (127)$$

Coefficients of terms up to κ^{12} were computed by *Mathematica*. Those relevant for parameter selection are

$$\begin{aligned} C_6 &= -\Phi/12 - \Psi^2, \\ C_8 &= \big[2 - 15\mu_{R2} - \mu_{T2} + 5\Phi(1+\Phi) \\ &\quad + 60(1+3\Phi)\Psi^2 + 720\Psi^4\big]/720, \\ C_{10} &= \big[-44 + 35\mu_{T2} - 3\mu_{T3} - 282\Phi + 525\mu_{R2}(1+\Phi) \\ &\quad - 105\mu_{R3}(1+\Phi) \\ &\quad + 1575\mu_{R2}\Phi(1+\Phi) - \Phi(3\mu_{T3} - 35\mu_{T2}(4+3\Phi) \\ &\quad + 35\Phi(17 + 5\Phi(3+\Phi))) \\ &\quad + (-2940 + 12600\mu_{R2}(1+\Phi) + 420(2\mu_{T2}(1+\Phi) \end{aligned}$$

$$
\begin{aligned}
&\quad -5\Phi(7+6\Phi(2+\Phi))))\Psi^2\\
&\quad -25200(2+\Phi(7+6\Phi))\Psi^4\\
&\quad -302400(1+\Phi)\Psi^6\big]/\big[302400(1+\Phi)\big],\\
D_0 &= 25200(1+\Phi)/\big[7+105\mu_{R2}+3\mu_{T3}+2100\Phi^2\Psi^2\big],\\
D_2 &= \big[2100(1+\Phi)(-56-35\mu_{T2}+3\mu_{T3}-63\Phi\\
&\quad +3\mu_{T3}\Phi+105\mu_{R3}(1+\Phi)\\
&\quad -525\mu_{R2}(1+\Phi)^2-35\mu_{T2}\Phi(2+\Phi))\\
&\quad +2100(1+\Phi)(3360\Phi+6300\Phi^2\\
&\quad +2100\Phi^3)\Psi^2+52920000\Phi^2(1+\Phi)\Psi^4\big]/\big[7\\
&\quad +105\mu_{R2}+3\mu_{T3}+2100\Phi^2\Psi^2\big]^2. \qquad (128)
\end{aligned}
$$

For the block-diagonal template (123):

$$
\begin{aligned}
\Omega_a^2 &= \kappa^4+F_6\kappa^6+F_8\kappa^8+F_{10}\kappa^{10}+\cdots,\\
\Omega_o^2 &= G_0+G_2\kappa^2+\cdots \qquad (129)
\end{aligned}
$$

in which

$$
\begin{aligned}
F_6 &= -24\nu_2-\Phi,\\
F_8 &= \frac{2880\nu_2-5\Phi+360\nu_2\Phi-1-5\Phi+5\Phi^2}{720}\\
G_0 &= \frac{6}{\nu_2(1+\Phi)},\quad G_2=\frac{24\nu_2+\Phi-2}{2\nu_2(1+\Phi)}. \qquad (130)
\end{aligned}
$$

Expansions for the 7-parameter template (124) are considerably more involved than the above ones, and are omitted for brevity.

7.7 Ti-Beam Selected Template Instances

Seven useful instances of the foregoing templates are identified and described in Table 11. Table 12 lists the template signatures that produce those instances. These tables include two well known mass matrices (CMM and DLMM) re-expressed in the template context, and five new ones. The latter were primarily obtained by matching series such as (128) and (129) to the continuum ones (107) and (108), up to a certain number of terms as indicated in Table 12.

For the spectral template it is possible to match the flexure branch up to $O(\kappa^{10})$. Trying to match $O(\kappa^{12})$ leads to complex solutions. For the diagonal template the choice is more restrictive. It is only possible to match flexure up to $O(\kappa^6)$, which leads to the instance called FLMM. Trying to go further gives imaginary solutions. For the 7-parameter template (124) it is again possible to match up to $O(\kappa^{10})$ but no further. The instance that exhibits least truncation error while retaining positivity is FBMG. This is globally optimal for the BE limit $\Phi=\Psi=0$, but the results are only slightly better for the reasons discussed below. Matching both flexure and shear branches leads to instances SBM0 and SBM2, which have the disadvantages noted in Table 11.

The exact dispersion curves of these instances are shown in Fig. 17 for $\Phi=48/125$ and $\Psi^2=1/75$, which pertains to a thick beam. On examining Fig. 17 it is obvious that trying to match the shear branch is quite difficult; the fit only works well over a tiny range near $\kappa=0$.

7.8 Ti-Beam Vibration Analysis Example

The vibration analysis performance of the seven Ti-beam template instances listed in Tables 11 and 12 is evaluated on a simply supported (SS) prismatic plane beam. The beam has length L and is divided into N_e identical elements. The cross section is rectangular with width b and height h. The material is isotropic with Poisson's ratio $\nu=0$. Three different height-to-span ratios h/L that characterize a thin, moderately thick and thick beam, respectively, are considered. Results for the three configurations are collected in Figs. 18, 19 and 20, respectively, for the first three vibration frequencies. All calculations are rendered dimensionless using appropriate scaling.

The accuracy of the computed frequencies is depicted using log-log plots of dimensionless natural frequency error versus N_e. The error is displayed as $d=\log_{10}(|\Omega_{comp}-\Omega_{exact}|$, which gives at a glance the number of correct digits d, versus $\log_2 N_e$ for $N_e=1$ through 32. If the LF error is approximately controlled by a truncation term of the form $\propto\kappa^m$, the log-log plot should be roughly a straight line of slope $\propto m$, inasmuch as $\kappa=k\ell=kL/N_e$ (note that the accuracy curves for CMM and FLMM are virtually on top of each other for $N_e\geq 4$, although errors have opposite signs; that is why their average CDLA does much better).

The results for the BE model, shown in Fig. 18, agree perfectly with the truncation error in the Ω_f^2 branch as listed in Table 11. For example, the top performers FBMG and FBMS gain digits twice as fast as CMM, DLMM and SBM2, since the formers match Ω_f^2 to $O(\kappa^{10})$ whereas the latter do that only to $O(\kappa^6)$. Instances CDLA and SMB0, which agree through $O(\kappa^8)$, come in between. The highly complicated FBMG is only slightly better than the much simpler FBMS. The case for their high accuracy should be emphasized. For example, four FBMS elements give Ω_1 to six figures: 9.86960281... versus $\pi^2=9.86960440...$, whereas CMM gives less than three: 9.87216716.... The "accuracy ceiling" of about 11 digits for FBMS and FBMG observable for $N_e>16$ is due to the eigensolver working in double precision ($\approx$ 16 digits). Rerunning with higher (quad) floating point precision, the plots continues marching up as straight lines before leveling off at approximately 25 digits.

On passing to the Timoshenko model, the well ordered BE world of Fig. 18 unravels. The culprits are Φ and Ψ. These figure prominently in the branch series and grow without bound as N_e increases, as discussed in Sect. 7.2. Figure 19

Table 11 Ti-beam selected template instances

Instance name	Description	Comments
CMM	Consistent mass matrix derived in Sect. 1. Matches FFB up to $O(\kappa^6)$	A popular choice. Fairly inaccurate, however, as beam gets thicker. Grossly overestimates intermediate frequencies
FBMS	FFB matched to $O(\kappa^{10})$ with spectral (Legendre) template (121)	Converges faster than CMM. Performance degrades as beam gets thicker, however, and becomes inferior to CDLA
SBM0	SFB matched to $O(\kappa^0)$ while flexure fitted to $O(\kappa^{10})$	Custom application: to roughly match SBF and cutoff frequency as mesh is refined. Warning: indefinite for certain ranges of Φ and Ψ: use with caution
SBM2	SBF matched to $O(\kappa^2)$ while flexure fitted to $O(\kappa^8)$	Custom application: to finely match SFB and cutoff frequency as mesh is refined. Warning: indefinite for wide ranges of Φ and Ψ: use with extreme caution
FLMM	Diagonally lumped mass matrix with rotational mass picked to match FFB to $O(\kappa^6)$	Obvious choice for explicit DTI. Accuracy degrades significantly, however, as beam gets thicker. Underestimates frequencies. Becomes singular in the BE limit
CDLA	Average of CMM and FLMM. Matches FFB to $O(\kappa^8)$	Robust all-around choice. Less accurate than FBMS and FBMG for thin beams, but becomes top performer as beam gets thicker. Easily constructed if both CMM and FLMM are available
FBMG	FFB matched to $O(\kappa^{10})$ with 7-parameter template (124)	Known to be the globally optimal positive-definite choice for matching flexure in the BE limit. Accuracy, however, is only marginally better than FBMS. As in the case of the latter, performance degrades as beam gets thicker

Table 12 Signatures of selected Ti-beam template Instances

Instance name	Templ. form	Template signature							Fit to continuum freqs.	
		μ_{T2}	μ_{T3}	μ_{R2}	μ_{R3}	ν_1	ν_2	μ_0	Ω_f^2 (flexural)	Ω_s^2 (shear)
CMM	(121)	1	1	$4\Psi^2$	$4\Psi^2$				up to κ^6	none
FBMS	(121)	2	26/3	$4\Psi^2+\Phi/3$	c_1				up to κ^{10}	none
SMB0	(121)	2	$-7/3$	$4\Psi^2+\Phi/3$	$20\Phi\Psi^2$				up to κ^{10}	up to κ^0
SMB2	(121)	2	$-7/3$	c_2	$20\Phi\Psi^2$				up to κ^8	up to κ^2
FLMM	(123)					0	$\Psi^2/2$		up to κ^6	none
CDLA	(124)	1	1	$4\Psi^2$	$4\Psi^2$	0	$\Psi^2/2$	1/2	up to κ^8	none
FBMG	(124)	c_3	c_4	c_5	c_6	1/12	$\Psi^2/2$	c_7	up to κ^{10}	none

$c_1 = \big(25\Phi^3 + 120\Psi^2 + \Phi^2(45 - 300\Psi^2) + 3\Phi(7 - 20\Psi^2 + 1200\Psi^4)\big)/\big(15(1+\Phi)\big)$,

$c_2 = \big(-19 + 10\Phi^2(90\Psi^2 - 1) - 30\Phi(1 - 26\Psi^2 + 120\Psi^4)\big)/\big(75(1+\Phi)^2\big)$,

$c_3 = (9 + \sqrt{105})/10, \quad c_4 = (61\sqrt{105} - 483)/18, \quad c_5 = (\sqrt{105} - 1)\Phi/30,$

$c_6 = \big(-48\Phi + 727\Phi^2 + 840\Phi^3 + 22128\Psi^2 + 19848\Phi\Psi^2 - 10080\Phi^2\Psi^2 - 113040\Psi^4$
$+120960\Phi\Psi^4 + 5\sqrt{105}\,(48\Phi + 87\Phi^2 + 40\Phi^3) - 24(6 + 21\Phi + 20\Phi^2)\Psi^2$
$+720(3 + 8\Phi)\Psi^4\big)/\big(60(21 + \sqrt{105})(1+\Phi)\big), \quad c_7 = (3 - 5\sqrt{5/21})/8$

collects results for a moderately thick beam with $h/L = 1/8$, which corresponds to $\Phi_0 = 3/80$ and $\Psi_0^2 = 1/768$. The BE top performers, FBMS and FBMG, gradually slow down and are caught by CDLA by $N_e = 32$. All other instances trail, with the standard ones: CMM and FLMM, becoming the worst performers. Note that for $N_e = 32$, CMM and FLMM provide only 1 digit of accuracy in Ω_3, although there are $32/1.5 \approx 21$ elements per wavelength.

Figure 20 collects results for a thick beam with $h/L = 2/5$, corresponding to $\Phi_0 = 24/625$ and $\Psi_0^2 = 1/75$. The trends of Fig. 19 are exacerbated, with FBMS and FBMG running out of steam by $N_e = 4$ and CDLA clearly emerging as best for $N_e \geq 8$. Again CMM and FLMM trail badly.

The reason for the performance degradation of FBMS and FBMG as the Ti-beam gets thicker is unclear as of this writing. Eigensolver accuracy is not responsible since rerunning

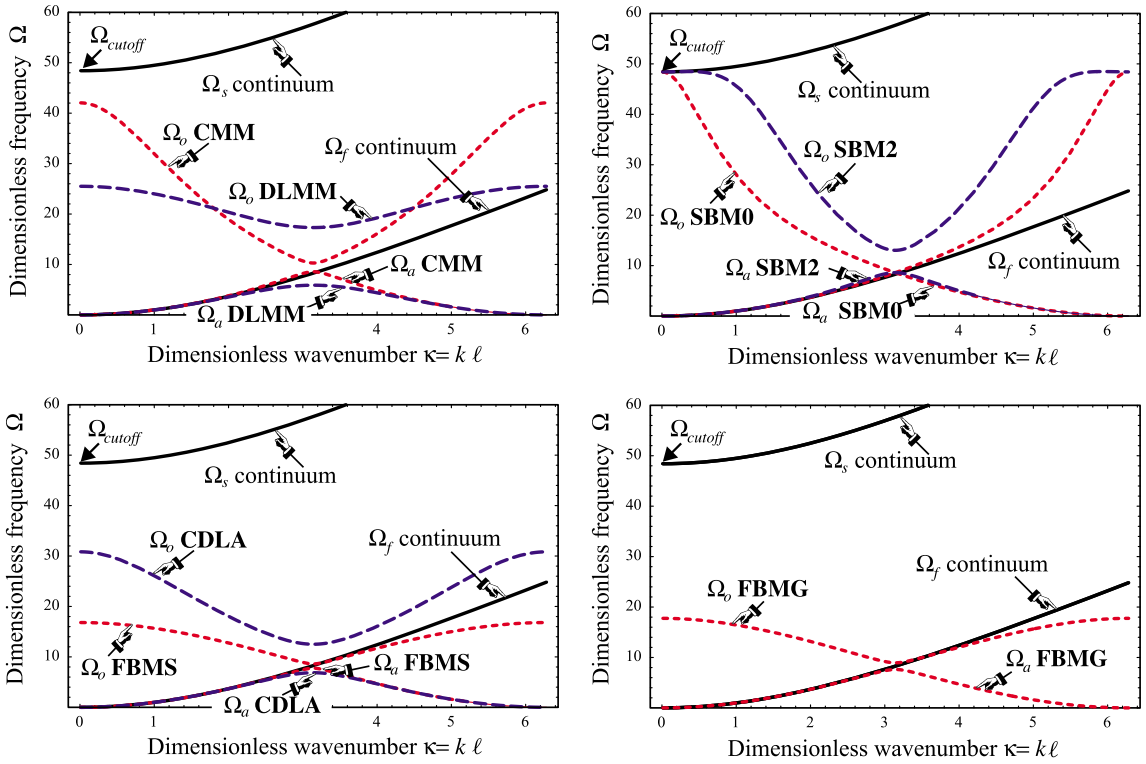

Fig. 17 DDD for selected Ti-beam mass template instances with $\Phi = 48/125$ and $\Psi^2 = 1/75$

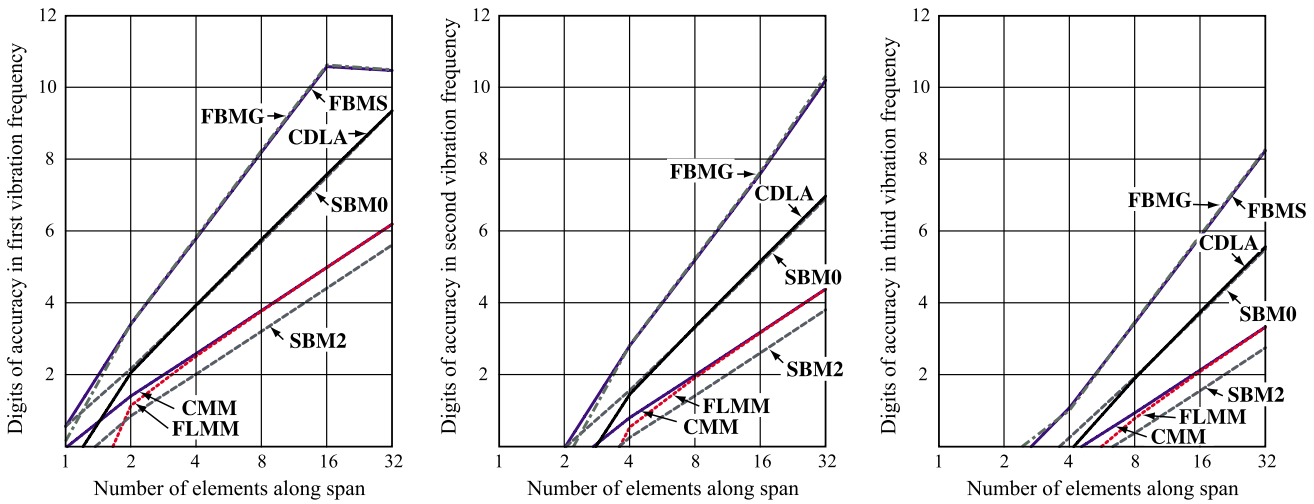

Fig. 18 Accuracy of first 3 natural vibration frequencies of SS prismatic beam using mass matrices of instances listed in Tables 11 and 12. BE model with $\Phi_0 = \Psi_0 = 0$. Exact (12-decimal) frequencies $\Omega_1 = \pi^2 = 9.869604401089$, $\Omega_2 = 4\pi^2 = 39.478417604357$ and $\Omega_3 = 9\pi^2 = 88.826439609804$. Cutoff frequency $+\infty$

the cases of Figs. 19 and 20 in quad precision did not change the plots. A numerical study of the Ω_f^2 truncation error shows that FBMS and FBMG fit the continuum branch better than CDLA even for very thick beams. Possible contamination of vibration mode shapes with the shear branch was not investigated.

8 Conclusions and Future Work

It is clear from the previous studies that mass matrix customization by templates can be effective in structural dynamics. The examples of Sects. 4.9, 5.14 and 7.8 illustrates two typical advantages:

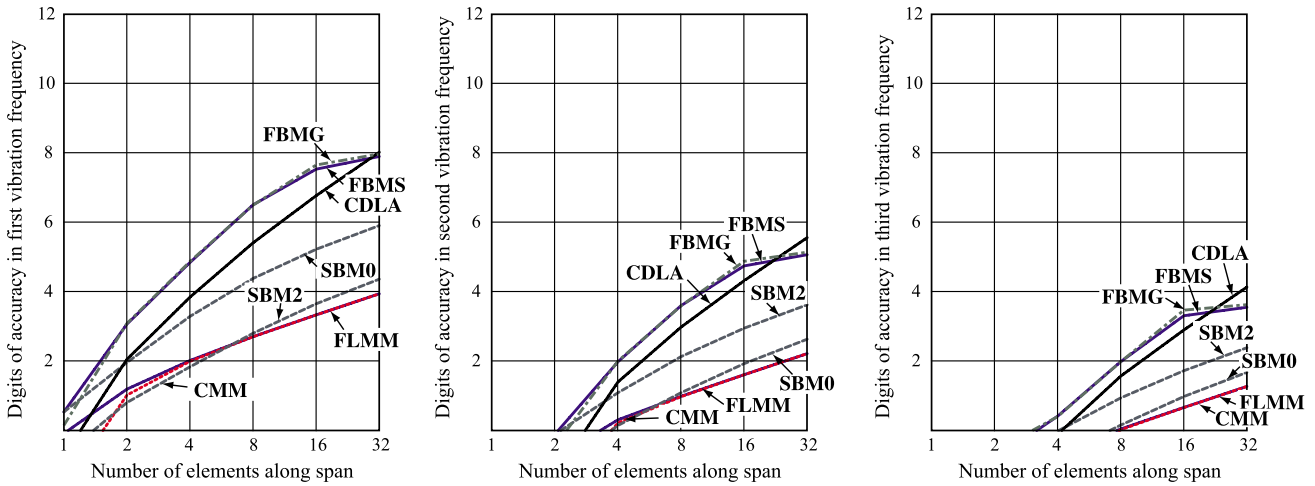

Fig. 19 Accuracy of first 3 natural vibration frequencies of SS prismatic beam using mass matrices of instances listed in Tables 11 and 12. Timoshenko model with $\Phi_0 = 3/80 = 0.0375$ and $\Psi_0^2 = 1/768 = 0.00130$, pertaining to a rectangular x-section with $h/L = 1/8$ and $\nu = 0$. Exact (12-decimal) frequencies $\Omega_1 = 9.662562122511$, $\Omega_2 = 36.507937703548$ and $\Omega_3 = 75.894968024537$. Cutoff frequency $\Omega_{cut} = 12/(\Phi_0\Psi_0^2) = 495.741868314549$

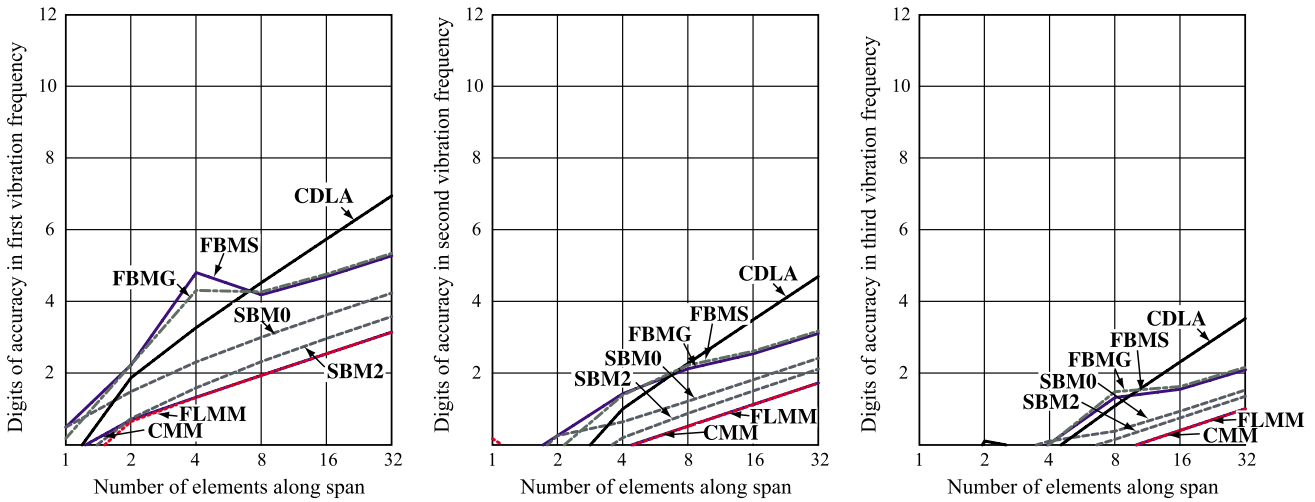

Fig. 20 Accuracy of first 3 natural vibration frequencies of SS prismatic beam using mass matrices of instances listed in Tables 11 and 12. Timoshenko model with $\Phi_0 = 24/625 = 0.384$ and $\Psi_0^2 = 1/75 = 0.0133$, pertaining to a rectangular x-section with $h/L = 2/5$ and $\nu = 0$. Exact (12-decimal) frequencies $\Omega_1 = 8.287891683498$, $\Omega_2 = 24.837128591729$ and $\Omega_3 = 43.182948411234$. Cutoff frequency $\Omega_{cut} = 12/(\Phi_0\Psi_0^2) = 48.412291827593$

- Orders of magnitude improvements in frequency accuracy can be achieved for the *same* computational effort.
- The space discretization need not be changed at all. Only the template free parameters need to be adjusted by supplying the appropiate signature.

These should be attractive to engineers for practical FEM computations. The last one is particularly important, since redoing a structural dynamics model not amenable to mesh generation may take a significant portion of a design and analysis process.

Would availability of customized templates eliminate the need for h and p adaptivity? Certainly not. Elements have performance limits, so such refinement schemes cannot be ruled out. It should be noted, however, that mesh adaptivity is less effective in dynamics, particularly in problems with rapid transients and shocks. Irregular meshes and high order elements are notorious sources of HF pollution, and adaptivity can make things worse by exacerbating nonphysical dispersion.

As regards future work, the most ambitious plan is extension to multiple space dimensions. Additional challenges emerge there:

- *Directionality*. This means that the dynamic accuracy of the FEM model, as compared to the continuum, depends

on the direction of plane wave propagation. This is a phenomenon missing in 1D. Integration averaging over propagation angles necessarily appears as another component of the Fourier analysis.
- *Material property dependence*. Optimal free parameters become dependent on additional elastic material properties missing from the 1D treatment. For example if the material is isotropic Poisson's ratio appears. This is not actually unique to mass templates, but affects stiffness templates as well.
- *Multiple plane wave types*. In isotropic 2D and 3D continua, one needs to consider two types: pressure (P-waves) and shear (S-waves). Plainly this impacts customization. If the medium is non-isotropic, more complicated wave types may have to be considered.
- *Parameter explosion*. This can be expected to hinder symbolic calculations. At first sight it seems inevitable given the rapidly increasing size of the element matrices. Growth can be controlled, however, by making use of *a priori* reduction techniques such as those mentioned in Sects. 3.1, 3.2, and 3.4.

These challenges are illustrated for a simple 2D element (three-node linear triangle) in Appendix 5.

Less ambitious research thrusts may focus on extending the results presented here for 1D elements. For example:

- Assess the performance of different template variant construction approaches to reduce high-frequency pollution caused in DTI. Three were described for the Bar3 element: singular mass, SMS and constant OB. As of this writing, no comparative rating based on numerical experiments is available.
- Find out whether the impressive gains in accuracy observed in LFF-customized templates survive in irregular meshes and/or heterogeneous element mixtures.
- Unfinished business remains for the Timoshenko beam. First, the unexpected deterioration in vibration accuracy as the coefficients $\mathbf{\Phi}$ and $\mathbf{\Psi}$ increase is presently unexplained. Could the degradation be arrested using MS template pairs? Prior experience with the BE-beam, referenced in Appendix Sect. 1.7, shows only modest improvements, but such continuum model is comparatively well behaved. Second, the relative performnace of the various template instances listed in Tables 11 and 12 for direct time integration (DTI) remains to be assessed.

Acknowledgments The first version of this paper was written during the 2004-2005 summer academic recesses while the first author was a visitor at CIMNE (Centro Internacional de Métodos Numéricos en Ingenieria) at Barcelona, Spain. The visits were partly supported by fellowships awarded by the Spanish Ministerio de Educación y Cultura during May-June of those years, and partly by the National Science Foundation under grant High-Fidelity Simulations for Heterogeneous Civil and Mechanical Systems, CMS-0219422. Thanks are due to Eugenio Oñate, director of CIMNE, for encouraging expanding the material to an expository paper. Thanks are also given to Manfred Bischoff and Anton Tkachuk for calling attention to recent work at the University of Stuttgart on mass modification methods, and providing articles in press.

Appendix 1: A Short History of Mass Matrices

This Appendix summarizes previous developments on various topics addressed by this paper.

Appendix 1.1: Pre-FEM Work

The first appearance of a structural mass matrix in a journal article occurs in two papers by Duncan and Collar [23,24], which appeared in the mid 1930s. The authors were members of the world famous aeroelasticity team at the National Physics Laboratory in Teddington (UK), led by Frazier. As narrated in [32] those two papers actually represent the birth of Matrix Structural Analysis (MSA). Befitting the overdesigned aircraft structures of the time, the focus is on dynamics and vibrations rather than on statics. In [23] the mass matrix is called "inertia matrix" and denoted by $[m]$. The first example [23, p. 869] displays the 3×3 diagonal mass of a triple pendulum. In the 1938 book [45], which collects that early work plus intermediate papers, the notation changes to A.

DLMM were strongly preferred in early publications. In fact they dominate all pre-1963 work. Three reasons may be adduced for the preference:

- The three-century astronomical heritage of Newtonian Mechanics. For unperturbed orbit calculations, celestial bodies were idealized as point masses regardless of actual size.
- Computational simplicity in vibration analysis and explicit direct time integartion (DTI).
- Direct lumping gives an obvious way to account for *nonstructural masses* in simple discrete models of the spring-dashpot-point-mass variety. For example, in a multistory building "stick model" wherein each floor is treated as one DOF in lateral sway under earthquake or wind action, it is natural to take the entire mass of the floor (including furniture, insulation, etc.) and assign it to that freedom.

Nondiagonal (but not consistent) masses pop up ocassionally in pre-1960 aircraft matrix analysis—e.g. wing oscillations in [45, §10.11] as a result of measurements. As such they necessarily account for nonstructural masses due to fuel, avionics equipment, etc.

Appendix 1.2: Consistent Mass Matrices Appear

The formulation of the CMM in structural mechanics by Archer [5,6] was a major advance. Most of the CMM derived in Appendix 3 appear in those papers. The underlying idea, however, is older. In fact, Irons and Ahmad observe [62] that consistent masses had been used in acoustics for over two decades before Archer's papers; see e.g., the textbook [116].

The CMM at the system (master) level follow directly from the Lagrange dynamic equations established in the late XVIII Century [67]. If T is the kinetic energy of a FEM-discretized structural system occupying volume V, and $\dot{u}_i(x_i)$ the velocity field defined by the nodal velocities collected in $\dot{\mathbf{u}}$, the master CMM is simply the Hessian of T with respect to nodal velocities:

$$T = \tfrac{1}{2}\int_V \rho\, \dot{u}_i\, \dot{u}_i\, dV, \quad u_i = u_i(\dot{\mathbf{u}}), \quad \mathbf{M} = \frac{\partial^2 T}{\partial \dot{\mathbf{u}}\, \partial \dot{\mathbf{u}}}. \tag{131}$$

This matrix is constant if T is quadratic in $\dot{\mathbf{u}}$, as happens in linear structural dynamics. Two key decisions had to be reached, however, before this idea was applicable to FEM.
Localization: (131) is applied element by element, and the master $\mathbf{M}$ assembled through the standard steps of the Direct Stiffness Method (DSM).
Consistent Interpolation: the interpolation of velocities and displacements is identical. That is, VSF and DSF coincide.

These in turn had to wait until three major ingredients became slowly established during the 1960s: (i) the DSM of Turner [105,106], (ii) the concept of shape functions progressively evolving in early FEM publications [26,28,60,61,74], and (iii) the FEM connection to Rayleigh-Ritz. The last one was critical. It was established in Melosh's thesis work [74,75]. The link to dynamics was closed with Archer's contributions, and CMM became a staple of FEM. But only a loose staple. Problems persisted:

(a) Nonstructural masses are not naturally handled by CMM. In vehicle systems such as ships or aircraft, the structural mass is only a fraction (10–20 %) of the total.
(b) It is inefficient in explicit DTI, since $\mathbf{M}$ is never diagonal.
(c) It may not give the best results compared to other alternatives. Why? If $\mathbf{K}$ results from a conforming displacement interpolation, pairing it with the CMM is a form of the conventional Rayleigh-Ritz, and thus guaranteed to provide upper bounds on natural frequencies. This is not necessarily a good thing. In practice it is observed that errors increase rapidly as one moves up the frequency spectrum. If the response is strongly influenced by intermediate and high frequencies, as in contact-impact and wave propagation dynamics, the CMM may give poor results.
(d) For elements derived outside the assumed-displacement framework, the DSF may be either unknown or altogether missing.

Problem (a) can be addressed by "rigid mass elements" accounting for inertia (and possibly gravity or centrifugal forces) but no stiffness. Nodes of these elements are linked to structural (elastic) nodes by multifreedom kinematic constraints. This is more of an implementation issue than a research topic, although numerical difficulties typical of multibody dynamics may crop up.

Problems (b,c,d) can be attacked by parametrization. MacNeal was the first to observe [4,71,73] that averaging the DLMM and CMM of Bar2 produced better results than using either alone. This idea was further examined by Belytschko and Mullen [8] using Fourier analysis; they also studied the CMM and SLMM of Bar3 but not their parametrizations. Krieg and Key [66] had emphasized that in transient analysis by DTI the introduction of a time discretization operator brings new compensation phenomena, and consequently the time integrator and the mass matrix should not be chosen separately. The template approach addresses this problem by allowing and encouraging customizing of the mass and stiffness to the problem at hand.

Appendix 1.3: Dynamic Model Reduction

Concurrently with advances in variational mass lumping leading to the CMM, the 1960s and early 1970 were a fertile time for the development of reduced order dynamic models based on component mode synthesis (CMS), a name coined by Hurty [58,59]. These were motivated by the high cost of dynamic and vibration analysis in the computers of the time, and blended well with the emerging use of substructuring methods in aerospace engineering, as summarized in [88].

Seminal publications of the period include [20,52,72,91], which originated the widely used Craig-Bampton and MacNeal–Rubin CMS methods. There is abundant literature since. Good textbook-level descriptions are provided in [21,48].

Appendix 1.4: Selective Mass Scaling

The SMS method, proposed in the mid 2000s [78,79], has attracted attention for rapid-transient simulations involving contact-impact, such as vehicle crash or explosions. Those are typically treated by explicit DTI, in which ephemeral high frequencies produced by transient shocks may require extremely small timesteps for stability, as well as producing significant spurious noise (pollution). In this approach, a DLMM is augmented by a scaled version of the stiffness matrix. The underlyting idea is to knock down the high fre-

quency of the "mesh modes," as quantitatively shown in Sect. 3.5

The derivation of the SMS variant for Bar3 in Sect. 5.12 shows that for the three-node bar, SMS can be presented as a subset of the general mass template. Nevertheless, it deserves consideration on its own because of two attractive features:

- It involves only *one* free parameter, which may be adjusted during the response simulation process. This makes it especially suitable for multidimensional elements.
- It does not depends on knowledge of element shape functions. In fact it may be used without knowing the source of the FEM matrices, which is an attractive feature for some commercial codes.

These are counteracted, however, by two disadvantages:

- Loss of low-frequency accuracy in the AB. Consequently SMS is not recommended for conventional structural dynamics and vibration analysis.
- Adding the stiffness term necessarily makes **M** nondiagonal, complicating explicit DTI. If the stiffness contribution is relatively small, however, DLMM diagonal dominance might be retained, which permits the use of iterative schemes [81].

The method has been further explored in several recent publications, some of which focus on the use of singular mass matrices as well as connection with parametrized variational principles (PVP) [64,90,101,102]. The variational connection outlined in Appendix 5, in which VSF and DSF are independent, has the potential to link templates to that recent line of research as well as earlier work cited there.

Appendix 1.5: Singular Mass Matrices

This approach to RHFP has been primarily developed with an applied mathematics flavor and with multibody dynamics as focus [14,107–110]. The key idea is to get the OB (or branches) out of the way at low frequencies to increase the acoustoptical gap. It can be readily subsumed under templates through spectral parametrization, as worked out for the Bar3 element in Sect. 5.11. While the BSSM instance constructed there shows promise in meeting both LFCF and RHFP customization goals, more numerical experimentation will be required to substantiate that promise.

Appendix 1.6: Frequency Dependent Matrices

Making mass and stiffness frequency dependent (FD) was proposed by Przemieniecki [88], who expanded both $\mathbf{M}^e(\omega)$ and $\mathbf{K}^e(\omega)$ as Taylor series in ω^2. An indirect derivation scheme, which preceeds [88], consists of starting from dynamic transfer matrices and convert them to mass and stiffness by partial inversion [117]. The procedure is described in detail in [85]. It is restricted to 1D elements.

The idea was subsequently pursued by other authors. Pilkey [86,87] derived such matrices by using exact solutions of the unforced EOM as shape functions. For the two-node bar, those matrices are not instances of the FDMS template presented in Sect. 4.12 because the baseline mass matrix for zero frequency is the CMM.

Since such exact solutions are available only for a limited number of 1D models, the approach is hardly extendible beyond prismatic bars and beams. More general 1D elements have been handled by numerical ODE integration [69,70] on the way to transfer matrices.

The approach can be generalized to the template context by making free parameters frequency dependent, as illustrated in Sect. 4.12 for Bar2. As noted there, this extension might be of interest for problems dominated by a driving frequency, such as some electronic and optical devices. For more general use, keeping the parameters frequency independent is far more practical. In multiple dimensions it merges with boundary integral and spectral element methods in elastodynamics. These are specialized topics beyond the scope of this historical review; for recent work and references, see [69,92,94,115].

Appendix 1.7: Templates

The template approach originally evolved in the late 1980s and early 1990s to construct high-performance *stiffness* matrices [30,31]. Its roots can be traced back to the Free Formulation of Bergan [10–13,29], in which the stiffness matrix was decomposed into basic and higher order components. A historical account is provided in a tutorial chapter [36]. The general concept of template as parametrized forms of FEM matrix equations is discussed in [31,35,39].

Mass templates in the form presented here were first described in [33,34] for a BE plane beam analyzed with Fourier methods. The study addressed MS pairs. The idea was extended to other elements in [40].

The Bar3 stiffness template (41) was first stated in [30], in which the only free parameter has a slightly different definition. The Timoshenko beam model first appeared in [99]; see also [100]. The symbolic derivation scheme used for the Timoshenko beam EOM in (104) is due to Flaggs [43]; see also [82–84]. The optimal static stiffness matrix (112) for the Ti-beam element appeared originally in [104]. A detailed derivation may be found in [88, §5.6]. It is an instance of a template given in [38].

Two powerful customization techniques used regularly for templates are Fourier analysis and modified differential equa-

tions (MoDE). Fourier analysis is limited to separable systems but is straightforward to apply, requiring only undergraduate mathematics (as tutorials for applied Fourier analysis, Hamming's textbooks [53,54] are highly recommended). MoDE methods, first published in correct form in 1974 [112] are less restrictive but more demanding on two fronts: mathematical ability and support of a CAS. Processing power limitations presently restrict MoDE to two-dimensional elements and regular meshes. In the present exposition, only Fourier methods are used since those are likely to be more familiar to potential readers.

The selection of *a priori* constraint criteria for template free parameters is not yet on firm ground. For example: is conservation of angular momentum useful in mass templates? The answer seem to depend on element type and complexity.

Appendix 1.8: Multidimensional Elements

Stiffness templates for 2D and 3D structural elements have been considered since a modest beginning in the 1980s, as Free Formulation plate elements that incorporated a scaling parameter for the higher order stiffness [13,29]. A significant number has been developed since; see references in Appendix Sect. 1.7. The development of mass matrix templates for multidimensional elements has lagged because of four complications:

- Mesh directionality effects that require angular averaging
- Additional dependence on elastic material properties
- Multiple plane wave types (pressure and shear waves in the case of an isotropic material)
- The free parameter explosion as matrices get larger

The first study of this nature for a nontrivial 2D element has appeared as a 2012 thesis [50], which dealt with triangular membrane elements with and without corner node drilling freedoms. An example extracted from this thesis is presented in Appendix 5.

Appendix 1.9: Connection To Molecular Physics

DLMM results for regular lattices of structural elements have counterparts in a very different area: molecular physics. More precisely, the wave mechanics of crystalline solids created in the XX Century by particle mechanicians; e.g., [15,89,118]. In crystal models, lattice nodes are occupied by molecules interacting with adjacent ones. Thus the "element dimension" ℓ acquires the physical meaning of molecular gap. Both acoustic and optical branches have physical significance.

In such models masses are always *lumped* at molecule locations, and atoms vibrate as harmonic oscillators in the potential well of the force fields of their neighbors. Dispersion curves govern energy transmission. In a linear atomic chain, the dimensionless wavenumber range $\kappa \in [-\pi, \pi]$, or $\kappa \in [0, 2\pi]$, is called the first Brillouin zone [16,63]. The happy connection of mass templates to periodic materials may be of interest as FEM and related discretization methods are extended into multiscale applications of crystal, micro- and nano-mechanics, and phononics [7,22].

Appendix 2: Standard Mass Matrix Derivation Methods

Appendix 2.1: Overview

This Appendix and the next one are written for readers unfamiliar with the standard (a.k.a. classical, conventional) approaches for constructing finite element mass matrices. The intention is to make the overall paper reasonably self-contained. Readers knowledgeable of those techniques should skip this material.

As a general rule, the construction of the master (system level) mass matrix $\mathbf{M}$ largely parallels that of the master stiffness matrix $\mathbf{K}$. Mass matrices for individual elements are formed in local coordinates, transformed to the global frame if necessary, and merged into the master mass matrix following exactly the same techniques used for $\mathbf{K}$. In practical terms, the assemblers for $\mathbf{K}$ and $\mathbf{M}$, before application of boundary conditions, can be made identical (except for obvious indexing shortcuts in the case of diagonal mass matrices). This procedural uniformity is one of the strengths of the DSM.

A notable difference with the stiffness matrix is the possibility of using a DLMM based on direct lumping to nodes. A master DLMM can be stored as a vector. If all entries are nonzero, it is easily inverted in place, since the inverse of a diagonal matrix is also diagonal. Plainly the use of a DLMM entails significant computational advantages in calculations that involve $\mathbf{M}^{-1}$; for example explicit DTI [9,111] and some symmetric eigenproblem solution methods [80]. This is counteracted by negative features.

Appendix 2.2: Element Mass Matrix Construction

The master mass matrix is built up from element contributions, and we start at that level. The construction of the mass matrix of individual elements with *continuous mass density* can be carried out through several methods. These can be categorized into three groups: direct mass lumping, variational mass lumping, and template mass lumping. The last group is more general in that includes others through parameterization; in fact it covers all admissible mass matrices. Variants of direct and variational lumping are by now standard in the literature at the textbook level; see e.g., [18,21,48,88,93], and references therein. They are implemented in all general purpose FEM codes. This Appendix covers the two standard

approaches. Template mass lumping is the subject of the main body of the paper.

Appendix 2.2.1: Direct Mass Lumping

This is the simplest procedure. The total mass of element e is directly apportioned to nodal freedoms, ignoring any cross coupling. The goal is to build a DLMM, denoted here by $\mathbf{M}^e_L$.

As the simplest example, consider a 2-node prismatic bar element with length ℓ, cross section area A, and mass density ρ, which can only move in the axial direction x, as depicted in Fig. 21a. The total mass of the element is $m^e = \rho A\ell$. This is divided into two equal parts and assigned to each end node. The element is endowed with the two freedoms shown in Fig. 21b. Thus

$$\mathbf{M}^e_L = \tfrac{1}{2}\rho A\ell \begin{bmatrix} 1 & 0 \\ 0 & 1 \end{bmatrix} = \tfrac{1}{2}\, m^e\, \mathbf{I}_2, \tag{132}$$

in which $m^e = \rho A\ell$ is the element mass and $\mathbf{I}_2$ denotes the 2×2 identity matrix. As sketched in Fig. 21, we have effectively replaced the continuum bar with a dumbbell: two masses separated by a massless connector.

This process conserves the translational kinetic energy or, equivalently, the linear momentum. To check this property for the bar example, take the constant x-velocity vector $\dot{\mathbf{u}}^e = v[1 \;\; 1]^T$. The kinetic energy of the element is $T^e = \frac{1}{2}(\dot{\mathbf{u}}^e)^T\, \mathbf{M}^e_L\, \dot{\mathbf{u}}^e = \frac{1}{2}\rho A\ell\, v^2 = \frac{1}{2}m^e v^2$. Thus the linear momentum $p^e = \partial T^e/\partial v = m^e v$ is preserved. When applied to simple elements that can rotate, however, the direct lumping process may not necessarily preserve *angular* momentum.

Historical motivations for direct lumping are noted in Appendix Sect. 1.1. Most crucial, it covers naturally the case where concentrated (point) masses are natural part of model building. For example, in aircraft engineering it is common to idealize nonstructural masses (fuel, cargo, engines, etc.) as concentrated at given locations (such concentrated masses in general have rotational freedoms; rotational inertia lumping is then part of the modeling process).

Appendix 2.2.2: Variational Mass Lumping

The second standard procedure is based on a variational formulation. This is done by taking the *kinetic energy* as part of the governing functional. The kinetic energy of an element of mass density ρ that occupies the domain Ω^e and moves with velocity field $\vec{\mathbf{v}}^e$ is

$$T^e = \tfrac{1}{2}\int\limits_{\Omega^e} \rho(\vec{\mathbf{v}}^e)^T \vec{\mathbf{v}}^e\, d\Omega^e. \tag{133}$$

Following the conventional FEM philosophy, the element velocity field is interpolated using *shape functions*: $\vec{\mathbf{v}}^e = \mathbf{N}_v\, \dot{\mathbf{u}}^e$, in which $\dot{\mathbf{u}}^e$ are node DOF velocities and $\mathbf{N}_v$ a shape function matrix (for 1D elements, $\mathbf{N}_v$ is a row vector). Inserting into (133) and taking the node velocities out of the integral yields

$$T^e = \tfrac{1}{2}(\dot{\mathbf{u}}^e)^T \int\limits_{\Omega^e} \rho(\mathbf{N}_v)^T\, \mathbf{N}_v\, d\Omega\, \dot{\mathbf{u}}^e \stackrel{\text{def}}{=} \tfrac{1}{2}(\dot{\mathbf{u}}^e)^T \mathbf{M}^e\, \dot{\mathbf{u}}^e, \tag{134}$$

whence the element mass matrix follows as the Hessian of T^e:

$$\mathbf{M}^e = \frac{\partial^2 T^e}{\partial \dot{\mathbf{u}}^e \partial \dot{\mathbf{u}}^e} = \int\limits_{\Omega^e} \rho\, (\mathbf{N}^e_v)^T\, \mathbf{N}_v\, dst\Omega. \tag{135}$$

If the same shape functions used in the derivation of the stiffness matrix are chosen, that is, $\mathbf{N}^e_v = \mathbf{N}^e_u$, (135) is called the CMM. It is denoted here by $\mathbf{M}^e_C$. A better name for (135) would be stiffness-consistent mass matrix. The shorter sobricket has the unfortunate implication that other choices are "inconsistent," which is far from the truth. In fact, the consistent mass is not necessarily the best performer, a feature already noted. The shorter name is, however, by now ingrained in the FEM literature.

For the 2-node prismatic bar element moving along x, pictured in Fig. 21a, the well known stiffness shape functions are $N_1 = 1-(x-x_1)/\ell = (1-\xi)/2$ and $N_2 = (x-x_2)/\ell = (1+\xi)/2$, in which $\xi = 2(x-x_1)/\ell - 1$ is the isoparametric natural coordinate that varies from -1 at node 1 to $+1$ at node 2. With $dx = \frac{1}{2}\ell\, d\xi$, the consistent mass is easily obtained as

$$\begin{aligned} \mathbf{M}^e_C &= \int\limits_0^\ell \rho\, A\, (\mathbf{N}^e)^T \mathbf{N}^e\, dx \\ &= \tfrac{1}{4}\rho\, \ell A \int\limits_{-1}^{+1} \begin{bmatrix} 1-\xi \\ 1+\xi \end{bmatrix} \begin{bmatrix} 1-\xi & 1+\xi \end{bmatrix} d\xi \\ &= \tfrac{1}{6}\, m^e \begin{bmatrix} 2 & 1 \\ 1 & 2 \end{bmatrix}. \end{aligned} \tag{136}$$

It can be verified that this mass matrix preserves linear momentum along x. If allowed to move in the xy plane, as considered in Appendix Sect. 2.5, it also preserves angular momentum about z.

Appendix 2.3: Mass Matrix Properties

Mass matrices must comply with conditions that can be used for verification and debugging at the element level. They

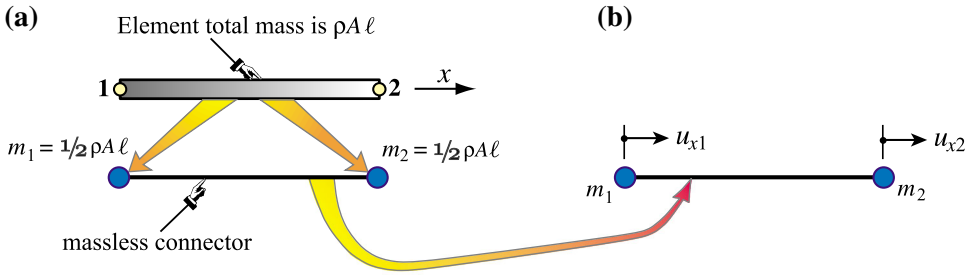

Fig. 21 Direct mass lumping for two-node prismatic bar element: **a** lumping element mass to end nodes, **b** assigning degrees of freedom

are: matrix symmetry, physical symmetries, conservation and positivity.

Matrix Symmetry This means $(\mathbf{M}^e)^T = \mathbf{M}^e$, which is easy to check. For a variationally derived mass matrix this follows directly from the definition (135), whereas for a DLMM is automatic.

Physical Symmetries Also called *geometric* or *fabrication symmetries*. They are dictated by the physical configuration. For example, the CMM or DLMM of the prismatic Bar2 element must be symmetric about the antidiagonal: $M_{11} = M_{22}$. To see this, flip the end nodes: the element remains the same and so does the mass matrix.

Conservation At a minimum, total element mass must be preserved (we are talking about classical mechanics here; in relativistic mechanics mass and energy can be exchanged). This is easily verified by applying a uniform translational velocity and checking that linear momentum is conserved. Higher order conditions, such as conservation of angular momentum, are optional and not necessarily desirable.

Positivity For any nonzero velocity field defined by the node values $\dot{\mathbf{u}}^e \neq \mathbf{0}$, $(\dot{\mathbf{u}}^e)^T \mathbf{M}^e \dot{\mathbf{u}}^e \geq 0$. That is, $\mathbf{M}^e$ must be nonnegative. Unlike the previous three conditions, this constraint is nonlinear in the mass matrix entries. It can be checked in two ways: through the eigenvalues of $\mathbf{M}^e$, or the sequence of principal minors. The second technique is more practical if the entries of $\mathbf{M}^e$ are symbolic.

A stricter form of the last condition requires that $\mathbf{M}^e$ be PD: $(\dot{\mathbf{u}}^e)^T \mathbf{M}^e \dot{\mathbf{u}}^e > 0$ for any $\dot{\mathbf{u}}^e \neq \mathbf{0}$. This is physically reassuring because one half of that form is the kinetic energy associated with the velocity field defined by $\dot{\mathbf{u}}^e$. In a continuum T can vanish only for zero velocities (a rest state). But allowing $T^e = 0$ for some nonzero $\dot{\mathbf{u}}^e$ makes life easier in some situations; e.g., elements with rotational or multiplier freedoms, or in the rapid-transient applications noted in Appendix Sect. 1.4.

The $\dot{\mathbf{u}}^e$ for which $T^e = 0$ collectively form the *null space* of $\mathbf{M}^e$. Because of the conservation requirement, a rigid velocity field (that is, the time derivative $\dot{\mathbf{u}}^e_R$ of a rigid body mode $\mathbf{u}^e_R$) cannot be in the mass matrix null space, as it would imply zero total mass. This scenario is dual to that of the element stiffness matrix. For the latter, $\mathbf{K}^e \mathbf{u}^e_R = \mathbf{0}$ because a rigid body motion produces no strain energy. Thus $\mathbf{u}^e_R$ must be in the null space of the stiffness matrix.

Appendix 2.4: Rank and Numerical Integration

Suppose the element has a total of n^e_F freedoms. A mass matrix $\mathbf{M}^e$ is called *rank sufficient* or of *full rank* if its rank is $r^e_M = n^e_F$. Because of the positivity requirement, a rank-sufficient mass matrix must be PD. Such matrices are preferred from a numerical stability standpoint.

If $\mathbf{M}^e$ has rank $r^e_M < n^e_F$ the mass is called rank deficient by $d^e_M = n^e_F - r^e_M$. Equivalently $\mathbf{M}^e$ is d^e_M times singular. For a numerical matrix the rank is easily computed by taking its eigenvalues and looking at how many of them are zero. The null space can be extracted by functions such as `NullSpace` in *Mathematica* without the need of computing eigenvalues.

The computation of $\mathbf{M}^e$ by the variational formulation (135) is often done using Gauss numerical quadrature. Each Gauss points adds n_D to the rank, where n_D is the row dimension of the shape function matrix $\mathbf{N}^e$, up to a maximum of n^e_F. For most elements n_D is the same as element spatial dimensionality; that is, $n_D = 1,\ 2$ and 3 for 1, 2 and 3 dimensions, respectively. This property can be used to pick the minimum Gauss integration rule that makes $\mathbf{M}^e$ PD.

Appendix 2.5: Globalization

Like their stiffness counterparts, mass matrices are often developed in a local or element frame. Should globalization be necessary before merge, a congruent transformation is applied:

$$\mathbf{M}^e = (\mathbf{T}^e)^T \bar{\mathbf{M}}^e \mathbf{T}^e. \tag{137}$$

Here $\bar{\mathbf{M}}^e$ is the element mass referred to a local frame $\bar{x}_i$ (a.k.a. element frame), whereas $\mathbf{T}^e$ is the local-to-global displacement transformation matrix. The recipe (137) follows readily from the Principle of Virtual Work, or equivalently the invariance of the first variation of the element kinetic energy:

$$\delta \bar{T}^e = (\dot{\bar{\mathbf{u}}}^e)^T\, \bar{\mathbf{M}}^e\, \delta \dot{\bar{\mathbf{u}}} = (\dot{\mathbf{u}}^e)^T\, (\mathbf{T}^e)^T\, \bar{\mathbf{M}}^e\, \mathbf{T}^e\, \delta \dot{\mathbf{u}}^e$$
$$= (\dot{\bar{\mathbf{u}}}^e)^T\, \mathbf{M}^e\, \delta \dot{\mathbf{u}}^e = \delta T^e. \tag{138}$$

Matrix $\mathbf{T}^e$ is in principle the same used for the stiffness globalization. Some procedural differences, however, must be noted. For stiffness matrices $\mathbf{T}^e$ is often *rectangular* if the local stiffness has lower dimensionality. For example, two-node bar, shaft and spar elements have 2×2 local stiffnesses. Globalization to 2D and 3D involves application of 2×4 and 2×6 transformation matrices, respectively. This works fine because the local element has zero stiffness in some directions, and those zero rows and columns may be omitted at the local level.

In contrast to stiffnesses, *translational masses never vanish*. One way to realize this is to think of an element moving in a translational rigid motion u_R with acceleration $\ddot{u}_R$. According to Newton's second law, $f_R = m^e \ddot{u}_R$, where m^e is the element translational mass. Regardless of direction, this inertia force cannot vanish.

The conclusion is: *all translational masses must be retained in the local mass matrix*. A two-node prismatic bar moving in the $\{x, y\}$ plane as in Fig. 22, furnishes a simple illustration. With the element freedoms arranged as $\mathbf{u}^e = \begin{bmatrix} u_{x1} & u_{x2} & u_{y1} & u_{y2} \end{bmatrix}^T$, the local mass matrix constructed by variationally consistent and diagonalized lumping are, respectively,

$$\bar{\mathbf{M}}^e_C = \tfrac{1}{6} m^e \begin{bmatrix} 2 & 1 & 0 & 0 \\ 1 & 2 & 0 & 0 \\ 0 & 0 & 2 & 1 \\ 0 & 0 & 1 & 2 \end{bmatrix},$$
$$\bar{\mathbf{M}}^e_L = \tfrac{1}{2} m^e \begin{bmatrix} 1 & 0 & 0 & 0 \\ 0 & 1 & 0 & 0 \\ 0 & 0 & 1 & 0 \\ 0 & 0 & 0 & 1 \end{bmatrix} = \tfrac{1}{2} m^e\, \mathbf{I}_4, \tag{139}$$

in which $m^e = \rho\, A\, \ell$. For 3D, repeat the diagonal block once more.

Appendix 2.5.1: Directional Invariance

For the case illustratedin in Fig. 22 the local-to-global freedom transformation $\bar{\mathbf{u}}^e = \mathbf{T}^e\, \mathbf{u}^e$ is

$$\begin{bmatrix} \bar{u}_{x1} \\ \bar{u}_{x2} \\ \bar{u}_{y1} \\ \bar{u}_{y2} \end{bmatrix} = \begin{bmatrix} c & 0 & s & 0 \\ 0 & c & 0 & s \\ -s & 0 & c & 0 \\ 0 & -s & 0 & c \end{bmatrix} \begin{bmatrix} u_{x1} \\ u_{x2} \\ u_{y1} \\ u_{y2} \end{bmatrix}, \quad \text{in which}$$
$$c = \cos\varphi, \quad s = \sin\varphi. \tag{140}$$

Now apply (137) to either $\mathbf{M}^e_C$ or $\mathbf{M}^e_L$ of (139) using (140). The result is $\mathbf{M}^e_C = \bar{\mathbf{M}}^e_C$ and $\mathbf{M}^e_L = \bar{\mathbf{M}}^e_L$: no change.

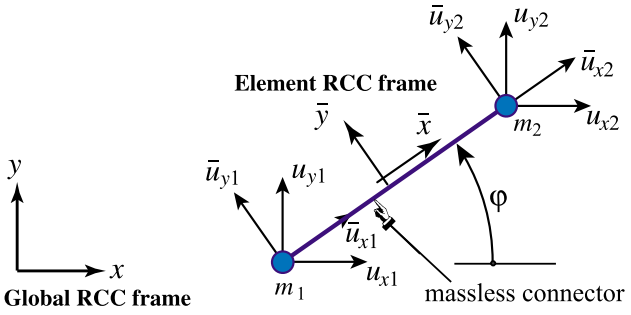

Fig. 22 Diagonally lumped mass Bar2 element moving in 2D

We say that these mass matrices *repeat*. Verification for the DLMM is easy because $\mathbf{T}^e$ is orthogonal: $(\mathbf{T}^e)^T\, \bar{\mathbf{M}}^e_L\, \mathbf{T}^e = \frac{1}{2} m^e\, (\mathbf{T}^e)^T\, \mathbf{I}_4 \mathbf{T}^e = \frac{1}{2} m^e\, (\mathbf{T}^e)^T\, \mathbf{T}^e = \frac{1}{2} m^e\, \mathbf{I}_4$. For the CMM, however, repetition is not obvious. It can be shown to hold by expressing $\mathbf{M}^e_C$ and $\mathbf{T}^e$ in 2×2 partitioned form

$$\bar{\mathbf{M}}^e_C = \begin{bmatrix} \tilde{\mathbf{M}} & \mathbf{0} \\ \mathbf{0} & \tilde{\mathbf{M}} \end{bmatrix}, \quad \mathbf{T}^e = \begin{bmatrix} c\mathbf{I}_2 & s\mathbf{I}_2 \\ -s\mathbf{I}_2 & c\mathbf{I}_2 \end{bmatrix},$$
$$\text{with } \tilde{\mathbf{M}} = \tfrac{1}{6} m^e \begin{bmatrix} 2 & 1 \\ 1 & 2 \end{bmatrix}. \tag{141}$$

Carrying out the congruent transformation in block form gives

$$\mathbf{M}^e_C = (\mathbf{T}^e)^T\, \mathbf{M}_C\, \mathbf{T}^e = \begin{bmatrix} (c^2+s^2)\tilde{\mathbf{M}} & (cs-cs)\tilde{\mathbf{M}} \\ (cs-cs)\tilde{\mathbf{M}} & (c^2+s^2)\tilde{\mathbf{M}} \end{bmatrix}$$
$$= \begin{bmatrix} \tilde{\mathbf{M}} & \mathbf{0} \\ \mathbf{0} & \tilde{\mathbf{M}} \end{bmatrix} = \bar{\mathbf{M}}^e_C. \tag{142}$$

A mass matrix that repeats upon transformation to any global frame is called a *directionally invariant mass matrix*, or DIMM. Note that the contents and order of $\tilde{\mathbf{M}}$ are irrelevant to the result (142). Hence the following generalization follows. If upon rearranging the element DOF so they are grouped node by node:

(i) $\bar{\mathbf{M}}^e$ has a repeating block diagonal form, and
(ii) $\mathbf{T}^e$ is configured as the block form shown above,

then local and global matrices will coalesce. For (ii) to hold, it is sufficient that all nodal DOF be translational and be referred to the same coordinate system. The same conclusion is easily extended to 3D, and to any arrangement of the element freedoms. This *repetition rule* can be summarized as follows:

> A local mass matrix is DIMM if all element DOFs are translational and all of them are referred to the same global system.

(143)

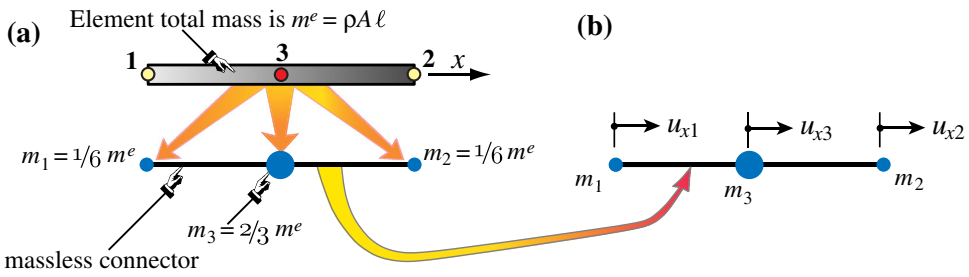

Fig. 23 Diagonal mass lumping for 3-node bar element **a** lumping as per Simpson's integration rule, **b** assigning element

This property should be taken advantage of to skip superfluous local-to-global transformations. Such operation may cost more than forming the local mass matrix. If the rule fails on actual computation, something (mass matrix or transformation) is wrong and must be fixed.

Appendix 2.5.2: Failure of Repetition Rule

The repetition rule can be expected to fail if $\bar{\mathbf{M}}^e$ is not a DIMM. This occurs under the following scenarios:

1. The element has non-translational freedoms; for example node rotations, or displacement derivatives (occasionally the rule may work, but that should not be taken for granted).
2. The mass blocks are different in content and/or size. This occurs if different continuum models are used in different local directions. Examples are furnished by beam-column elements, shell elements, and elements with curved sides or faces.
3. Nodes are referred to different coordinate frames in the global system. This can happen if certain nodes are referred to special frames to facilitate the application of boundary conditions.

Appendix 3: Standard Mass Matrix Derivation Examples

In this Appendix the DLMM and CMM of a few simple 1D and 2D elements are worked out to illustrate the standard lumping methods outlined in Appendix 2. Since all examples pertain to the element level, overbars to distinguigh local and global frames are omitted for brevity.

Appendix 3.1: The Three-Node Bar

The three-node bar element, usually abbreviated to Bar3, is shown in Fig. 7a. It is prismatic with length ℓ, area A, and uniform mass density ρ, Midnode 3 is at the center. The DOFs are arranged $\mathbf{u}^e = \begin{bmatrix} u_{x1} & u_{x2} & u_{x3} \end{bmatrix}^T$. The shape function matrix is

$$\begin{aligned} \mathbf{N}^e &= \begin{bmatrix} N_1(\xi) & N_2(\xi) & N_3(\xi) \end{bmatrix} \\ &= \begin{bmatrix} \xi(1-\xi)/2 & \xi(1+\xi)/2 & 1-\xi^2 \end{bmatrix}. \end{aligned} \tag{144}$$

in which ξ is the isoparametric natural coordinate pictured in Fig. 7a. The consistent mass follows as

$$\mathbf{M}^e_{CMM} = \rho A \int_{-1}^{1} (\mathbf{N}^e)^T \mathbf{N}^e\, J\, d\xi = \frac{m^e}{30} \begin{bmatrix} 4 & -1 & 2 \\ -1 & 4 & 2 \\ 2 & 2 & 16 \end{bmatrix}, \tag{145}$$

in which the Jacobian $J = dx/d\xi = \ell/2$, and $m^e = \rho\, A\, \ell$. To produce a DLMM, the total mass of the element is divided into three parts: $\alpha\rho A\ell$, $\alpha\rho A\ell$, and $(1-2\alpha)\rho A\ell$, which are assigned to nodes 1, 2 and 3, respectively. See Fig. 23. As discussed below the standard choice is $\alpha = 1/6$. Consequently 2/3 of the total mass goes to the midpoint, and what is left to the corners, giving

$$\mathbf{M}^e_{SLMM} = \tfrac{1}{6} m^e \begin{bmatrix} 1 & 0 & 0 \\ 0 & 1 & 0 \\ 0 & 0 & 4 \end{bmatrix}. \tag{146}$$

The 1:1:4 allocation happens to be Simpson's rule for integration, whence the label SLMM. This meshes in with the interpretation of diagonal mass lumping as a Lobatto integration rule, a topic discussed in Appendix Sect. 4.2. Both (145) and (146) are DIMM, and may be used as 3×3 building blocks to expand the element to 2D or 3D space. The repetition rule (143) holds.

Appendix 3.2: The Plane BE Beam

The two-node plane BE-beam element has length ℓ, cross section area A and uniform mass density ρ. Only the translational inertia due to the lateral motion of the beam is considered in the kinetic energy $T = \frac{1}{2}\int_0^\ell \rho \dot{v}(\bar{x})^2\, d\bar{x}$ of the element, whereas its rotational inertia is ignored. The freedoms are arranged as $\mathbf{u}^e = \begin{bmatrix} v_1 & \theta_1 & v_2 & \theta_2 \end{bmatrix}^T$. The natural coordinate ξ varies from $\xi = -1$ at node 1 ($x = 0$) to $\xi = +1$ at node 2 ($x = \ell$), whence $dx/d\xi = \frac{1}{2}\ell$ and $d\xi/dx = 2/\ell$. The well

known cubic shape functions in terms of ξ are collected in the shape function matrix

$$\mathbf{N}^e = \left[\tfrac{1}{4}(1-\xi)^2(2+\xi) \quad \tfrac{1}{8}\ell(1-\xi)^2(1+\xi) \quad \tfrac{1}{4}(1+\xi)^2(2-\xi) \quad -\tfrac{1}{8}\ell(1+\xi)^2(1-\xi)\right] \tag{147}$$

The CMM obtained by analytical integration is

$$\mathbf{M}^e_{CMM} = \rho A \int_{-1}^{1} J\,(\mathbf{N}^e)^T\mathbf{N}^e\,d\xi = \frac{m^e}{420}\begin{bmatrix} 156 & 22\ell & 54 & -13\ell \\ 22\ell & 4\ell^2 & 13\ell & -3\ell^2 \\ 54 & 13\ell & 156 & -22\ell \\ -13\ell & -3\ell^2 & -22\ell & 4\ell^2 \end{bmatrix}. \tag{148}$$

in which the Jacobian $J = dx/d\xi = \ell/2$ and $m^e = \rho\, A\, \ell$. The mass matrices obtained with Gauss integration rules of 1, 2 and 3 points are

$$C_1\begin{bmatrix} 16 & 4\ell & 16 & -4\ell \\ 4\ell & \ell^2 & 4\ell & -\ell^2 \\ 16 & 4\ell & 16 & -4\ell \\ -4\ell & -\ell^2 & -4\ell & \ell^2 \end{bmatrix},$$

$$C_2\begin{bmatrix} 86 & 13\ell & 22 & -5\ell \\ 13\ell & 2\ell^2 & 5\ell & -\ell^2 \\ 22 & 5\ell & 86 & -13\ell \\ -5\ell & -\ell^2 & -13\ell & 2\ell^2 \end{bmatrix},$$

$$C_3\begin{bmatrix} 444 & 62\ell & 156 & -38\ell \\ 62\ell & 11\ell^2 & 38\ell & -9\ell^2 \\ 156 & 38\ell & 444 & -62\ell \\ -38\ell & -9\ell^2 & -62\ell & 11\ell^2 \end{bmatrix}, \tag{149}$$

in which $C_1 = m^e/64$, $C_2 = m^e/216$, and $C_3 = m^e/1200$. Their eigenvalue analysis shows that all three are singular, with rank 1, 2 and 3, respectively. The result for 4 and more points agrees with (148), which has full rank. The main purpose of this example is to illustrate the rank property stated in Appendix Sect. 2.4: each Gauss point adds one to the rank up to 4, since the problem is 1D.

The matrix (148) conserves linear and angular momentum. So do the reduced-integration mass matrices (149) if the number of Gauss points is 2 or greater.

To get a DLMM is trickier. Obviously the translational nodal masses must be the same as that of a bar: $\frac{1}{2}\rho A\ell$. See Fig. 24. But there is no easy road to get rotational masses. To accommodate these variations, it is convenient to leave the latter parametrized as follows

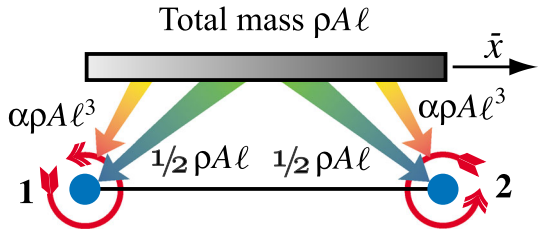

Fig. 24 Direct mass lumping for two-node plane BE beam element

$$\bar{\mathbf{M}}^e_L = m^e\begin{bmatrix} \frac{1}{2} & 0 & 0 & 0 \\ 0 & \alpha\ell^2 & 0 & 0 \\ 0 & 0 & \frac{1}{2} & 0 \\ 0 & 0 & 0 & \alpha\ell^2 \end{bmatrix}, \quad \alpha \ge 0. \tag{150}$$

Here α is a nonnegative parameter, typically between 0 and 1/100. The choice of α has been argued in the FEM literature over several decades, but the whole discussion is largely futile. Matching the angular momentum of the beam element gyrating about its midpoint gives $\alpha = -1/24$. This violates the positivity condition. It follows that the *best possible* α as opposed to possible best is zero. This choice gives, however, a singular mass matrix. This is undesirable in scenarios where a mass-inverse appears.

This result can be readily understood physically. The $m^e/2$ translational end node masses grossly overestimate (in fact, by a factor of 3) the angular momentum of the element. Hence adding any rotational lumped mass only makes things worse.

Appendix 3.3: The Plane Timoshenko Beam

The Timoshenko beam (Ti-beam) incorporates two refinements over the BE model:

1. For both statics and dynamics: plane sections remain plane but not necessarily normal to the deflected mid-surface. See Fig. 16 for the kinematics. This assumption allows the averaged shear distortion to be included in both strain and kinetic energies.
2. In dynamics: the rotary inertia is included in the kinetic energy.

This model is more important for dynamics and vibration than BE, and indispensable for rapid transient and wave propagation analysis. More specifically, the BE beam has infinite phase velocity, because the EOM is parabolic, and thus becomes useless for high-fidelity wave propagation.

According to the second assumption, the kinetic energy of the Ti-beam element is given by

$$T = \tfrac{1}{2}\int_0^\ell \left(\rho A\, \dot{v}(x)^2 + \rho I_R\, \dot{\theta}(x)^2\right) dx. \tag{151}$$

Here I_R is the second moment of inertia to be used in the computation of the rotary inertia and $\theta = v' + \gamma$ is the cross-section rotation angle shown in Fig. 16; $\gamma = V/(GA_s)$ being the section-averaged shear distortion. The element DOF are ordered $\mathbf{u}^e = \left[\, v_1\ \theta_1\ v_1\ \theta_2 \,\right]^T$. The lateral displacement interpolation is

$$v(\xi) = v_1 N^e_{v1}(\xi) + v'_1 N^e_{v'1}(\xi) + v_2 N^e_{v2}(\xi) + v'_2 N^e_{v'2}(\xi), \quad \xi = \frac{2x}{\ell} - 1, \tag{152}$$

in which cubic interpolation functions are used. A complication over BE is that the rotational freedoms are θ_1 and θ_2 but the interpolation (152) is in terms of the neutral surface end slopes: $v'_1 = (dv/dx)_1 = \theta_1 - \gamma$ and $v'_2 = (dv/dx)_2 = \theta_2 - \gamma$. From a kinematic analysis we can derive the relation

$$\begin{bmatrix} v'_1 \\ v'_2 \end{bmatrix} = \frac{1}{1+\Phi}\begin{bmatrix} -\frac{\Phi}{\ell} & 1+\frac{\Phi}{2} & \frac{\Phi}{\ell} & -\frac{\Phi}{2} \\ -\frac{\Phi}{\ell} & -\frac{\Phi}{2} & \frac{\Phi}{\ell} & 1+\frac{\Phi}{2} \end{bmatrix}\begin{bmatrix} v_1 \\ \theta_1 \\ v_2 \\ \theta_2 \end{bmatrix}, \tag{153}$$

in which the dimensionless parameter $\Phi = 12EI/(GA_s\,\ell^2)$ characterizes the ratio of bending and shear rigidities. The end slopes of (153) are replaced into (152), the interpolation for θ obtained, and v and θ inserted into the kinetic energy (151).

After lengthy algebra the CMM emerges as the sum of two contributions:

$$\mathbf{M}^e_{CMM} = \mathbf{M}^e_{CT} + \mathbf{M}^e_{CR}$$

$$= C_T \begin{bmatrix} \frac{13}{35}+\frac{7}{10}\Phi+\frac{1}{3}\Phi^2 & \left(\frac{11}{210}+\frac{11}{120}\Phi+\frac{1}{24}\Phi^2\right)\ell & \frac{9}{70}+\frac{3}{10}\Phi+\frac{1}{6}\Phi^2 & -\left(\frac{13}{420}+\frac{3}{40}\Phi+\frac{1}{24}\Phi^2\right)\ell \\ & \left(\frac{1}{105}+\frac{1}{60}\Phi+\frac{1}{120}\Phi^2\right)\ell^2 & \left(\frac{13}{420}+\frac{3}{40}\Phi+\frac{1}{24}\Phi^2\right)\ell & -\left(\frac{1}{140}+\frac{1}{60}\Phi+\frac{1}{120}\Phi^2\right)\ell^2 \\ & & \frac{13}{35}+\frac{7}{10}\Phi+\frac{1}{3}\Phi^2 & \left(\frac{11}{210}+\frac{11}{120}\Phi+\frac{1}{24}\Phi^2\right)\ell \\ \text{symmetric} & & & \left(\frac{1}{105}+\frac{1}{60}\Phi+\frac{1}{120}\Phi^2\right)\ell^2 \end{bmatrix}$$

$$+ C_R \begin{bmatrix} \frac{6}{5} & \left(\frac{1}{10}-\frac{1}{2}\Phi\right)\ell & -\frac{6}{5} & \left(\frac{1}{10}-\frac{1}{2}\Phi\right)\ell \\ & \left(\frac{2}{15}+\frac{1}{6}\Phi+\frac{1}{3}\Phi^2\right)\ell^2 & \left(-\frac{1}{10}+\frac{1}{2}\Phi\right)\ell & -\left(\frac{1}{30}+\frac{1}{6}\Phi-\frac{1}{6}\Phi^2\right)\ell^2 \\ & & \frac{6}{5} & \left(-\frac{1}{10}+\frac{1}{2}\Phi\right)\ell \\ \text{symmetric} & & & \left(\frac{2}{15}+\frac{1}{6}\Phi+\frac{1}{3}\Phi^2\right)\ell^2 \end{bmatrix}. \tag{154}$$

in which $C_T = \rho\, A\, \ell/(1+\Phi)^2 = m^e/(1+\Phi)^2$ and $C_R = \rho\, I_R/((1+\Phi)^2\,\ell)$. Matrices $\mathbf{M}_{CT}$ and $\mathbf{M}_{CR}$ account for translational and rotary inertia, respectively. Caveat: the I in $\Phi = 12EI/(GA_s\,\ell^2)$ is the second moment of inertia that enters in the elastic flexural elastic rigidity. If the beam is homogeneous $I_R = I$, but that is not necessarily the case if, as sometimes happens, the beam has nonstructural attachments that contribute rotary inertia.

The scale factor of $\mathbf{M}^e_{CR}$ can be further transformed to facilitate parametric studies by introducing $r_R^2 = I_R/A$ as cross-section gyration radius and $\Psi = r_R/\ell$ as element slenderness ratio. Then $C_R = \rho I_R/((1+\Phi)^2\,\ell) = \rho A\,\ell\,\Psi^2/(1+\Phi)^2 = m^e\,\Psi^2/(1+\Phi)^2$. If $\Phi = 0$ and $\Psi = 0$, $\mathbf{M}^e_{CR}$ vanishes and $\mathbf{M}^e_{CT}$ in (154) reduces to (148).

A DLMM can be obtained through the HRZ scheme explained in Appendix Sect. 4.1. The optimal lumped mass is derived in Sect. 7.5. via templates.

Appendix 3.4: The Plane Stress Linear Triangle

We consider the three-node linear displacement triangle to model a plate in plane stress. The element will be identified as Trig3 in the sequel. Its formulation using triangular natural coordinates ζ_i is available online [42]. For the following $\mathbf{M}^e$ derivations, the plate is assumed to have constant mass density ρ, area A, and uniform thickness h. The motion is restricted to the $\{x, y\}$ plane.

The six DOFs are arranged as $\mathbf{u}^e = \left[u_{x1}\ u_{y1}\ u_{x2}\ u_{y2}\ u_{x3}\ u_{y3}\right]^T$. The CMM is obtained using the well known DSF, which are simply the triangular coordinates ζ_i. Accordingly the shape function matrix is

$$\mathbf{N}^e = \begin{bmatrix} \zeta_1 & 0 & \zeta_2 & 0 & \zeta_3 & 0 \\ 0 & \zeta_1 & 0 & \zeta_2 & 0 & \zeta_3 \end{bmatrix}. \tag{155}$$

Expanding $(\mathbf{N}^e)^T\mathbf{N}^e$ gives a 6×6 matrix quadratic in the triangular coordinates. This can be area-integrated with formulas exemplified by $\int_{\Omega^e}\zeta_1^2\,d\Omega = A/3$, $\int_{\Omega^e}\zeta_1\zeta_2\,d\Omega = A/6$, etc. The result is

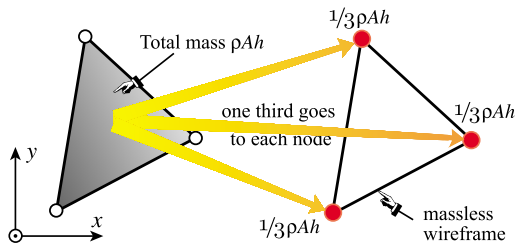

Fig. 25 Diagonal mass lumping for the Trig3 element in plane stress

$$\mathbf{M}^e_{CMM} = \rho h \int_{\Omega^e} \begin{bmatrix} \zeta_1\zeta_1 & 0 & \zeta_1\zeta_2 & 0 & \zeta_1\zeta_3 & 0 \\ 0 & \zeta_1\zeta_1 & 0 & \zeta_1\zeta_2 & 0 & \zeta_1\zeta_3 \\ \zeta_2\zeta_1 & 0 & \zeta_2\zeta_2 & 0 & \zeta_2\zeta_3 & 0 \\ 0 & \zeta_2\zeta_1 & 0 & \zeta_2\zeta_2 & 0 & \zeta_2\zeta_3 \\ \zeta_3\zeta_1 & 0 & \zeta_3\zeta_2 & 0 & \zeta_3\zeta_3 & 0 \\ 0 & \zeta_3\zeta_1 & 0 & \zeta_3\zeta_2 & 0 & \zeta_3\zeta_3 \end{bmatrix} d\Omega$$
$$= \frac{m^e}{12} \begin{bmatrix} 2 & 0 & 1 & 0 & 1 & 0 \\ 0 & 2 & 0 & 1 & 0 & 1 \\ 1 & 0 & 2 & 0 & 1 & 0 \\ 0 & 1 & 0 & 2 & 0 & 1 \\ 1 & 0 & 1 & 0 & 2 & 0 \\ 0 & 1 & 0 & 1 & 0 & 2 \end{bmatrix} \tag{156}$$

in which $m^e = \rho Ah$. This computation may be done by numerical integration, using Gauss rules. Since the order of $\mathbf{M}^e$ is 6, and each Gauss point adds two (the number of space dimensions) to the rank, a rule with 3 or more points is required to reach full rank, as can be verified by simple numerical experiments.

The DLMM is constructed by taking the total element mass element, which is ρAh, dividing it by 3 and assigning those to the corner nodes. See Fig. 25. This process produces a diagonal matrix:

$$\mathbf{M}^e_{DLMM} = \frac{\rho Ah}{3}\mathbf{diag}\begin{bmatrix} 1 & 1 & 1 & 1 & 1 & 1 \end{bmatrix} = \frac{m^e}{3}\mathbf{I}_6. \tag{157}$$

If this element is used in three dimensions (for example as membrane component of a shell element), it is necessary to insert the normal-to-the-plate z mass components in either (156) or (157). According to the invariance rule (143) the globalization process is trivial because $\mathbf{M}^e_C$ or $\mathbf{M}^e_L$ becomes a DIMM upon grouping element DOFs component-wise, and the local element mass matrix repeats in the global frame.

Appendix 3.5: The Plane Stress Bilinear Quadrilateral

We finally consider the 4-node, 8 DOF bilinear quadrilateral modeling a plate in plane stress. The element is identified as Quad4 in the sequel. It is assumed homogeneous with density ρ and constant thickness h. It moves in the x, y plane. The nodal displacement vector is $\mathbf{u}^e = \begin{bmatrix} u_{x1} & u_{y1} & u_{x2} & \dots & u_{y4} \end{bmatrix}$. The shape functions and appropriate Gauss quadrature rules are described in [42].

The integration is carried out numerically using a $p\times p$ Gauss product rule, with p variable. Testing the mass matrix module on a *rectangular* element of dimensions a and b in the x and y directions, respectively, returns the following CMMs for the 1×1 and 2×2 Gauss rules:

$$\mathbf{M}^e_{CMM1} = C_1 \begin{bmatrix} 1 & 0 & 1 & 0 & 1 & 0 & 1 & 0 \\ 0 & 1 & 0 & 1 & 0 & 1 & 0 & 1 \\ 1 & 0 & 1 & 0 & 1 & 0 & 1 & 0 \\ 0 & 1 & 0 & 1 & 0 & 1 & 0 & 1 \\ 1 & 0 & 1 & 0 & 1 & 0 & 1 & 0 \\ 0 & 1 & 0 & 1 & 0 & 1 & 0 & 1 \\ 1 & 0 & 1 & 0 & 1 & 0 & 1 & 0 \\ 0 & 1 & 0 & 1 & 0 & 1 & 0 & 1 \end{bmatrix}, \quad \mathbf{M}^e_{CMM2}$$
$$= C_2 \begin{bmatrix} 4 & 0 & 2 & 0 & 1 & 0 & 2 & 0 \\ 0 & 4 & 0 & 2 & 0 & 1 & 0 & 2 \\ 2 & 0 & 4 & 0 & 2 & 0 & 1 & 0 \\ 0 & 2 & 0 & 4 & 0 & 2 & 0 & 1 \\ 1 & 0 & 2 & 0 & 4 & 0 & 2 & 0 \\ 0 & 1 & 0 & 2 & 0 & 4 & 0 & 2 \\ 2 & 0 & 1 & 0 & 2 & 0 & 4 & 0 \\ 0 & 2 & 0 & 1 & 0 & 2 & 0 & 4 \end{bmatrix},$$

in which $C1 = \rho abh/32 = m^e/32$ and $C_2 = \rho abh/72 = m^e/72$. The mass given by 1-point integration has rank 2 and 6 zero eigenvalues, and thus it is rank-deficient by 6. The mass given by the 2×2 rule is rank-sufficient and PD. Either matrix repeats on globalization. Using rules with 3 or more points returns the same matrix. The DLMM is obtained by assigning one fourth of the total element mass $m^e = \rho abh$ to each freedom.

For a quadrilateral of general geometry, use of the 2×2 Gauss quadrature rule is recommended, as it provides full mass matrix rank.

Appendix 4: Mass Diagonalization Methods

The construction of the CMM is fully defined by the choice of kinetic energy functional and shape functions. No significant procedural deviation is possible, other than possibly using reduced integration to obtain a singular matrix. On the other hand, the construction of a DLMM is not so clear cut, except for simple elements in which the lumping is uniquely defined by conservation and symmetry considerations. A consequence of this ambiguity is that various methods have been proposed in the literature, ranging from heuristic through algorithmic. A good discussion of mass diagonalization schemes starting from the CMM can be found in the textbook by Cook et al. [19]. Its use in explicit DTI is well covered in [9]. This Appendix gives a quick overview

of proven methods, as well as a promising but as yet untried one.

Appendix 4.1: HRZ Lumping

This scheme is acronymed after the authors of [57]. It produces a DLMM given the CMM. Let m^e denote the total element mass. The procedure is as follows.

1. For each coordinate direction, select the DOFs that contribute to motion in that direction. From this set, separate translational DOF and rotational DOF subsets.
2. Add up the CMM diagonal entries pertaining to the translational DOF subset only. Call the sum S.
3. Apportion m^e to DLMM entries of both subsets on dividing the CMM diagonal entries by S.
4. Repeat for all coordinate directions.

The see HRZ in action, consider the three-node prismatic bar with CMM given by (145). Only one direction (x) is involved and all DOFs are translational. Excluding the factor $\rho A\ell/30$, which does not affect the results, the diagonal entries are 4, 4 and 16, which add up to $S = 24$. Apportion the total element mass $\rho A\ell$ to nodes with weights $4/S = 1/6$, $4/S = 1/6$ and $16/S = 2/3$. The result is the DLMM (146).

Next consider the 2-node BE plane beam element. Again only one direction (y) is involved but now there are translational and rotational freedoms. Excluding the factor $\rho A\ell/420$, the diagonal entries of the CMM (148), are 156, $4\ell^2$, 156 and $4\ell^2$. Add the translational DOF entries: $S = 156+156 = 312$. Apportion the element mass $\rho A\ell$ to the four DOFs with weights $156/312 = 1/2$, $4\ell^2/312 = \ell^2/78$, $156/312 = 1/2$ and $4\ell^2/312 = \ell^2/78$. The result is the DLMM (150) with $\alpha = 1/78$.

The procedure is heuristic but widely used on account of three advantages: easy to explain and implement, applicable to any element as long as a CMM is available, and able to retain nonnegativity. The last attribute is particularly important: it means that the DLMM is physically admissible, precluding numerical instability headaches. As a general assessment, it gives reasonable results if the element has only translational freedoms. If there are rotational freedoms the results can be poor compared to customized templates.

Appendix 4.2: Lobatto Mass Lumping

A DLMM with n_F^e diagonal entries m_i is formally equivalent to a numerical integration formula with n_F^e points for the element kinetic energy:

Table 13 1D Lobatto integration rules

Points	Abscissas $\xi_i \in [-1, 1]$	Weights w_i
2	$-\xi_1 = 1 = \xi_2$	$w_1 = w_2 = 1$
3	$-\xi_1 = 1 = \xi_3,\ \xi_2 = 0$	$w_1 = w_3 = \frac{1}{3},\ w_2 = \frac{4}{3}$
4	$-\xi_1 = 1 = \xi_4,\ -\xi_2 = 1/\sqrt{5} = \xi_3$	$w_1 = w_4 = \frac{1}{6},\ w_2 = w_3 = \frac{5}{6}$

Common names: Trapezoidal rule and Simpson's rule for $p = 2, 3$, respectively. In the $p = 4$ rule, interior points are not thirdpoints, since $1/\sqrt{5} \approx 0.447213596 \neq \frac{1}{3}$. Lobatto rules with $5 \leq p \leq 10$, rarely important in FEM work, are tabulated in [1, Table 25.6]

$$T^e = \sum_{i=1}^{n_F^e} m_i T_i, \quad \text{where} \quad T_i = \tfrac{1}{2}\dot{u}_i^2 \tag{158}$$

Assume the element is 1D, possesses only translational DOF, and that its geometry is described by the natural coordinate ξ that varies from -1 through 1 at the end nodes. Then (158) can be placed in correspondence with the so-called *Lobatto quadrature* in numerical analysis (also called Radau quadrature by some authors, e.g. [17]; however the handbook [1, p. 888] says that Lobatto and Radau rules are slightly different).

A Lobatto rule is a 1D Gaussian quadrature formula in which the endpoints of the interval $\xi \in [-1, 1]$ are sample points. If the formula has $p \geq 2$ abscissas, only $p-2$ of those are free. Abscissas are symmetric about the origin $\xi = 0$ and all weights are positive. The general form is

$$\int_{-1}^{1} f(\xi)\, d\xi = w_1 f(-1) + w_p f(1) + \sum_{i=2}^{p-1} w_i f(\xi_i). \tag{159}$$

The rules for $p = 2, 3, 4$ are collected in Table 13. Comparing (158) with (159) clearly indicates that if the nodes of a 1D element are placed at the Lobatto abscissas, the diagonal masses m_i are simply the weights w_i. This correspondence was first observed in [46], and further explored in [76,77]. For the type of elements noted, the equivalence works well for $p = 2, 3$. For $p = 4$ a minor difficulty arises: the interior Lobatto points are not at the thirdpoints, as can be seen in Table 13. If the element nodes are collocated there, one must switch to the "Simpson 3/8 rule", which is a Newton–Cotes formula listed in Table 14 and adjust diagonal masses accordingly.

As a generalization to multiple dimensions, for conciseness we call *FEM Lobatto quadrature* one in which the DOF-endowed element nodes are sample points of an integration rule (sample points at other than nodal locations are precluded). If so, the equivalence with (158) still holds. But one quickly runs into difficulties:

Table 14 1D Newton–Cotes integration rules

Points	Abscissas $\xi_i \in [-1, 1]$	Weights w_i
2	Same as 2-point Lobatto; see Table 13	
3	Same as 3-point Lobatto; see Table 13	
4	$-\xi_1 = 1 = \xi_4,\ -\xi_2 = 1/3 = \xi_3$	$w_1 = w_4 = \frac{1}{4},\ w_2 = w_3 = \frac{3}{4}$
5	$-\xi_1 = 1 = \xi_5,\ -\xi_2 = 1/2 = \xi_4,\ \xi_3 = 0$	$w_1 = w_5 = \frac{7}{90},\ w_2 = w_3 = \frac{32}{90},\ w_3 = \frac{12}{90}$

Common names for $p = 4, 5$: Simpson's 3/8 rule and Boole's rule, respectively. Additional NC formulas may be found in [1, Table 25.4]. For $p > 5$ they have negative weights

Negative Masses If one insists in higher order accuracy, weights of 2D and 3D Lobatto rules are not necessarily positive, a feature noted in [28]. The subject is studied in detail in [46]. This shortcoming can be alleviated, however, by accepting lower accuracy, or sticking to product rules in suitable geometries. For example, applying a product 1D Lobatto rule over each side of a triangle or quadrilateral. Of course a more flexible alternative is provided by templates, because these allow the stiffness to be concurrently adjusted.

Rotational Freedoms If the element has rotational DOF, Lobatto rules do not exist. Any attempt to extend (159) to node rotations inevitably leads to translation-rotation coupling.

Varying Properties If the element is nonhomogeneous or has varying properties (for instance, a tapered bar element, or a plate of variable thickness) the construction of accurate Lobatto rules runs into additional difficulties, for the problem effectively becomes the construction of a quadrature formula with non-unity kernel.

As a general assessment, Lobatto mass lumping is useful when the diagonalization problem happens to fit a Gaussian quadrature rule with *element nodes as sample points* and *nonnegative weights*. Formulas of that type were developed for multidimensional domains of simple geometry during the 1950s and 1960s. They are can be found in handbooks such as [95,96], along with many other rules. As noted above, an obvious hindrance is the *emergence of negative weights* as the rule degree gets higher. This feature excludes those from contention except under extreme caution, whereas zero weights are less deadly. Rules useful for FEM work are compiled in [37], as well as Appendix I of [41], for seven element geometries.

The six-node plane stress triangle, shown in Fig. 26(a), illuminates obstacles typically encountered in multiple space dimensions. The total element mass is $m^e = \rho\, A\, h$, in which A denotes the plane area and h the plate thickness, assumed uniform. There are two 3-point Gauss quadrature rules of degree 2 for a constant metric triangle, shown in Fig. 26b, c, which is extracted from [42]. The midpoint rule, illustrated in Fig. 26c, is also a Lobatto rule for this element, but the 3-interior-point rule pictured in Fig. 26b is not.

Using the midpoint rule to build the DLMM results in three masses of $m^e/3$ collocated at the midpoints, while all corner masses vanish [28]. The HRZ scheme leads to the same result. This DLMM has rank 6 and rank deficiency 6. To attain full rank one must take some mass from the midpoints and move it to the corners: not a well defined process. An heuristic way out would be to apply the Simpson rule line lumping along the three edges. This results in $m^e/9$ at corners and $2m^e/9$ at midpoints but the degree drops to 1. To retain accuracy, a simultaneous change of the stiffness matrix could be tried within the template framework.

For a curved-side six-node triangle with variable metric, a case illustrated in Fig. 27, node and sample points remain at the same location in terms of natural coordinates, but local Jacobian determinants enter the formula.

Appendix 4.3: Nonconforming Velocity Shape Functions

This is a variational technique based on assuming VSF that differ from the usual DSF. To produce a diagonal mass matrix, the VSF must satisfy additional "mass orthogonality" conditions that effectively decouples each VSF with respect to all others in the kinetic energy integral. This can be practically realized by making each VSF vanish at all points of a Gauss

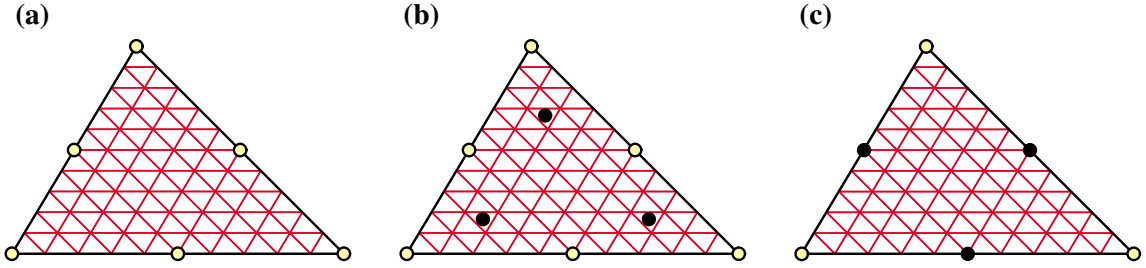

Fig. 26 A pair of degree-2, 3-point Gauss quadrature rules for the six-node plane stress triangle with constant metric: **a** node configuration, **b** the 3-interior point rule, **c** the 3-midpoint rule, which is a Lobatto rule for this node configuration. All weights are 1/3. *Lines* within *triangle mark* triangular natural coordinates (a.k.a. barycentric coordinates) of constant value, to illustrate constant metric

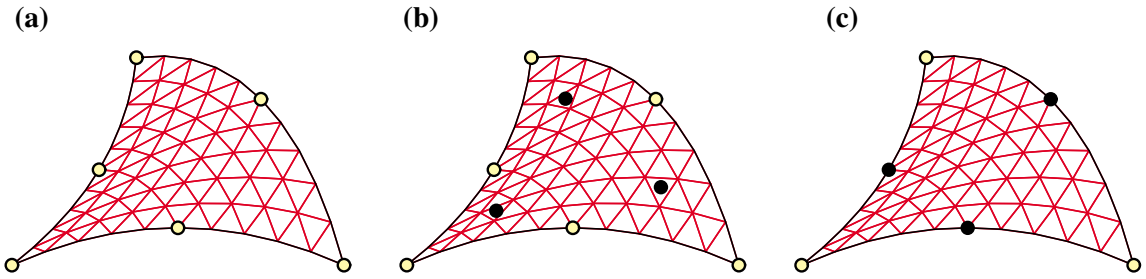

Fig. 27 As in Fig. 26, but triangle has now curved sides and variable metric

integration rule except one. Which rule? That appropriate to the correct integration of the kinetic energy over the element.

Rather than explaining the technique further, the interested reader may want to study the examples provided in Appendix 6.

Appendix 4.4: Congruential Mass Transformation

A *congruential mass transformation*, or CMT, is a general framework than can be applied to transform a given *source* mass matrix into a *target* one. In particular all model reduction techniques mentioned in Appendix Sect. 1.3. Here it is specialized to the following case of importance in diagonalization:

(i) The source mass matrix $\mathbf{M}_S$ is nondiagonal and PD; for example a CMM.
(ii) The target mass matrix $\mathbf{M}_T$ is diagonal and nonnegative (that is, zero diagonal entries are permitted)

Both matrices have order n_{DOF}. The congruential transformation that converts source to target is

$$\mathbf{M}_T = \mathbf{H}^T \mathbf{M}_S \mathbf{H}. \tag{160}$$

If $\mathbf{H}$ is nonsingular, the inverse mapping is $\mathbf{M}_S = \mathbf{G}^T \mathbf{M}_T \mathbf{G}$, in which $\mathbf{G} = \mathbf{H}^{-1}$. We will say that $\mathbf{M}_S$ and $\mathbf{M}_T$ are *congruentially linked* through $\mathbf{H}$. Even if $\mathbf{M}_S$ and $\mathbf{M}_T$ are both given and parameter-free, there are generally many $\mathbf{H}$ matrices that satisfy (160). In fact the number of solutions typically grows exponentially with n_{DOF}.

One particular form, however, is unique under conditions (i)-(ii). Perform the Cholesky factorization $\mathbf{M}_S = \mathbf{L}_S \mathbf{L}_S^T = \mathbf{L}_S \mathbf{U}_S$, where $\mathbf{L}_S$ is lower triangular and $\mathbf{U}_S = \mathbf{L}_S^T$ is upper triangular. If $\mathbf{M}_S$ is PD, this factorization is unique and both $\mathbf{L}_S$ and $\mathbf{U}_S$ are nonsingular [113]. Let $\mathbf{M}_T^{1/2}$ be the principal square root of $\mathbf{M}_T$, obtained by taking the positive square root of each diagonal entry. By inspection

$$\mathbf{H} = \mathbf{U}_S \mathbf{M}_T^{1/2}, \qquad \mathbf{H}^T = \mathbf{M}_T^{1/2} \mathbf{L}_S^{-1}. \tag{161}$$

This will be called the *Cholesky form* of $\mathbf{H}$, and identified by subscript 'CF' if necessary. Since the inverse of a nonsingular upper triangular matrix is also lower triangular, and scaling by the diagonal matrix $\mathbf{M}_T^{1/2}$ does not alter that configuration, $\mathbf{H}^T$ and $\mathbf{H}$ are lower and upper triangular, respectively.

As an example, the CMM and DLMM of the two-node prismatic bar given in (7) are linked by the Cholesky form

$$\mathbf{H}_{CF} = \frac{1}{\sqrt{2}} \begin{bmatrix} \sqrt{3} & -1 \\ 0 & 2 \end{bmatrix} = \begin{bmatrix} 1.22474 & -0.707107 \\ 0 & 1.41421 \end{bmatrix}. \tag{162}$$

For the CMM and DLMM of the three-node prismatic bar studied in Sect. 5.2, the Cholesky form is

$$\mathbf{H}_{CF} = \begin{bmatrix} \sqrt{5}/2 & 1/(2\sqrt{3}) & -\sqrt{2/3} \\ 0 & 2/\sqrt{3} & -\sqrt{2/3} \\ 0 & 0 & \sqrt{3/2} \end{bmatrix} = \begin{bmatrix} 1.180303 & 0.288675 & -0.816497 \\ 0 & 1.154701 & -0.816497 \\ 0 & 0 & 1.224745 \end{bmatrix}. \tag{163}$$

The Cholesky form of (160) is unique and easy to obtain, but does not link naturally to the algebraic Riccati equation mentioned below. For that purpose finding a symmetric $\mathbf{H}$ is more convenient. Those will be identified by subscript 'Sy' if necessary. Symmetric forms are not unique; in fact typically one generally finds $2^{n_{DOF}}$ different solutions. It is rather easy, however, to extract a principal solution.

For the two-node prismatic bar, the transformation (160) from CMM to DLMM with symmetric $\mathbf{H}$ has $2^2 = 4$ solutions. The only one with positive eigenvalues is

$$\mathbf{H}_{Sy} = \tfrac{1}{2} \begin{bmatrix} 1+\sqrt{3} & 1-\sqrt{3} \\ 1-\sqrt{3} & 1+\sqrt{3} \end{bmatrix} = \begin{bmatrix} 1.366025 & -0.366025 \\ -0.366025 & 1.366025 \end{bmatrix}. \tag{164}$$

For the 3-node pristamic bar, one gets $2^3 = 8$ solutions. The only one with all eigenvalues positive is (only given numerically, as its analytical expression is complicated):

$$\mathbf{H}_{Sy} = \begin{bmatrix} 1.2051889 & 0.2051889 & -0.1472036 \\ 0.2051889 & 1.2051889 & -0.1472036 \\ -0.1472036 & -0.1472036 & 1.1518024 \end{bmatrix}. \tag{165}$$

The determination of $\mathbf{H}$ in (160) is related to the quadratic matrix equation $\mathbf{X}^T\mathbf{A}\mathbf{X} = \mathbf{B}$, where $\mathbf{M}_S \to \mathbf{A}$ and $\mathbf{M}_T \to \mathbf{B}$ are data and $\mathbf{H} \to \mathbf{X}$ the unknown. If $\mathbf{H} \to \mathbf{X}$ is symmetric so $\mathbf{X}^T = \mathbf{X}$, the equation $\mathbf{X}\mathbf{A}\mathbf{X} = \mathbf{B}$ is a specialization of the algebraic Riccati equation extensively studied in optimal control systems [3,68]. Hopefully this interdisciplinary resource could be eventually be applied to devise robust mass diagonalization schemes using a matrix function library [56,114]. But as of now, templates remain the most practical method to find optimal diagonalizations.

Appendix 5: A Two-Dimensional Template

This appendix presents an example of the construction and LFF customization of a mass template for the simplest two-dimensional element, namely the three-node plane stress (membrane) linear triangle, identified as Trig3 in the sequel. The example is intended to illustrate three additional features that must be considered in multiple dimensions; in particular mesh directionality, multiple plane wave types, and (for an isotropic material) Poisson's ratio. It is the only multidimensional template presented in this paper, since the subject has barely lifted off the ground. The results are taken from the a recent thesis [50] in which intermdiate calculation details (omitted here for brevity) may be found. The thesis also works out a more complicated version of this element type that includes corner drilling freedoms. That development is too complex to be briefly covered here.

Appendix 5.1: Longitudinal Wave Propagation in a Continuum Thin Plate

Wave propagation in continuum models of elastic solids is a classical subject of elastodynamics that is well covered in several textbooks and monographs; e.g., [2,27,49,55,65]. Here we consider *longitudinal* waves propagating in an isotropic, homogeneous, elastic flat thin plate. Thickness effects are ignored. The continuum model has elastic modulus E, Poisson's ratio ν, shear modulus $G = E/(2(1+\nu))$, mass density ρ, and uniform thickness h. Two plane wave types are possible in that model:

Pressure waves or P-waves, in which material points harmonically oscillate in the direction of the wave propagation. Also known as longitudinal, dilatational and "push" waves. A P-wave propagates at speed c_{P0}, in which $c_{P0}^2 = \hat{E}/\rho$, with $\hat{E} = E/(1-\nu^2)$.

Shear waves or S-waves, in which material points harmonically oscillate in the direction normal to wave propagation. Also known as transverse, rotational and "shake" waves. An S-wave propagates at speed c_{S0}, in which $c_{S0}^2 = G/\rho$. The dispersion equations are

$$\omega_{P0}^2 = c_{P0}^2\,k^2, \qquad \omega_{S0}^2 = c_{S0}^2\,k^2, \tag{166}$$

in which k is the wavenumber while ω_{P0} and ω_{S0} denote the characteristic frequencies for the P- and S-wave, respectively. In dimensionless variables $\kappa = k\,a$, $\Omega_{P0}^2 = \omega_P^2\,a^2/c_{P0}^2$, and $\Omega_{S0}^2 = \omega_S^2\,a^2/c_{S0}^2$, these reduce to

$$\Omega_{P0}^2 = \kappa^2, \qquad \Omega_{S0}^2 = \kappa^2. \tag{167}$$

Note that both plane wave types are nondispersive (i.e., speed is independent of frequency) and can propagate along any in-plane direction, as befits isotropy. That is not the case in a FEM lattice of Trig3 elements, as studied next.

Appendix 5.2: Trig3 LCD Template

The Trig3 mass template is assumed to be of the LCD form (2): it linearly combines the CMM and DLMM given in (156) and (157), respectively, through a weight parameter:

$$\begin{aligned}\mathbf{M}_\mu^e &= (1-\mu)\mathbf{M}_{CMM}^e + \mu\,\mathbf{M}_{DLLM}^e \\ &= \frac{m^e(1-\mu)}{12}\begin{bmatrix} 2 & 0 & 1 & 0 & 1 & 0\\ 0 & 2 & 0 & 1 & 0 & 1\\ 1 & 0 & 2 & 0 & 1 & 0\\ 0 & 1 & 0 & 2 & 0 & 1\\ 1 & 0 & 1 & 0 & 2 & 0\\ 0 & 1 & 0 & 1 & 0 & 2 \end{bmatrix} + \frac{m^e\,\mu}{3}\,\mathbf{I}_6\end{aligned} \tag{168}$$

This is paired with the well known Trig3 stiffness $\mathbf{K}^e$, which is kept fixed. To study the performance of (168) an infinite 2D regular lattice such as pictured in Fig. 28a was chosen. The triangles form square cells of side a. To account for the effect of wave directionality in the FEM lattice, the direction of propagation of the P- and S-waves is assumed to be always along the x axis. The lattice is rotated by an angle ϕ with respect to x, as illustrated in Fig. 28b. Thus the mesh symmetry axes $\{x_m, y_m\}$ forms an angle ϕ with the propagation axis $\{x, y\}$. The advantage of this choice, as opposed to rotating the propagation direction, is that the wave functions are kept simple. The kinematic expressions for the P- and S-waves are

$$\begin{aligned}&\text{P-wave:}\quad u_x = B_x\,\exp(k\,x - \omega_P\,t), \quad u_y = 0,\\ &\text{S-wave:}\quad ux = 0, \quad u_y = B_y\,\exp(k\,x - \omega_S\,t).\end{aligned} \tag{169}$$

in which B_x and B_y are nonzero amplitudes. Note that the wavenumber k is kept the same in both expressions. All calculations summarized below were carried out symbolically with *Mathematica*.

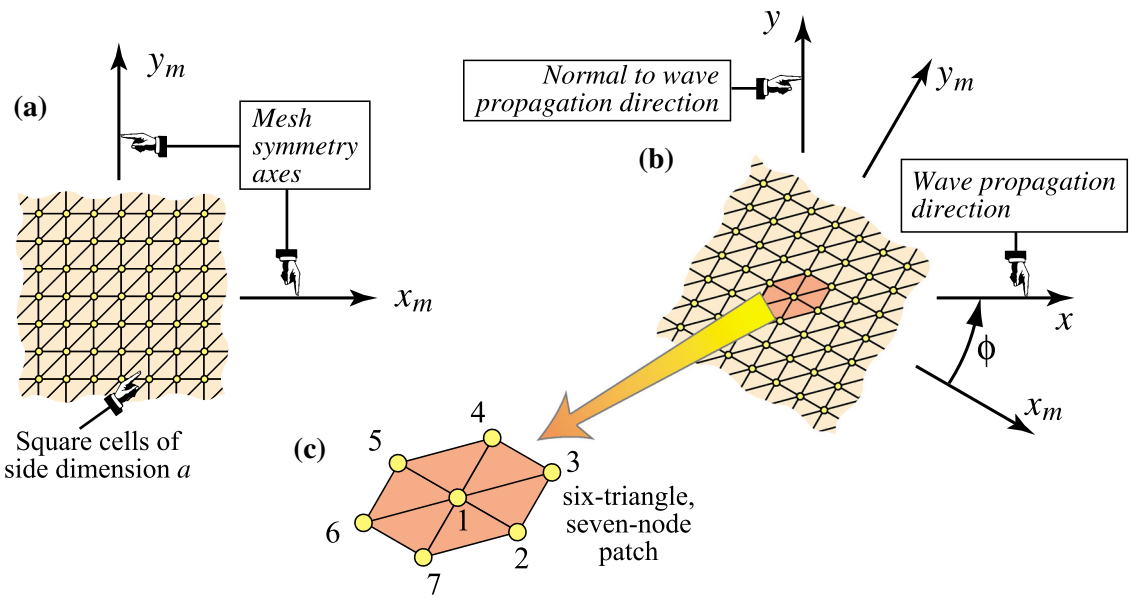

Fig. 28 Mesh for Fourier analysis of Trig3 LCD mass template: **a** infinite regular lattice of square cells, **b** rotated lattice to account for wave propagation directionality, forming angle ϕ with respect to wave propagation direction (x-axis), **c** six-triangle, seven-node patch

Appendix 5.3: Trig3 Template Fourier Analysis

From the 2D infinite lattice pictured in Fig. 28b, extract a (repeating) six-triangle, seven-node patch highlighted in (c) of that Figure. Assemble the 14×14 patch mass matrix $\mathbf{M}_p$ from (168), and the 14×14 patch stiffness matrix $\mathbf{K}_p$. From these extract the 2×14 mass matrix $\widehat{\mathbf{M}}_p$ and the 2×14 stiffness matrix $\widehat{\mathbf{K}}_p$ for the patch center node. The dynamic force residual equations at that node are

$$\mathbf{r} = (\widehat{\mathbf{K}}_p - \omega^2\, \widehat{\mathbf{M}}_p)\, \mathbf{u}_B, \tag{170}$$

in which $\mathbf{r} = \begin{bmatrix} r_x & r_y \end{bmatrix}^T$ is the residual vector measuring force equilibrium in the x and y directions, and $\mathbf{u}_p$ is a 14-vector containing wave displacements of the seven patch nodes. Two $\mathbf{u}_P$: $\mathbf{u}_{pP}$ and $\mathbf{u}_{pS}$ are constructed by evaluating the P- and S- plane waves, respectively at the patch nodes, and inserted in (170). For the P-wave, $u_y = 0$ and setting $r_x = 0$ we solve for ω^2, renamed ω_P^2. For the S-wave, $u_x = 0$ and setting $r_y = 0$ we solve for ω^2, renamed ω_S^2. Thse are then Taylor series expanded at $k = 0$ in powers of k, up to k^4. Passing to dimensionless variables: $\kappa = k\,a$, $\Omega_P^2 = \omega_P^2\, a^2/c_{P0}^2$, and $\Omega_S^2 = \omega_S^2\, a^2/c_{S0}^2$, the result for the P-wave is

$$\Omega_P^2 = \kappa^2 - \frac{2C_1 + 2(1-3\nu)\cos(4\phi) + C_2 \sin(2\phi) - 3(1+\nu)\sin(6\phi)}{384}\kappa^4 + \cdots \tag{171}$$

in which $C_1 = 32\mu + 3\nu - 17$ and $C_2 = 32\mu + 9\nu - 23$. For the S-wave:

$$\Omega_S^2 = \kappa^2 - \frac{2D_1 + 2(5+\nu)\cos(4\phi) + D_2 \sin(2\phi) + 3(1+\nu)\sin(6\phi)}{192(1-\nu)}\kappa^4 + \cdots \tag{172}$$

in which $D_1 = 7\nu + 16\mu(1-\nu) - 13$ and $D_2 = 7\nu + 16\mu(1-\nu) - 25$. Comparing to the continuum expressions (167), which may be rewritten we observe a $O(\kappa^4)$ error than depends on ϕ and ν. To eliminate the effect of ϕ we integrate that error term over $\phi \in [-\pi/2, \pi/2]$ and divide by π to get an average error. Setting that to zero and solving for μ, we get two "averaged-optimal" values for the free parameter, one for each wave type, denoted by μ_P and μ_S:

$$\mu_P(\nu) = \frac{-45 + 40\sqrt{3} - (45 - 24\sqrt{3})\nu}{48},$$
$$\mu_S(\nu) = \frac{45 - 16\sqrt{3} + (45 + 32\sqrt{3})\nu}{24(1-\nu)}, \tag{173}$$

These are plotted as functions of Poisson's ratio in Fig. 29. As can be observed, the dependence on ν is failrly mild. For the S-wave it is approximately 0.5 whereas for the S-wave it varies from 0.72 to 1.00. Which one to pick? Assuming the given ν is uniform, select either μ_P or μ_S according to the wave type expected to dominate the solution. This may require some interaction. If S-waves dominate $\mu = 1/2$ is recommended for any Poisson's ratio.

Appendix 5.4: Can Plane Waves Actually Propagate Over a 2D FEM Lattice?

The answer to the title question is: only for selected direction angles. To check that for the P-wave, pick the frequency ω_P^2

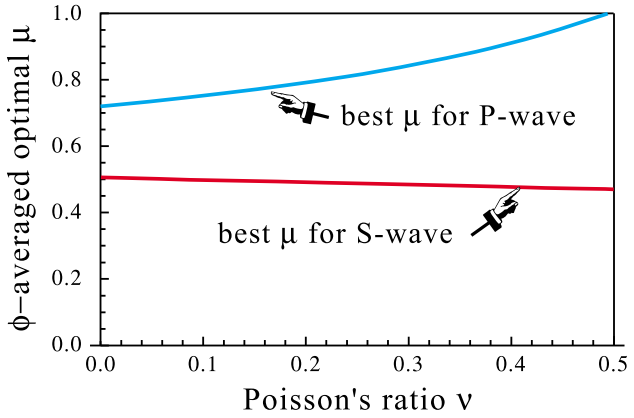

Fig. 29 Best ψ-averaged values of free parameter μ as function of Poisson's ratio ν, for two plane wave types (P and S)

obtained by solving $r_x = 0$, and insert that solution into r_y. It will be observed that for $\phi \in [-90°, 90°]$, $r_y = 0$ is only satisfied exactly at $\phi = \pm 90°$, $\phi = \pm 45°$, and $\phi = 0°$. For those angles the assumption of plane wave propagation is exact. Othwerwise $r_y \neq 0$ means that the plane wave is distorted by the FEM discretization even if the lattice is regular. A similar result is obtained for the S-wave on replacing ω_S^2 into r_x. In practice the distortion is not of great concern since the goal of this analysis is to find reasonable values for the free parameter, rather than finding a solution to the dynamic problem. Those are two distict objectives.

Appendix 6: Mass Templates in a Variational Framework

A question that may be interest to FEM theoreticians: can any mass template be produced by a conventional variational framework? By "conventional" is meant based on shape functions injected in the kinetic energy. More precisely: velocities are interpolated over the element from nodal velocities using VSF, and the element kinetic energy T^e evaluated by integration. The mass matrix follows as the Hessian of T^e with respect to nodal velocities, as per (135). In short, a variationally derived mass matrix (VDMM). For practical template construction and customization, the variational interpretation is superfluous, since templates can be expediently postulated and algebraically customized. The reformulation may be worthwhile, however, for mathematical investigations, as well as linkage to work conducted by other researchers.

Presently it is unknown whether the template-to-VDMM connection for arbitrary elements can be established. It has been only investigated for the two simplest bar elements: Bar2 and Bar3. In both cases, the general template was considered. The findings may be summarized as follows:

(1) VSF that reproduce the general template as a VDMM can be found. They are not unique.
(2) For any template instance that deviates from the CMM, the VSF do not coincide with the DSF used in the derivation of the element stiffness.
(3) VSF that deviate from the DSF are noninterpolatory and nonconforming with respect to nodal velocities computed from the displacements by time differentiation. They do *not* necessarily satisfy the unit-sum condition (also called partition of unity in the literature). A uniform velocity field, however, must produce the exact kinetic energy.

Two simple elements are analyzed below.

Appendix 6.1: Variationally Derived Bar2 Mass Template

We investigate whether the general one-parameter Bar2 mass template (9) can be produced as a VDMM. The velocity field derived from the axial displacement $u^e(x,t)$ is $\dot{u}^e(x,t) = d^e(x,t)/dt$. Evaluation at the nodes yields the nodal velocities $\dot{u}_1$ and $\dot{u}_2$, collected in $\dot{\mathbf{u}}^e = \begin{bmatrix} \dot{u}_1 & \dot{u}_2 \end{bmatrix}^T$. Let $N_1(\xi) = (1-\xi)/2$ and $N_2(\xi) = (1+\xi)/2$ denote the well known displacement shape functions (DS)F of Bar2, ξ being the usual iso-P natural coordinate. The element velocity interpolation is taken to be

$$v^e(\xi) = \dot{u}_1\, N_{v1}(\xi) + \dot{u}_2\, N_{v2}(\xi), \tag{174}$$

in which the VSF N_{v1} and N_{v2} are linked to the DSF through the linear map

$$\begin{aligned} N_{v1}(\xi) &= (1 + \tfrac{1}{2}\delta_1)\, N_1(\xi) + \tfrac{1}{2}\delta_2\, N_2(\xi), \\ N_{v2}(\xi) &= \tfrac{1}{2}\delta_2\, N_2(\xi) + (1 + \tfrac{1}{2}\delta_1)\, N_1(\xi). \end{aligned} \tag{175}$$

In (175), δ_1 and δ_2 are functions of the template parameter (but not of ξ), representing the deviations of the VSF from the DSF. Note that prismatic bar symmetry is built-in: $N_{v1}(\xi) = N_{v2}(-\xi)$. The associated kinetic energy T^e is $\rho\, A\, (\ell/2) \int_{-1}^{1} \left(v^e(\xi)\right)^2 d\xi$, which can be evaluated either analytically or through 2-point Gauss integration. Taking its Hessian with respect to $\dot{\mathbf{u}}^e$ gives a mass matrix denoted by $\mathbf{M}_\delta^e$ below. As for the Bar2 template, it is preferable to use the alternative form $\mathbf{M}_\chi^e$ of (10) rather than $\mathbf{M}_\mu^e$ of (9) because solutions are simpler. Summarizing, the two matrices to be matched are

$$\mathbf{M}_\delta^e = \tfrac{1}{24}\,\rho\, A\, \ell \begin{bmatrix} \psi_{11} & \psi_{12} \\ \psi_{21} & \psi_{22} \end{bmatrix},$$

$$\mathbf{M}_\chi^e = \tfrac{1}{12}\,\rho A\, \ell \begin{bmatrix} 3+\chi & 3-\chi \\ 3-\chi & 3+\chi \end{bmatrix},$$

$$\psi_{11} = \psi_{22} = 2(4 + 4\delta_1 + 2\delta_2 + \delta_1^2 + \delta_1\delta_2 + \delta_2^2),$$

$$\psi_{12} = \psi_{21} = 4 + 4\delta_1 + 8\delta_2 + \delta_1^2 + 4\delta_1\delta_2 + \delta_2^2,$$

$$\chi = 1 + 2\mu, \quad \mu = \tfrac{1}{2}(\chi - 1), \tag{176}$$

in which (10) is reproduced for convenience.

On equating $\mathbf{M}^e_\delta = \mathbf{M}^e_\chi$ we get four solutions: $\{\delta_1 = -3-\sqrt{\chi}, \delta_2 = -1+\sqrt{\chi}\}$, $\{\delta_1 = -1-\sqrt{\chi}, \delta_2 = 1+\sqrt{\chi}\}$, $\{\delta_1 = -3+\sqrt{\chi}, \delta_2 = -1-\sqrt{\chi}\}$, and $\{\delta_1 = -1+\sqrt{\chi}, \delta_2 = 1-\sqrt{\chi}\}$. Only the last one reduces the VSF to DSF when $\mu = 0$ or $\chi = 1$. Inserting it into (175) and simplifying yields

$$\begin{aligned} N_{v1}(\xi) &= \tfrac{1}{2}(1 - \xi\sqrt{\chi}) = \tfrac{1}{2}(1 - \xi\sqrt{1+2\mu}), \\ N_{v2}(\xi) &= \tfrac{1}{2}(1 + \xi\sqrt{\chi}) = \tfrac{1}{2}(1 + \xi\sqrt{1+2\mu}). \end{aligned} \tag{177}$$

These VSF satisfy the conservation condition $N_{v1} + N_{v2} = 1$ for any μ and ξ. They are plotted in Fig. 30 for three instances: $\mu = 0$ (CMM) $\mu = \frac{1}{2}$ (BLFM), and 1 (DLMM). If $\mu \neq 0$, the VSF depart from the DSF, and are plainly nonconforming.

The two VSF for $\mu = 1$, namely $(1 \pm \xi\sqrt{3})/2$, display a distinguishing geometric feature: each VSF vanishes at one of the sample points $\xi = \pm 1/\sqrt{3}$ of the 2-point Gauss rule; see Fig. 30c. This effectively orthogonalizes them in the sense that the kinetic energy cross integral $\int_{-1}^{1} N_{v1}\, N_{v2}\, d\xi$ is zero. The result is the diagonal mass matrix $\mathbf{M}^e_L$ of (7).

Comparing the results (177) with the ansatz (175), clearly shows that the latter was too elaborate. Little harm is done, however, for this simple element. For more complicated ones, such as the Bar3 studied next, a recursive adjustment is recommended using an interactive CAS.

Appendix 6.2: Variationally Derived Bar3 Mass Template

Next we find whether the general mass template for Bar3 can be derived variationally. The well known DSF are $N_1(\xi) = -\xi(1-\xi)/2$, $N_2(\xi) = \xi(1+\xi)/2$, and $N_3(\xi) = 1 - \xi^2$. The velocity interpolation is assumed to be

$$v^e(\xi) = \dot{u}_1\, N_{v1}(\xi) + \dot{u}_2\, N_{v2}(\xi) + \dot{u}_3\, N_{v3}(\xi), \tag{178}$$

in which

$$\begin{aligned} N_{v1}(\xi) &= N_1(\xi) - \tfrac{1}{2}\xi(\delta_1 - \delta_2\,\xi), \\ N_{v2}(\xi) &= N_2(\xi) + \tfrac{1}{2}\xi(\delta_1 + \delta_2\,\xi), \\ N_{v3}(\xi) &= N_3(\xi) + (\delta_3 + \delta_4\,\xi^2). \end{aligned} \tag{179}$$

Here δ_1 through δ_4 are functions of the template parameters to be determined. The VSF ansatz (179) was obtained after some simplifying initial computations. Note that prismatic bar symmetry is preimposed: $N_{v1}(\xi) = N_{v2}(-\xi)$ and $N_{v3}(\xi) = N_{v3}(-\xi)$. The associated kinetic energy T^e can be evaluated either analytically or from 3-point Gauss integration. Taking its Hessian with respect to $\dot{\mathbf{u}}^e$ gives the mass matrix

$$\mathbf{M}^e_\delta = \frac{\rho\, A\, \ell}{30}\begin{bmatrix} \psi_{11} & \psi_{12} & \psi_{13} \\ \psi_{21} & \psi_{22} & \psi_{23} \\ \psi_{31} & \psi_{32} & \psi_{33} \end{bmatrix},$$

$$\begin{aligned} \psi_{11} &= \psi_{22} = 2(2 + 5\delta_1 + 5\delta_1^2 + 3\delta_2 + 3\delta_2^2), \\ \psi_{12} &= \psi_{21} = -1 - 10\delta_1 - 10\delta_1^2 + 6\delta_2 + 6\delta_2^2, \\ \psi_{13} &= \psi_{23} = \psi_{31} = \psi_{32} = (1 + 2\delta_2)(2 + 5\delta_3 + 3\delta_4), \\ \psi_{33} &= 2(8 + 15\delta_3^2 + 4\delta_4 + 3\delta_4^2 + 10\delta_3(2 + \delta_4)). \end{aligned} \tag{180}$$

It is convenient to match $\mathbf{M}^e_\delta$ to the 3-parameter, χ-form of mass matrix template (44) instead of against (39). Matching entries gives 8 solutions, of which the one that yields $\delta_1 = \delta_2 = \delta_3 = \delta_4 = 0$ for the CMM ($\chi_1 = 5/2$, $\chi_2 = 3/2$, $\chi_3 = 2/3$) is picked:

$$\begin{aligned} &\delta_1 = \phi_1 - 1/2, \quad \delta_2 = \phi_2 - 1/2, \quad \delta_3 = 3\phi_3/2 - 1, \\ &\delta_4 = 1 - 2\phi_2 + \phi_3 - 5\phi_4/2, \end{aligned} \tag{181}$$

in which $\phi_1 = \sqrt{\chi_2/10}$, $\phi_2 = \sqrt{\chi_1/6}$, $\phi_3 = \sqrt{\chi_3/\chi_1}$, and $\phi_4 = \sqrt{5(1 - \chi_3/\chi_1)}$. Except for the CMM, these VSF do not verify the strong (pointwise) unit sum condition $N_{v1} + N_{v2} + N_{v3} = 1$ for each ξ, but do satisfy the more lenient element mass conservation constraint

$$\tfrac{1}{2}\int_{-1}^{1} (N_{v1} + N_{v2} + N_{v3})^2\, d\xi = 1. \tag{182}$$

In terms of the δ_i, (182) is $12\delta_2^2 + 15\delta_3^2 + 10\delta_3(3 + \delta_4) + \delta_4(10 + 3\delta_4) + 4\delta_2(5 + 5\delta_3 + 3\delta_4) = 0$.

The VSF produced by (181) are plotted in Fig. 31 for nine Bar3 mass instances, as labeled therein. Except for the CMM they depart from the DSF, and are nonconforming. Some mass matrix properties can be discerned visually:

- For the diagonally lumped instances SLMM and BLFD shown in Fig. 31b, e, two VSF vanish at each of the sample points $\xi \in \{0, \pm\sqrt{3/5}\}$ of the 3-point Gauss rule. Those points are marked in the Figure. This feature effectively energy-orthogonalizes the VSF in the sense of kinetic energy, since all cross integrals $\int_{-1}^{1} N_{vi}\, N_{vj}\, d\xi$ for $i \neq j$ vanish. As a result, diagonal mass matrices are produced.
- The VSF for the singular mass instance BSSM shown in Fig 31f, clearly displays linear dependence among the VSF.

Aside from those special cases, it is difficult to draw general conclusions from a glance at Fig. 31 as to performance. For example, why does the VSF displayed in Fig. 31d provides the best low frequency matching? Shapes for say, (a) through (e), look quite similar (once you've seen one

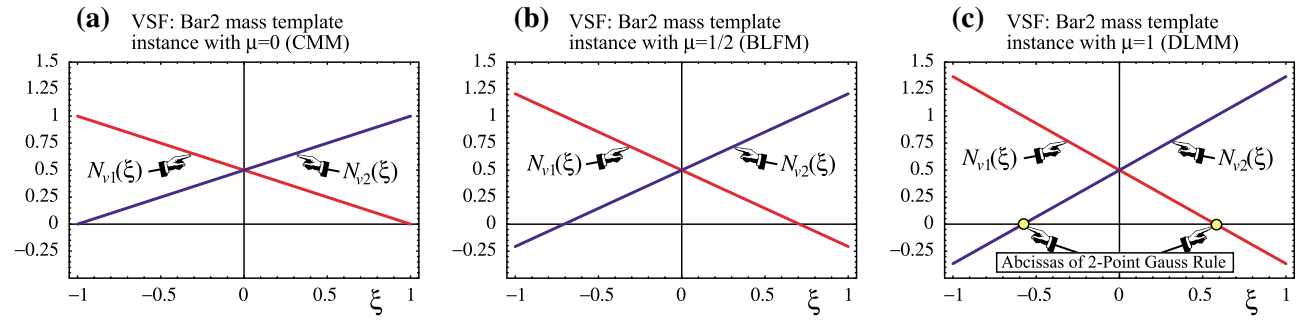

Fig. 30 VSF that produce the general Bar2 mass template (8) in a variational framework, for three instances

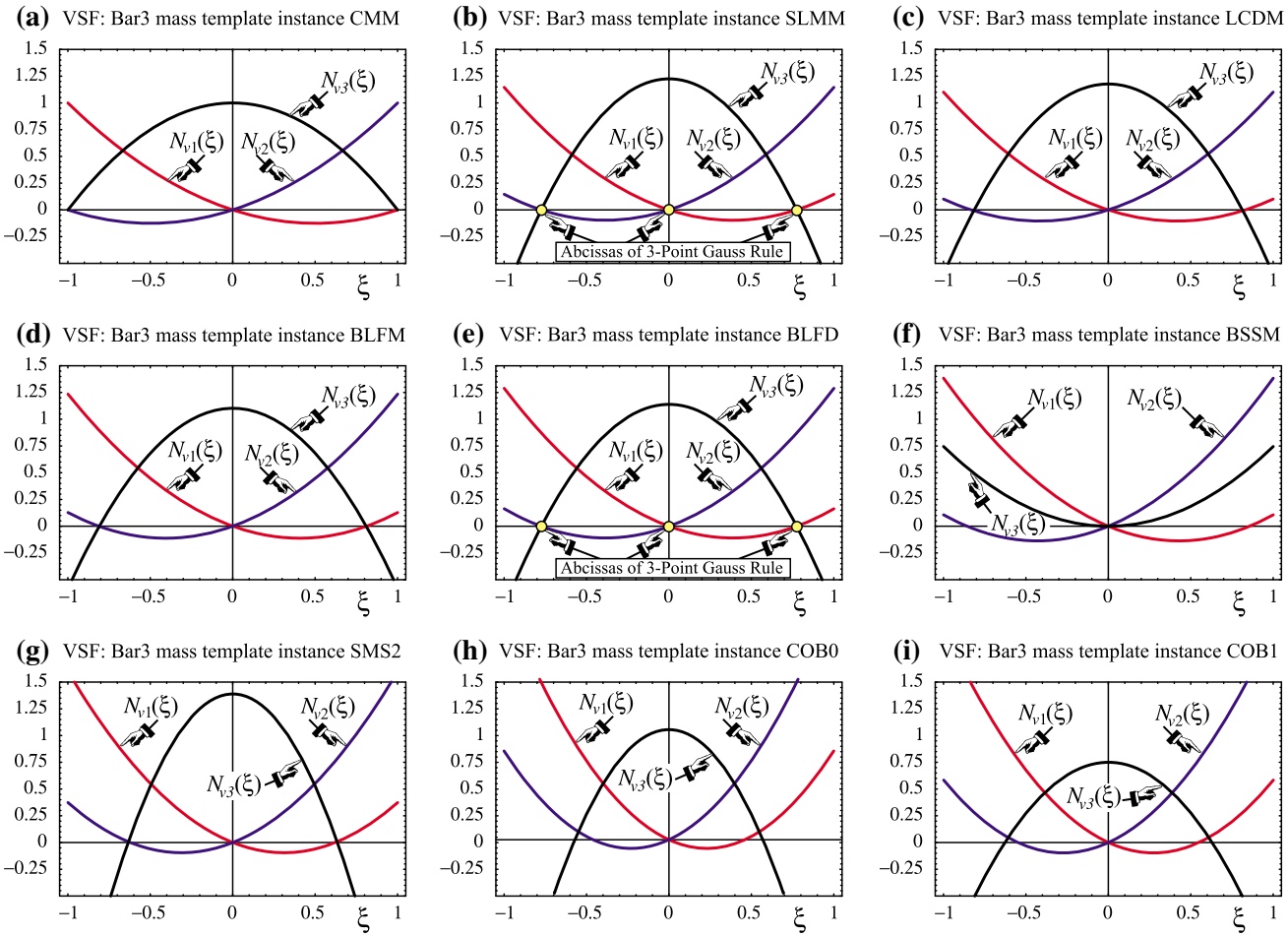

Fig. 31 VSF that produce the general Bar3 mass template (44) in a variational framework, for the nine labeled instances

parabola...). The obvious conclusion: Fourier analysis is a much sharper tool in dynamics.

Appendix 6.3: A Comment on the Variational Formulations of Elastodynamics

The use of VSF that differ from DSF dates back to the early days of FEM. It was done, for example, in [28] for the HCT plate bending element, following suggestions by R. W. Clough (the consistent mass of that tricubic macroelement was too complicated for hand derivations in 1966). The idea can be incorporated into the well-known stationary-action variational principle (VP) of elastodynamics, called Hamilton-Kirchhoff by Gurtin [51, p. 225], by weakening the temporal kinematic link.

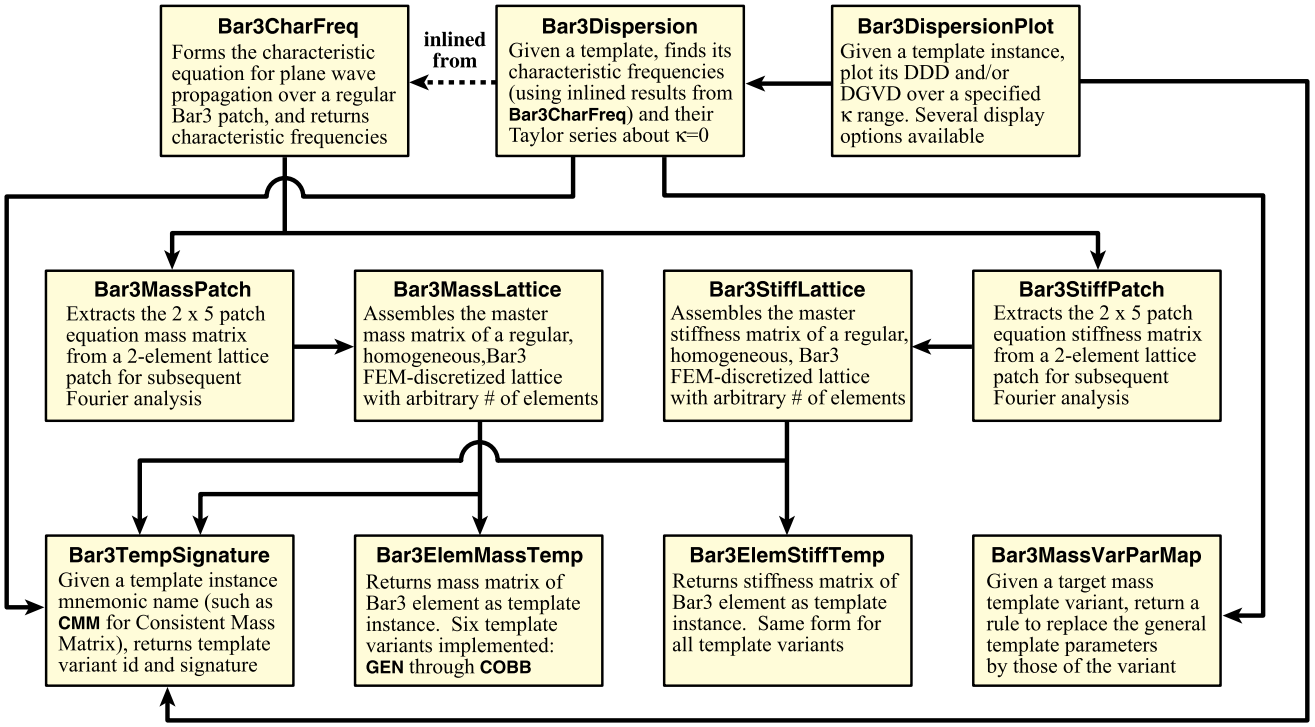

Fig. 32 Organization of Bar3 template analysis modules presented in this Appendix

That minor generalization of the primal VP of elastodynamics should not be confused with the use of dual (also called complementary or reciprocal) forms. Research in that subject took off with Toupin's formulation [103] of a dual form of Hamilton's principle for a system of mass particles with interaction impulses as unknown variables. For corrections and evolution into continua see [25,98] and references therein. FEM applications to vibrations and dynamics emerged during the early 1970s; see e.g., [44,47,97], but have stagnated since. Reason: impulse DOF are foreign to the DSM, which dominates general purpose codes.

Appendix 7: Implementation of Bar3 Template

This Appendix presents the computer implementation of the MS template pair for the three-node bar element, abbreviated to Bar3. It is written in the *Mathematica* language. Although the element is admittedly simple it is not trivial. In fact the implementation illustrates the use of template variants to simplify customization. Why *Mathematica*?. As observed in the Introduction, use of a CAS is essential for template development because analytical derivations soon exceed human endurance. Once the development phase is completed, a production version in a compilable language such as C can be easily produced. But the CAS version should not be discarded.

The hierarchical organization of the modules presented in this Appendix is shown in Fig. 32. The bottom-up description that follows starts from the lowest level of that chart, going up and traversing against the arrows.

Appendix 7.1: Auxiliary Modules

The two outside modules at the lowest level of the chart of Fig. 32 provide auxiliary services to modules at all levels.

Appendix 7.1.1: Name To Signature Mapper

Auxiliary module `Bar3TempSignature`, listed at the top of Fig. 33, maps an abbreviated template instance name to its full signature definition. It is invoked by

```
tsign = Bar3TempSignature[name]
```
(183)

The only argument is `name`: a character string of 3 or 4 letters that abbreviates a template instance. Examples: `"CMM"` for the CMM or `"SLMM"` for Simpson-lumped mass matrix. Names currently implemented can be gathered by examining the code. Some of these are also listed in Table 10.

The function returns `tsign` as template signature. This is a list of the form

```
{tvar, {kpars}, {mpars}}
```
(184)

Here `tvar` is a character string that identifies template variants, `kpars` a list of stiffness parameters, and `mpars` a list of

```
Bar3TempSignature[name_]:=Module[{a1,a2,β,μL1,μS1,μS2,μK,
 modname="Bar3TempSignature"},
 If [name=="CMM",  Return[{"GEN",{1},{0,0,0,0}}]];
 If [name=="SLMM", Return[{"LUM",{1},{0,0}}]];
 If [name=="BLCD", Return[{"GEN",{1},{2,8,2,-4}/3}]];
 If [name=="BLFM", a1=375^(1/4); a2=Sqrt[15];
                   Return[{"GEN",{1},{91-12*a1-7*a2,64-16*a2,
                   61-12*a1-a2,-92+12*a1+8*a2}/6}]];
 If [name=="BLFD", β=3/(4*(Sqrt[3]-1)); μL1=5*(2-Sqrt[3]);
                   Return[{"LUM",{β},{μL1,-2*μL1}}]];
 If [name=="BSSM", β=(5+Sqrt[10])/12; μS1=3*(5+Sqrt[10])/2;
                   Return[{"SPE",{β},{μS1,0}}]];
 If [name=="SMS1", μK=1/24;  β=1/(1-12*μK); Return[{"SMS",{β},{0,0,μK}}]];
 If [name=="SMS2", μK=1/2;   β=1; Return[{"SMS",{β},{0,0,μK}}]];
 If [name=="SMS3", μK=2;     β=1; Return[{"SMS",{β},{0,0,μK}}]];
 If [name=="COB0", Return[{"COBA",{1},{-5/3}}]];
 If [name=="COB1", Return[{"COBA",{1},{0}}]];
 If [name=="COB2", Return[{"COBB",{1},{0}}]];
 Print[modname,": illegal template name ",name," CMM assumed"];
 Return[{"GEN",{0},{0,0,0,0}}]];

Bar3MassVarParMap[gmpars_,tsign_]:=Module[{tvar,β,mpars,μ1,μ2,μ3,μ4,
  ν1,ν2,ν3,ν4,χ1,χ2,χ3,μL1,μL2,μS1,μS2,μK,νA,νB,s,d,r,kw,rep={}},
 {μ1,μ2,μ3,μ4}=gmpars; {tvar,{β},mpars}=tsign; kw=ToUpperCase[tvar];
 If [kw=="GEN", {ν1,ν2,ν3,ν4}=mpars; rep={μ1->ν1,μ2->ν2,μ3->ν3,μ4->ν4}];
 If [kw=="GEX", {χ1,χ2,χ3}=mpars; r=Sqrt[30]*Sqrt[χ1-χ3]-2*χ1; s=χ1+χ2;
                 d=χ1-χ2; rep={μ1->s-4,μ2->14-4*χ1-4*r,μ3->d+1,μ4->r-2}];
 If [kw=="LUM", {μL1,μL2}=mpars; rep={μ1->μL1+1,μ2->μL2+4,μ3->1,μ4->-2}];
 If [kw=="SPE", {μS1,μS2}=mpars; rep={μ1->(μS1+μS2-2)/3,μ2->(4*μS2-38)/3,
                 μ3->(13-μS1+μS2)/3,μ4->(4-2*μS2)/3}];
 If [kw=="SMS", {μL1,μL2,μK}=mpars; rep={μ1->1+μL1+10*(4*β+3)*μK,
                 μ2->4+μL2+160*β*μK,μ3->1+10*(4*β-3)*μK,μ4->-2-80*β*μK}];
 If [kw=="COBA",{νA}=mpars; rep={μ1->11-5*νA/2,μ2->-2*(3+5*νA),
                 μ3->6-5*νA/2,μ4->-7+5*νA}];
 If [kw=="COBB",{νB}=mpars; rep={μ1->8/3-5*νB/2-5*νB^2/72,μ2->32/3,
                 μ3->8/3-5*νB/6+(5*νB^2)/72,μ4->(5*νB-16)/3}];
 Return[rep]];
```

Fig. 33 Two auxiliary modules. `Bar3TempSignature` maps a template name to its signature. `Bar3MassVarParMap` returns a replacement rule that maps the general mass template to a target variant

Table 15 Bar3 template signature list specification

Template variant	Ref. Eqs.	# Of pars	Signature format, identified as `tsign` in Mathematica code	Mass conservation constraint[a]
General, μ_i pars	(39)	5	{ "GEN",{ β },{ $\mu_1, \mu_2, \mu_3, \mu_4$ } }	$2\mu_1+\mu_2+2\mu_3+4\mu_4 = 0$
General, χ_i pars	(44)	4	{ "GEX",{ β },{ χ_1, χ_2, χ_3 } }	preimposed
Lumped	(63)	3	{ "LUM",{ β },{ μ_{L1}, μ_{L2} } }	$2\mu_{L1}+\mu_{L2} = 0$
Spectral	(71)	3	{ "SPE",{ β },{ μ_{S1}, μ_{S2} } }	preimposed
Selective mass scaling	(81)	4	{ "SMS",{ β },{ $\mu_{L1}, \mu_{L2}, \mu_K$ } }	$2\mu_{L1}+\mu_{L2} = 0$
Constant optical branch[b]	(84), (86)	1	{ "COBA",{ 1 },{ ν_A } }or { "COBB",{ 1 },{ ν_B } }	preimposed

[a] When doing symbolic work, the mass conservation constraint is not always preimposed in some template variants, as that may complicate intermediate expressions

[b] For this variant, two families: COBA and COBB, are implemented. Cf. Sect. 5.13

mass parameters. Configuration details for this data structure are given in Table 15. If `name` is not recognized, a warning message is printed and `"CMM"` is assumed.

Example: `Bar3TempSignature["SLMM"]` returns `{"LUM",{1},{0,0}}` as function value.

Appendix 7.1.2: Mass Template Variant Parameter Mapper

Auxiliary module `Bar3MasVarParMap`, listed at the bottom of Fig. 33, returns a replacement rule that maps the four μ parameters of the Bar3 general mass template

(39) to those of a variant. The latter is called the *target* form. The rule is used to specialize results such as dispersion equations; cf. the link drawn in Fig. 32. It is invoked by

```
rule = Bar3MasVarParMap[gmpars, tsign]   (185)
```

The arguments are:

`gmpars`	A list of symbols used for the free parameters of of the Bar3 mass template (39). Normally the parameters are labeled { $\mu_1, \mu_2, \mu_3, \mu_4$ }. Those symbols will appear in the left side of the replacement rule.
`tsign`	Signature of the target form.

Items in `gmpars` must be individual symbols, while those in `tsign` may be symbolic or numeric (see examples below). Note that β in `tsign` is used if the target pertains to the SMS variant.

The function returns

`rule`	Replacement rule. If the target is not recognized, the empty list `{ }` is returned.

Example 1 Let `gmpars=`{ $\mu_1, \mu_2, \mu_3, \mu_4$ } and `tsign=` { `"LUM"`, { β }, { μ_{L1}, μ_{L2} } }. The module call `Bar3MasVarParMap[tsign,gmpars]` returns {μ_1 `->`μ_{L1} `+1`,μ_2`->`μ_{L2}`+4`, μ_3`->1`,μ_4`->-2` }, a rule that maps the general template (39) to the lumped mass variant as per (62).

Example 2 Same `gmpars` as above but now `tsign=` { `"LUM"`, { β }, { 0, 0 } }. The call returns {μ_1`->1`,μ_2 `->4`, μ_3`->1`, μ_4`->-2` }, a replacement rule that produces the SLMM instance.

Appendix 7.2: Element Level Modules

This section describes element modules that return mass and stiffness templates.

Appendix 7.2.1: Element Mass and Stiffness Modules

The Bar3 element mass and stiffness template modules are called `Bar3ElemMassTemp` and `Bar3ElemStiffTemp`, respectively. They are listed in Fig. 34. The call sequences are

```
Me = Bar3ElemMassTemp[Le, rho, A, tsign, numer]   (186)
Ke = Bar3ElemStiffTemp[Le, Em, A, tsign, numer]   (187)
```

The arguments are:

`Le`	Element length
`Em,A,rho`	Elastic modulus, cross section area, and mass density, respectively, of bar
`tsign`	Template signature. See Table 15 for configuration details.
`numer`	Logical flag. If `True`, process in floating point. If `False`, process symbolically.

As function values the modules return

`Me`	3×3 element mass matrix
`Ke`	3×3 element stiffness matrix

Appendix 7.3: Assembly Level Modules

This section covers modules that work at the assembly (master) level. These are the midlevel four pictured in Fig. 32.

Appendix 7.3.1: Lattice Master Mass and Stiffness Modules

Modules `Bar3ElemMassTempLattice` and `Bar3StiffTempLattice`, listed in Fig. 35, assemble the master mass and stiffness matrices, respectively, of a prismatic homogeneous bar member discretized as a regular lattice with a given number of elements. Since all elements are identical, only one call to the appropriate element-level module is made. The returning matrix is reused in the merge loop. The call sequences are similar:

```
M = Bar3MassTempLattice[numele, Le, rho, A,
    tdef, numer]                          (188)
K = Bar3StiffTempLattice[numele, Le, Em, A,
    tdef, numer]                          (189)
```

The arguments are:

`numele`	Number of elements in lattice. The number of freedoms is `numdof=2*numele+1`
`Le`	Element length. Total member length will be `Le*numele`
`Em,A,rho`	Elastic modulus, cross section area, and mass density, respectively, of bar
`tdef`	Template definition argument. Two possibilities: If a list, `tdef` is taken to be the template signature `tsign` configured as shown in Table 15, and thus passed directly to the element module If a character string (for example: `"CMM"`), `tdef` is interpreted as a template instance abbreviation and `Bar3TempSignature` called as per (185) to build `tsign`, which is then passed to the element modules
`numer`	Logical flag; see Sect. 1

Fig. 34 Bar3 element mass and stiffness template modules

```
Bar3MassTemp[Le_,ρ_,A_,tsign_,numer_]:=Module[
 {me=ρ*A*Le,μ1,μ2,μ3,μ4,μL1,μL2,μS1,μS2,μK,νA,νB,MKe,χ1,χ2,χ3,
 m1,m2,m3,tvar,β,mpars,kw,varOK,MeZ,Me,modname="Bar3MassTemp"},
 {tvar,{β},mpars}=tsign; varOK=False;
  kw=ToUpperCase[tvar]; MeZ=Table[0,{3},{3}];
  If [kw=="GEN", varOK=True; {μ1,μ2,μ3,μ4}=mpars;
      Me=me*{{4+μ1,-1+μ3,2+μ4},{-1+μ3,4+μ1,2+μ4},
             {2+μ4,2+μ4,16+μ2}}/30];
  If [kw=="GEX", varOK=True; {χ1,χ2,χ3}=mpars;
      m1=χ1+χ2; m2=χ1-χ2; m3=Sqrt[30]*Sqrt[χ1-χ3]-2*χ1;
      Me=me*{{m1,m2,m3},{m2,m1,m3},{m3,m3,30-4*χ1-4*m3}}/30];
  If [kw=="LUM", varOK=True; {μL1,μL2}=mpars;
      Me=me*{{5+μL1,0,0},{0,5+μL1,0},{0,0,20+μL2}}/30];
  If [kw=="SPE", varOK=True; {μS1,μS2}=mpars;
      Me=me*{{10+μS1+μS2, 10-μS1+μS2, 10-2*μS2},
             {10-μS1+μS2, 10+μS1+μS2, 10-2*μS2},
             {10-2*μS2,   10-2*μS2,   10+4*μS2}}/90];
  If [kw=="SMS", varOK=True; {μL1,μL2,μK}=mpars;
      MKe=μK*me*Bar3StiffTemp[1,1,1,tsign,numer];
      Me=me*{{5+μL1,0,0},{0,5+μL1,0},{0,0,20+μL2}}/30+MKe];
  If [kw=="COBA", varOK=True; {νA}=mpars;
      Me=me*{{  6-νA,    2-νA,-2+2*νA},
             {  2-νA,    6-νA,-2+2*νA},
             {-2+2*νA,-2+2*νA, 4-4*νA}}/12];
  If [kw=="COBB", varOK=True; {νB}=mpars;
      Me=me*{{96-36*νB-νB^2, 24-12*νB+νB^2, -48+24*νB},
             {24-12*νB+νB^2, 96-36*νB-νB^2, -48+24*νB},
             {-48+24*νB,    -48+24*νB,           384}}/432];
  If [!varOK, Print[modname,": bad template var ",tvar,
       ", zero matrix returned"]; Return[MeZ]];
  If [!numer, Me=Simplify[Me]];
  Return[Me]];

Bar3StiffTemp[Le_,Em_,A_,tsign_,numer_]:=Module[
 {ke=Em*A/Le,tvar,β,mpars,Keb,Keh,Ke},
 {tvar,{β},mpars}=tsign;
  Keb=ke*{{1,-1,0},{-1,1,0},{0,0,0}};
  Keh=(4/3)*β*ke*{{1,1,-2},{1,1,-2},{-2,-2,4}};
  Ke=Keb+Keh; If[!numer, Ke=Simplify[Ke]];
  Return[Ke]];
```

Fig. 35 Bar3 master mass and stiffness assembler modules

```
Bar3MassTempLattice[numele_,Le_,ρ_,A_,tdef_,numer_]:=Module[
 {tsign=tdef,e,i,j,ii,jj,eft,Me,M,numnod=2*numele+1},
 If [Head[tdef]==String, tsign=Bar3TempSignature[tdef]];
 M=Table[0,{numnod},{numnod}];
 Me=Bar3MassTemp[Le,ρ,A,tsign,numer];
 For [e=1,e<=numele,e++, eft={1,3,2}+(e-1)*{2,2,2};
     For [i=1,i<=3,i++, ii=eft[[i]];
         For [j=1,j<=3,j++, jj=eft[[j]];
                 M[[ii,jj]]+=Me[[i,j]]
             ];
         ];
     ]; If [!numer, M=Simplify[M]];
 Return[M] ];

Bar3StiffTempLattice[numele_,Le_,Em_,A_,tdef_,numer_]:=Module[
 {tsign=tdef,e,i,j,ii,jj,eft,Ke,K,numnod=2*numele+1},
  If [Head[tdef]==String, tsign=Bar3TempSignature[tdef]];
  K=Table[0,{numnod},{numnod}];
  Ke=Bar3StiffTemp[Le,Em,A,tsign,numer];
  For [e=1,e<=numele,e++, eft={1,3,2}+(e-1)*{2,2,2};
      For [i=1,i<=3,i++, ii=eft[[i]];
          For [j=1,j<=3,j++, jj=eft[[j]];
                 K[[ii,jj]]+=Ke[[i,j]]
              ];
          ];
      ]; If [!numer, K=Simplify[K]];
 Return[K] ];
```

```
Bar3StiffTempPatch[Le_,Em_,A_,tdef_,numer_]:=Module[
 {e,i,j,ii,jj,K},
  K=Bar3StiffTempLattice[2,Le,Em,A,tdef,numer];
  Return[{K[[2]],K[[3]]}] ];

Bar3MassTempPatch[Le_,ρ_,A_,tdef_, numer_]:=Module[
 {e,i,j,ii,jj,M},
  M=Bar3MassTempLattice[2,Le,ρ,A,tdef,numer];
  Return[{M[[2]],M[[3]]}] ];
```

Fig. 36 Bar3 mass and stiffness patch extraction modules

As function values the modules return

`M` Master mass matrix of order `ndof×ndof`
`K` Master stiffness matrix of order `ndof×ndof`

Appendix 7.3.2: Lattice Patch Modules

Modules `Bar3ElemMassPatch` and `Bar3StiffPatch`, listed in Fig. 36, return the assembled mass and stiffness matrices, respectively, of a patch of two identical Bar3 elements. This is done by calling `Bar3MassTempLattice` and `Bar3StiffTempLattice` with `numele=2` and returning only the second and third equations. The call sequences are similar:

$$\texttt{M} = \texttt{Bar3MassTempPatch[Le, rho, A, tdef, numer]} \tag{190}$$

$$\texttt{K} = \texttt{Bar3StiffTemppatch[Le, Em, A, tdef, numer]} \tag{191}$$

The arguments are identical to those for the lattice master mass and stiffness modules, respectively, described in Sect. 1, except that `numele` is not supplied.

As function values the modules return

`Mp` Patch mass equations as a coefficient matrix of order 2×5; see (46)–(47)
`Kp` Patch stiffness equations as a coefficient matrix of order 2×5; see (46)–(47)

Appendix 7.4: Dispersion Analysis and Display Modules

This section describe modules that produce and display dispersion diagrams. Those are the top three shown in Fig. 32.

Appendix 7.4.1: Characteristic Equation Module

Module `Bar3CharFreq`, listed in Fig. 37, forms the characteristic equation of a plane wave propagating over a regular Bar3 lattice patch and solves it for the two characteristic frequencies. The calling sequence is

$$\{\texttt{detCm}, \Omega\texttt{2aco}, \Omega\texttt{2opt}\} = \texttt{Bar3CharFreq[wavars, tdef, numer]} \tag{192}$$

The arguments are:

`wavars` A list of symbols representing plane wave dispersion analysis variables, configured as the list { κ, ζ, Ω, Ω2, τ,`Bc`, `Bm` }, in which
- κ Dimensionless wavenumber $\kappa = k\,\ell$
- ζ Dimensionless space coordinate $\zeta = x/\ell \in [-1, 1]$ over patch.
- Ω Dimensionless characteristic frequency $\omega\,\ell/c_0$
- Ω2 Dimensionless characteristic squared frequency
- τ Dimensionless time $\tau = t c_0/\ell$

`Bc`, `Bm` Corner and midpoint wave component amplitudes, respectively
These must be *individual symbols*. No numbers or expressions should be in this list, because they are internally used as variables. For instance, entering $\Omega * \Omega$ or Ω^2 for Ω2 will cause errors.
`tdef` Template definition argument; see Appendix Sect. 7.3.1
`numer` Logical flag; see Appendix Sect. 7.3.1

The module returns the list { `detCm`,Ω`2aco`,Ω`2opt` }, in which

`detCm` Determinant of characteristic matrix $\mathbf{C}_m$ as a function of κ and Ω^2
Ω`2aco` Dimensionless characteristic squared frequency Ω_a^2 of AB, expressed as function of κ
Ω`2opt` Dimensionless characteristic squared frequency Ω_a^2 of OB, expressed as function of κ

The last two expressions: Ω`2aco` and Ω`2opt`, collectively define the DDD for the template specified by `tdef`.

Appendix 7.4.2: Dispersion Branches And Taylor Series

Given a Bar3 template (or instance) definition, module `Bar3Dispersion`, listed in Fig. 38, returns the dimensionless characteristic squared frequencies Ω_a^2 and Ω_o^2 of the AB and OB as function of the dimensionless wavenumber κ. This module was built by inlining symbolic results produced by `Bar3CharFreq` with the goal of speeding up direct retrieval of those expressions. In addition, this module can compute and return their Taylor series expansions about $\kappa = 0$ up to specified orders. The calling sequence is

Fig. 37 Bar3 characteristic equation module

```
Bar3CharFreq[wavars_,tdef_,numer_]:=Module[
 {κ,ζ,Ω,Ω2,τ,Bc,Bm,Kp,Mp,up,fm,fc,mfac,cfac,Cm,detCm,
  Ω2sol,Ω21,Ω22,Ω2aco,Ω2opt}, {κ,ζ,Ω,Ω2,τ,Bc,Bm}=wavars;
  PlaneWave[k_,ω_,B_,x_,t_]:=B*Exp[I*(k*x-ω*t)];
  Mp=Bar3MassTempPatch [1,1,1,tdef,numer];
  Kp=Bar3StiffTempPatch[1,1,1,tdef,numer];
  up={PlaneWave[κ,Ω,Bc,-1,τ],PlaneWave[κ,Ω,Bm,-1/2,τ],
      PlaneWave[κ,Ω,Bc, 0,τ],PlaneWave[κ,Ω,Bm, 1/2,τ],
      PlaneWave[κ,Ω,Bc, 1,τ]};
 {fm,fc}=Simplify[ExpToTrig[(Kp-Ω2*Mp).up]];
  mfac=(Cos[κ/2+Ω*τ]-I*Sin[κ/2+Ω*τ]);
  cfac=(Cos[Ω*τ]-I*Sin[Ω*τ]);
  {fm,fc}=Simplify[{fm/mfac,fc/cfac}];
  Cm={{Coefficient[fm,Bm],Coefficient[fm,Bc]},
      {Coefficient[fc,Bm],Coefficient[fc,Bc]}};
  detCm=Simplify[Det[Cm]];
  Ω2sol=Simplify[Solve[detCm==0,Ω2]];
  Ω2aco=Ω21=Simplify[Ω2/.Ω2sol[[1]]];
  Ω2opt=Ω22=Simplify[Ω2/.Ω2sol[[2]]];
 {Ω210,Ω220}=Simplify[Limit[{Ω21,Ω22},κ->0]];
  If [Ω220==0, Ω2aco=Ω22; Ω2opt=Ω21];
  Return[{detCm,Ω2aco,Ω2opt}]];
```

Fig. 38 Bar3 dispersion module that returns dimensionless characteristic squared frequencies as function of dimensionless wavenumber, and their Taylor series up to given order about $\kappa = 0$

```
Bar3Dispersion[κv_,tdef_,{ma_,mo_},slevel_]:=Module[
 {κ=κv,kw,kw3,tsign=tdef,tvar,β,mpars,μ1,μ2,μ3,μ4,μL1,μL2,
  μS1,μS2,μK,νA,νB,P,Q,R,c1,c2,c3,c4,c5,c6,c7,c8,c9,
  assume,parmap,rep,Ω2aco,Ω2opt,Ω2acos=Null,Ω2opts=Null},
  If [Head[tdef]==String, tsign=Bar3TempSignature[tdef]];
 {tvar,{β},mpars}=tsign; kw=ToUpperCase[tvar]; kw3=StringTake[kw,3];
  parmap=MemberQ[{"GEX","LUM","SPE","SMS"},kw3]; assume=κ>=0&&β>=0;
  If [kw3=="COB", Ω2aco=12*(1-Cos[κ])/(5+Cos[κ]);
      If [kw=="COBA", νA=mpars[[1]]; Ω2opt=16/(1-νA)];
      If [kw=="COBB", νB=mpars[[1]]; Ω2opt=432/(36-12*νB-νB^2)];
      If [ma>=0, Ω2acos=Series[Ω2aco,{κ,0,ma}]];
      If [mo>=0, Ω2opts=Series[Ω2opt,{κ,0,mo}]];
      Return[{Ω2aco,Ω2opt,Ω2acos,Ω2opts}]];
  If [kw=="GEN", {μ1,μ2,μ3,μ4}=mpars];
  c1=4*β*(40+4*μ1+μ2+4*μ4); c2=16+μ2; c3=μ4*(4+μ4);
  c4=4*(5+μ3+μ4); c5=60+4*μ2+μ1*c2; c6=16*μ3-c3;
  c7=4*β*(μ2+c4); c8=c6+μ2*(μ3-1)-20; c9=c7-3*c2;
 {c1,c2,c3,c4,c5,c6,c7,c8,c9}=Simplify[{c1,c2,c3,c4,c5,c6,c7,c8,c9}];
  P=c1+3*c2+c9*Cos[κ]; R=c5-4*μ4-μ4^2+c8*Cos[κ];
  Q=192*β*(Cos[κ]-1)*(c5-c3+c8*Cos[κ])+(c1+3*c2+c9*Cos[κ])^2;
  If [parmap, rep=Bar3MassVarParMap[{μ1,μ2,μ3,μ4},tsign];
      {P,Q,R}={P,Q,R}/.rep];
  If [slevel==1, {P,Q,R}=Simplify[{P,Q,R},assume]];
  If [slevel>1,  {P,Q,R}=FullSimplify[{P,Q,R},assume]];
  Ω2aco=5*(P-Sqrt[Q])/R; Ω2opt=5*(P+Sqrt[Q])/R;
  If [slevel==1, {Ω2aco,Ω2opt}=Simplify[{Ω2aco,Ω2opt},assume]];
  If [slevel>1,  {Ω2aco,Ω2opt}=FullSimplify[{Ω2aco,Ω2opt},assume]];
  If [ma>=0, Ω2acos=Series[Ω2aco,{κ,0,ma}]];
  If [mo>=0, Ω2opts=Series[Ω2opt,{κ,0,mo}]];
  If [slevel==1,{Ω2acos,Ω2opts}=Simplify[{Ω2acos,Ω2opts},assume]];
  If [slevel>1, {Ω2acos,Ω2opts}=FullSimplify[{Ω2acos,Ω2opts},assume]];
  Return[{Ω2aco,Ω2opt,Ω2acos,Ω2opts}]];
```

$$\{\Omega 2aco, \Omega 2opt, \Omega 2acos, \Omega 2opts\} = \texttt{Bar3Dispersion}[\kappa, \texttt{tdef}, \{\texttt{ma}, \texttt{mo}\}, \texttt{slevel}] \tag{193}$$

The arguments are:

- κ Dimensionless wavenumber
- `tdef` Template definition argument; see Sect. 1
- `ma` If $\texttt{ma} \geq 0$, return AB Taylor series (ABTS): Ω_a^2 expanded in κ about $\kappa = 0$, up to and including order `ma`. If a negative integer, return `Null`.
- `mo` If $\texttt{mo} \geq 0$, return OB Taylor series (OBTS): Ω_o^2 expanded in κ about $\kappa = 0$, up to and including order `mo`. If a negative integer, return `Null`.
- `slevel` Simplification level for output results: an integer 0, 1 or 2.
  - `0` : (or negative): no simplifications

Fig. 39 Bar3 dispersion diagram plotting module

```
Bar3DispersionPlot[κ_,tdef_,plotwhat_,κrange_,DVrange_,
  imgsiz_,title_]:=Module[{κv,tsign=tdef,tvar,kpars,mpars,
  cat,Ω2aco,Ω2opt,Ω2acos,Ω2opts,κmin,κmax,Drange,Vrange,
  style,pD=False,pV=False,dfun=$DisplayFunction},
  If [Head[tdef]==String, tsign=Bar3TempSignature[tdef]];
 {tvar,kpars,mpars}=tsign;
  cat=tvar<>" "<>ToString[N[kpars]]<>ToString[N[mpars]];
  If [plotwhat=="D"||plotwhat=="DV", pD=True];
  If [plotwhat=="V"||plotwhat=="DV", pV=True];
 {κmin,κmax}=κrange; {Drange,Vrange}=DVrange;
  style={{AbsoluteThickness[1.80],RGBColor[1,0,0]},
         {AbsoluteThickness[1.80],RGBColor[0,1,0]},
         {AbsoluteThickness[1.80],RGBColor[0,0,0]}}; κv=κ;
  {Ω2aco,Ω2opt,Ω2acos,Ω2opts}=Bar3Dispersion[κv,tsign,{-1,-1},1];
  {Ω2aco,Ω2opt}={Ω2aco,Ω2opt}/.κv->κ;
  If [title!=" ", Print[title]];
  If [$VersionNumber>=6.0, dfun=Print];
  If [pD, Plot[{Sqrt[Ω2aco],Sqrt[Ω2opt],κ},{κ,κmin,κmax},
      PlotStyle->style, Frame->True, PlotRange->Drange,
      ImageSize->imgsiz, DisplayFunction->dfun,
      PlotLabel->"DDD for "<>cat]];
  caco=D[Sqrt[Ω2aco],κ]; copt=D[Sqrt[Ω2opt],κ];
  If [pV, Plot[{caco,copt,1},{κ,κmin,κmax},
      PlotStyle->style, Frame->True, PlotRange->Vrange,
      ImageSize->imgsiz, DisplayFunction->dfun,
      PlotLabel->"DGVD for "<>cat]];
  Return[]];
```

1 : ordinary simplification using the `Simplify` function

2 : more exhaustive simplification using the `Full Simplify` function. Note: this level should be used with caution. Reason: full simplification may return unexpected weird results with terms involving `Abs`, or conditional expressions.

The module returns the list `{ Ω2aco,Ω2opt,Ω2acos,Ω2opts }`, in which

`Ω2aco`	AB dimensionless characteristic squared frequency Ω_a^2 expressed as function of κ
`Ω2opt`	OB dimensionless characteristic squared frequency Ω_o^2 expressed as function of κ
`Ω2acos`	ABTS about $\kappa = 0$ up to and including order `ma`. If `ma` < 0, `Null` is returned.
`Ω2ocos`	OBTS about $\kappa = 0$ up to and inclusing order `ma`. If `mo` < 0, `Null` is returned.

Appendix 7.4.3: Dispersion Diagram Plotting

Given a Bar3 template *instance* (that is, with all-numeric signature) module `Bar3DispersionPlot`, listed in Fig. 39, can plot its DDD, which includes the acoustic and optical branches returned by `Bar3Dispersion`. It may also plot its DGVD, which is the ratio $\gamma_c = c/c_0$ of the FEM plane wave speed c to that of the continuum wave speed c_0. The module has been used to produce all Bar3 dispersion plots of this paper.

The call sequence is

`Bar3DispersionPlot[`κ`, tdef, plotwhat,`
κ`range, DVrange, imgsiz, title]` (194)

The arguments are:

κ	Dimensionless wavenumber
`tdef`	Template definition argument; see Section 1
`plotwhat`	A character string of the form `"D"`, `"V"`, or `"DV"`. If the letter `D` appears, plot the DDD (the so-called "D-plot"). If the letter `V` appears, plot the DGVD (the so-called "V-plot"). If none of those strings is given, no plot is produced.
κ`range`	A 2-item list `{` κ`min,`κ`max }` that specifies the (horizontal) plot range for κ. It is used for both DDD and DGVD plots. Usual range is `{ 0,2 Pi }`.
`DVrange`	A list of the form `{ Drange,Vrange }`. `Drange` is in turn a two-item list: `{` Ω`min, `Ω`max }` that specifies the DDD plot range for Ω. `Vrange` has a similar configuration: `{` γ`cmin,`γ`cmax }` and specifies the DGVD range for $\gamma_c = c/c_0$. Both lists must be supplied even if only one plot is requested. Common specifications are `{ 0,8 }` for `Drange` and $\{-2,2\}$ for `Vrange`.
`imgsiz`	Width of plot in points. Normally set to 300 to 400.
`title`	An optional character string to be printed before the plot. If `" "` no title appears.

The module does not return a value. Its output is the plot image object written to the *Mathematica* default display function. (Its name changed in Version 6.0 from `$DisplayFunction` to `Print`).

References

1. Abramowitz M, Stegun LA (eds) (1964) Handbook of Mathematical Functions with Formulas, Graphs and Mathematical Tables, Applied Mathematics Series 55, Natl. Bur. Standards, U.S. Department of Commerce, Washington, DC (reprinted by Wiley)
2. Achenbach JD (1973) Wave propagation in elastic solids. Elsevier, Amsterdam
3. Aitken AC (1939) Determinants and Matrices. Oliver and Boyd, Edinburgh and London (2nd-8th editions, 1942–56, 9th edition, reset and reprinted, 1967, Greenwood Press, Westport CN, 1983)
4. Anonymous The NASTRAN Theoretical Manual, NASA SP-221 (1970) The NASTRAN User's Manual, NASA SP-222, 1970; The NASTRAN Programmer's Manual, NASA SP-223, 1970; The NASTRAN Demonstration Problem Manual, NASA SP-223
5. Archer JS (1963) Consistent mass matrix for distributed mass systems. J ASCE Struct Div 89:161–178
6. Archer JS (1965) Consistent mass matrix formulation for structural analysis using finite element techniques. AIAA J 3:1910–1918
7. Banerjee B (2011) An introduction to metamaterials and waves in composites. Taylor and Francis, Boca Raton
8. Belytschko T, Mullen R (1978) On dispersive properties of finite element solutions. In: Miklowitz J, Achenbach JD (eds) Modern problems in elastic wave propagation. Wiley, New York, pp 67–82
9. Belytschko T, Hughes TJR (eds) (1983) Computational methods for transient analysis. Elsevier, Amsterdam
10. Bergan PG, Hanssen L (1976) A new approach for deriving 'good' finite elements. In: Whiteman JR (ed) The mathematics of finite elements and applications II. Academic Press, London, pp 483–497
11. Bergan PG (1980) Finite elements based on energy-orthogonal functions. Int J Numer Methods Eng 15:1141–1555
12. Bergan PG, Nygård MK (1984) Finite elements with increased freedom in choosing shape functions. Int J Numer Methods Eng 20:643–664
13. Bergan PG, Felippa CA (1985) A triangular membrane element with rotational degrees of freedom. Comput Methods Appl Mech Eng 50:25–69
14. Bhat SP, Bernstein DS (1996) Second-order systems with singular mass matrix and an extension of Guyan reduction. SIAM J Matrix Anal Appl 17:649–657
15. Born M, Huang K (1954) Dynamical theory of crystal Lattices. Oxford, London
16. Brillouin L (1946) Wave propagation in periodic structures. Dover, New York
17. Chandrasekhar S (1960) Radiative transfer. Dover, New York
18. Clough RW, Penzien J (1993) Dynamics of structures, 2nd edn. McGraw-Hill, New York
19. Cook RD, Malkus DS, Plesha ME (1989) Concepts and application of finite element methods, 3rd edn. Wiley, New York
20. Craig RR, Bampton MCC (1968) Coupling of substructures for dynamic analyses. AIAA J 6:1313–1319
21. Craig RR, Kurdila AJ (2006) Fundamentals of structural dynamics. Wiley, New York
22. Deymier PA (ed) (2013) Acoustic metamaterials and phononic crystals. Springer, New York
23. Duncan WJ, Collar AR (1934) A method for the solution of oscillations problems by matrices. Philos Mag Ser 7 17:865–885
24. Duncan WJ, Collar AR (1935) Matrices applied to the motions of damped systems. Philos Mag Ser 7 19:197–214
25. Elias ZM (1973) On the reciprocal form of Hamilton's principle. J Appl Mech 40:93–100
26. Ergatoudis J, Irons BM, Zienkiewicz OC (1968) Curved, isoparametric, "quadrilateral" elements for finite element analysis. Int J Solids Struct 4:31–42
27. Ewing WM, Jardetsky WS, Press F (1957) Wave propagation in layered media. McGraw-Hill, New York
28. Felippa CA (1966) Refined finite element analysis of linear and nonlinear two-dimensional structures, Ph.D. Dissertation, Department of Civil Engineering, University of California at Berkeley, Berkeley
29. Felippa CA, Bergan PG (1987) A triangular plate bending element based on an energy-orthogonal free formulation. Comput Methods Appl Mech Eng 61:129–160
30. Felippa CA (1994) A survey of parametrized variational principles and applications to computational mechanics. Comput Methods Appl Mech Eng 113:109–139
31. Felippa CA (2000) Recent advances in finite element templates. In: Topping BHV (ed) Computational Mechanics for the Twenty-First Century. Saxe-Coburn Publications, Edinburgh, Chapter 4, pp 71–98
32. Felippa CA (2001) A historical outline of matrix structural analysis: a play in three acts. Comput Struct 79:1313–1324
33. Felippa CA (2001) Customizing high performance elements by Fourier methods. In: Wall WA et al. (eds). Trends in Computational Mechanics, CIMNE, Barcelona, pp 283–296
34. Felippa CA (2001) Customizing the mass and geometric stiffness of plane thin beam elements by Fourier methods. Eng Comput 18:286–303
35. Felippa CA (2003) A study of optimal membrane triangles with drilling freedoms. Comput Methods Appl Mech Eng 192:2125–2168
36. Felippa CA (2004) A template tutorial. In: Mathisen KM Kvamsdal T, Okstad KM (eds) Computational mechanics: theory and practic, 29th edn. CIMNE, Barcelona, pp 29–66
37. Felippa CA (2004) A compendium of FEM integration rules for finite element work. Eng Comput 21:867–890
38. Felippa CA (2005) The amusing history of shear flexible beam elements. IACM Expr 17:15–19
39. Felippa CA (2006) Supernatural QUAD4: a template formulation, invited contribution to J. H. Argyris Memorial Issue. Comput Methods Appl Mech Eng 195:5316–5342
40. Felippa CA (2006) Construction of customized mass-stiffness pairs using templates, invited contribution to special Issue in honor of A. K. Noor. ASCE J Aerosp 19:4:241–258
41. Felippa CA Web-posted Lectures on Advanced Finite Element Methods. http://caswww.colorado.edu/courses.d/AFEM.d/Home.html. Accessed 2013
42. Felippa CA Web-posted Lectures on Introduction to Finite Element Methods http://caswww.colorado.edu/courses.d/IFEM.d/Home.html. Accessed 2013
43. Flaggs DL (1988) Symbolic analysis of the finite element method in structural mechanics, Ph.D. Dissertation, Dept of Aeronautics and Astronautics, Stanford University
44. Fraeijs de Veubeke BM (1971) Dual principles of elastodynamics: finite element applications, NATO Advanced Studies Institute Lecture Series in Finite Element Methods in Continuum Mechanics, Lisbon (reprinted in M. Geradin (ed.), B. M. Fraeijs de Veubeke Memorial Volume of Selected Papers, Sitthoff & Noordhoff, Alphen aan den Rijn, The Netherlands, pp 295–319)

45. Frazer RA, Duncan WJ, Collar AR (1938) Elementary matrices, and some applications to dynamics and differential equations, 1st edn. Cambridge University Press, Cambridge
46. Fried I, Malkus DS (1975) Finite element mass lumping by numerical integration with no convergence rate loss. Int J Solids Struct 11:461–466
47. Geradin M (1973) Computational efficiency of equilibrium models for eigenvalue analysis. In: Fraeijs de Veubeke B (ed) High speed computing of elastic structures. Université de Liège, Liège, pp 589–624
48. Geradin M, Rixen D (1997) Mechanical vibrations: theory and applications to structural dynamics. Wiley, New York
49. Graff KF (1991) Wave motion in elastic solids. Dover, New York
50. Guo Q (2012) Developing an optimal mass for membrane triangles with corner drilling freedoms, M.S. Dissertation, Department of Aerospace Engineering Sciences, University of Colorado at Boulder
51. Gurtin M (1972) The Linear Theory of Elasticity. In: Truesdell C (ed) Encyclopedia of Physics VIa, Vol II, Springer-Verlag, Berlin, pp 1–295 (reprinted as Mechanics of Solids, vol II. Springer, Berlin)
52. Guyan RJ (1965) Reduction of stiffness and mass matrices. AIAA J 3:380
53. Hamming RW (1986) Numerical methods for scientists and engineers, 2nd edn. Dover, New York
54. Hamming RW (1998) Digital filters, 3rd edn. Dover, New York
55. Harris JD (2001) Linear elastic waves. Cambridge University Press, Cambridge
56. Higham NJ (2008) Functions of matrices: theory and computation. SIAM, Philadelphia
57. Hinton E, Rock T, Zienkiewicz OC (1976) A note on mass lumping and related processes in the finite element method. Earthq Eng Struct Dyn 4:245–249
58. Hurty WC (1960) Vibrations of structural systems by component mode synthesis. J Eng Mech 86:51–69
59. Hurty WC (1965) Dynamic analysis of structural systems using component modes. AIAA J 3:678–685
60. Irons BM, Draper K (1965) Inadequacy of nodal connections in a stiffness solution for plate bending. AIAA J 3:965–966
61. Irons BM (1966) Engineering application of numerical integration in stiffness methods. AIAA J 4:2035–2037
62. Irons BM, Ahmad S (1980) Techniques of finite elements. Ellis Horwood Ltd., Chichester
63. Jones H (1960) The theory of Brillouin zones and electronic states in crystals. North Holland, Amsterdam
64. Khenous HB, Laborde P, Renard Y (2008) Mass redistribution method for finite element contact problems in elastodynamics. Eur J Mech A 27:918–932
65. Kolsky H (1953) Stress waves in solids. Oxford University Press, Oxford reprinted by Dover, 1963
66. Krieg RD, Key SW (1972) Transient shell analysis by numerical time integration. In: Oden JT, Clough RW, Yamamoto Y (eds) Advances in computational methods for structural mechanics and design. UAH Press, Huntsville, pp 237–258
67. Lagrange JL (1788) Méchanique Analytique, Paris (Reprinted by J. Gabay, Paris, 1989; downloadable as Google eBook)
68. Lancaster P, Rodman L (1995) Algebraic Riccati equations. Oxford University Press, Oxford
69. Lee U (2009) Spectral element method in structural dynamics. Wiley, Singapore
70. Leung AYT (1993) Dynamic stiffness and substructures. Springer, London
71. MacNeal RH (ed) (1970) The NASTRAN Theoretical Manual, NASA SP-221
72. MacNeal RH (1971) A hybrid method of component mode synthesis. Comput Struct 1:581–601
73. MacNeal RH (1994) Finite elements: their design and performance. Marcel Dekker, New York
74. Melosh RJ (1962) Development of the stiffness method to define bounds on the elastic behavior of structures, Ph.D. Dissertation, University of Washington, Seattle
75. Melosh RJ (1963) Bases for the derivation of matrices for the direct stiffness method. AIAA J 1:1631–1637
76. Malkus DS, Plesha ME (1986) Zero and negative masses in finite element vibration and transient analysis. Comput Methods Appl Mech Eng 59:281–306
77. Malkus DS, Plesha ME, Liu MR (1988) Reversed stability conditions in transient finite element analysis. Comput Methods Appl Mech Eng 68:97–114
78. Olovsson L, Unosson M, Simonsson K (2004) Selective mass scaling for thin wall structures modeled with trilinear solid elements. Comput Mech 34:134–136
79. Olovsson L, Simonsson K, Unosson M (2005) Selective mass scaling for explicit finite element analysis. Int J Numer Methods Eng 63:1436–1445
80. Parlett BN (1980) The symmetric eigenvalue problem. Prentice-Hall, Englewood Cliffs (Reprinted by SIAM Publications, 1980)
81. Park KC, Underwood PG (1980) A variable step central difference method for structural dynamics analysis: theoretical aspects. Comput Methods Appl Mech Eng 22:241–258
82. Park KC (1984) Symbolic Fourier analysis procedures for C^0 finite elements. In: Liu WK, Belytschko T, Park KC (eds) Innovative methods for nonlinear problems. Pineridge Press, Swansea, pp 269–293
83. Park KC, Flaggs DL (1984) An operational procedure for the symbolic analysis of the finite element method. Comput Methods Appl Mech Eng 42:37–46
84. Park KC, Flaggs DL (1984) A Fourier analysis of spurious modes and element locking in the finite element method. Comput Methods Appl Mech Eng 46:65–81
85. Pestel EC, Leckie FA (1963) Matrix methods in elastomechanics. McGraw-Hill, New York
86. Pilkey WD, Wunderlich W (1993) Mechanics of structures: variational and computational methods. CRC Press, Boca Raton
87. Pilkey WD (2002) Analysis and design of elastic beams. Wiley, New York
88. Przemieniecki JS (1968) Theory of matrix structural analysis. McGraw-Hill, New York (Dover edition 1986)
89. Raimes S (1967) The wave mechanics of electrons in metals. North-Holland, Amsterdam
90. Renard Y (2010) The singular dynamic method for constrained second order hyperbolic equations. J Comput Appl Methods 234:906–923
91. Rubin S (1975) Improved component-mode representation for structural dynamic analysis. AIAA J 13:995–1006
92. Song C (2009) The scaled boundary finite element method in structural dynamics. Int J Numer Methods Eng 77:1139–1171
93. Soutas-Little RW, Inman DJ (1998) Engineering mechanics: dynamics. Prentice-Hall, Upper Saddle River
94. Sprague MA, Geers TL (2007) Legendre spectral finite elements for structural dynamics analysis. Commun Numer Methods Eng 24:1953–1965
95. Stroud AH, Secrest D (1966) Gaussian quadrature formulas. Prentice-Hall, Englewood Cliffs
96. Stroud AH (1971) Approximate calculation of multiple integrals. Prentice-Hall, Englewood Cliffs
97. Tabarrok B (1973) Complementary energy methods in elastodynamics. In: Fraeijs de Veubeke B (ed) High speed computing of elastic structures. Université de Liège, Liège, pp 625–662
98. Tabarrok B, Rimrott FPJ (1994) Variational methods and complementary formulations in dynamics. Kluwer, Boston

99. Timoshenko SP (1921) On the correction for shear of the differential equation for transverse vibration of prismatic bars, Phil. Mag., XLI, pp 744–46 (Reprinted in The Collected Papers of Stephen P. Timoshenko, McGraw-Hill, London, 1953. See also S. P. Timoshenko and D. H. Young, Vibration Problems in Engineering, 3rd edition, Van Nostrand, pp 329–331, 1954)
100. Timoshenko SP, Young DH (1955) Vibration problems in engineering. Van Nostrand, Princeton
101. Tkachuk A, Bischoff M (2013) Variational methods for selective mass scaling. Comput Mech 52:563–576
102. Tkachuk A, Wolfmuth B, Bischoff M (2013) Hybrid-mixed discretization of elastodynamic contact problems using consistent singular matrices. Int J Numer Methods Eng 94:473–493
103. Toupin RA (1952) A variational principle for the mesh-type analysis of a mechanical system. Trans ASME 74:151–152
104. Turner MJ, Clough RW, Martin HC, Topp LJ (1956) Stiffness and deflection analysis of complex structures. J Acoust Soc Am 23:805–824
105. Turner MJ (1959) The direct stiffness method of structural analysis. Structural and Materials Panel Paper, Aachen
106. Turner MJ, Martin HC, Weikel BC (1964) Further developments and applications of the stiffness method. In: Fraeijs de Veubeke BM (ed) Matrix methods of structural analysis, AGARDograph 72. Pergamon Press, Oxford, pp 203–266
107. Udwadia FE, Kalaba RE (1996) Analytical dynamics. Cambridge University Press, Cambridge
108. Udwadia FE, Phohomshiri P (2006) Explicit equations of motion for constrained mechanical systems with singular mass matrices and applications to multi-body dynamics. Proc R Soc A 462:2097–2117
109. Udwadia FE, Schutte AD (2010) Equations of motion for general constrained systems in Lagrangian mechanics. Acta Mech 213:111–129
110. Udwadia FE, Wanichanon T (2012) Explicit equation of motion of constrained systems. In: Dai L, Jazar RN (eds) Nonlinear approaches in engineering applications. Springer, New York
111. Underwood PG, Park KC (1980) A variable-step central difference method for structural dynamics analysis, Part 2: implementation and performance evaluation. Comput Methods Appl Mech Eng 23:259–279
112. Warming RF, Hyett BJ (1974) The modified equation approach to the stability and accuracy analysis of finite difference methods. J Comput Phys 14:159–179
113. Wilkinson JH, Reinsch CH (eds) (1971) Handbook for automatic computation. Linear Algebra, vol 2, Springer, Berlin
114. Wimp J (1981) Sequence transformations and their applications. Academic Press, New York
115. Wolf A (2003) The scaled boundary finite element method. Wiley, Chichester
116. Wood A (1940) Acoustics. Blackie and Sons, London (Reprinted by Dover, 1966)
117. Zhang F (ed) (2005) The schur complement and its applications. Springer, New York
118. Ziman JM (1967) Principles of the theory of solids. North-Holland, Amsterdam